Topological and superconducting properties of Weyl and Dirac metals

by

Grigory Bednik

A thesis
presented to the University Of Waterloo
in fulfillment of the
thesis requirement for the degree of
Doctor of Philosophy
in
Physics

Waterloo, Ontario, Canada, 2018

© Grigory Bednik 2018

Examining committee membership

The following served on the Examining Committee for this thesis.
The decision of the Examining Committee is by majority vote.

External Examiner	Professor Igor Zutic
Supervisor	Professor Anton Burkov
Internal Member	Professor Roger Melko
Internal Member	Professor David Hawthorn
Internal-external Member	Associate Professor Jonathan Baugh

Author's declaration

This thesis consists of material all of which I authored or co-authored: see Statement of Contributions included in the thesis. This is a true copy of the thesis, including any required final revisions, as accepted by my examiners.

I understand that my thesis may be made electronically available to the public.

Statement of contributions

My thesis starts from introduction (Chap. 1), where I review general results and existing literature about topological materials, Weyl metals, and non-topological semimentals. I review their known properties in Secs. 2, 3, 4, 5.1, 5.2.1. The results for double Weyl metals and Luttinger model presented in the Secs. 5.1.2, 5.2.2 were obtained by me, but they are not new, and constitute common sense knowledge. The results presented in Secs. 5.3, 5.4 are new and constitute previously unpublished work. The most significant part of this work, presented in Chap. 6 - problem of superconductivity in Weyl metals - was studied by me in collaboration with my supervisor Anton Burkov and our colleague Alexander Zyuzin. With slight refinements, it has been published in the papers [1, 2]. Finally, the problem of mirror symmetry in Dirac metals, presented in Chap. 7 is published in a paper [3].

Abstract

In this work we explore superconductivity and surface states in topological semimetals. We start from general overview of basic properties of topological semimetals. We review general concepts of Chern insulators, their surface states, and use it as a building block for construction of Weyl metals. We also construct double Weyl metals, which are protected both by topology and discrete rotational symmetry. In addition, we study Luttinger model of semimetals - it the simplest case, it is non-topological, but it can acquire topological Weyl points in the presence of non-zero Zeeman field. We present study of its surface states, and also consider its possible critical points.

Next, we turn to the problem of superconductivity in Weyl metals. We demonstrate that Weyl metals are natural candidates for hosting unconventional superconductivity. Specifically, we consider two possible superconducting instabilities: unconventional finite momentum FFLO pairing, and zero momentum BCS pairing, which is also unconventional due to spin-momentum locking in Weyl metals. We demonstrate that its BCS phase is more favorable. In addition, we compute its anomalous Hall conductivity, and demonstrate that it is universal, i.e. not affected by the presence of superconductivity.

Finally, we consider Dirac metals, which are protected solely by rotational symmetry. We point out, that mirror symmetry along its Dirac points plays special role. We demonstrate, that by breaking the rotational symmetry, it is possible to convert Dirac metal into a topological crystalline insulator, and Dirac metal itself can be viewed as a critical point between its different topological phases. We explore surface states spectrum in the resulting picture, and demonstrate, that this mechanism can be used to show that surface states in Dirac metal always terminate at Dirac points despite being not topologically protected.

Acknowledgments

I would like to express my gratitude to my supervisor Professor Anton Burkov, without whom my research could not be possible. I also would like to thank our colleague Alexander Zyuzin, who collaborated on our papers, and had a few conversations with me. I would like to have my second supervisor Professor Roger Melko, working with whom, I have obtained a lot of scientific results. I would like to thank Lauren Sierens for the collaboration and significant support. I would like to thank Professor David Hawthorn for being my commitee member and various help.

Table of Contents

List of Figures

Chapter 1

Introduction

The concept of topological materials originates from the famous paper [4], where quantum Hall conductivity in two-dimensional electron gas was studied experimentally. It was found that it possesses flat plateaus, which are not affected by any perturbations. Soon after it, theory of quantum Hall effect was built: it was found that it is related to so called TKNN invariant: an integral of a matrix elements of wavefunctions over the Brillouin zone [5] , [6]. Later on, theory of quantum Hall effect was rebuilt in terms of Berry connection [7] - vector defined in terms of electron wavefunction, which has all properties of gauge field. Particularly, it was found [8] that quantum Hall conductivity can be expressed as a topological invariant of the wavefuction configuration, i.e. at integral of Berry curvature, which takes discrete values and is invariant under any continuous transformations. This discovery led to building the bridge between condensed matter physics and a mathematical area of topology, which establishes, whether manifolds or field configurations can be connected to each other by continous transformations.

Later, the area of topological materials was developed further. For example, there was proposed a famous Haldane model [9], which exhibits anomalous Hall effect - quantum Hall effect without external magnetic field. This model has never been realized experimentally. However, the Haldane model was built on two-dimensional honeycomb lattice, which later was experimentally realized in graphene [10]. At the same time, it was theoretically predicted, that graphene can be viewed as two copies of Chern insulators [11]: two spin components of its wavefunction exhibit anomalous Hall effect in

the opposite directions, thus forming spin Hall insulator. Strictly speaking, graphene electronic structure contains two almost massless Dirac cones, and it was suggested to be viewed as a spin Hall insulator only because of a very small mass gap present in these Dirac cones. However, spin Hall effect was discovered in a different material: HgTe quantum well [12, 13]. This led to a boom in the area of topological insulators. For example, in one of the first works, it was proposed that between the topological and normal insulating phase, there exists a critical point, where the band structure forms a Dirac cone. At the same time, it was discovered, that topological insulators can be characterized not only by Chern invariant, but also by Z_2 invariant (see [14] for review). Later on, the area of topological insulators expanded into many new matetrials. For example, there were proposed topological crystalline insulators, where, in a mirror invariant plane, bands are characterized by mirror Chern invariant, i.e. difference between Chern invariants for states with different mirror eigenvalues [15, 16, 17, 18]. Particular attention was attracted to the area of topological semimetals, such as, for instance, Weyl metals [19] (see [20, 21] for review), nodal line metals (see e.g. [22, 23]), double Weyl metals [24]. In addition, this area led to discovery of other related materials, such as e.g. Dirac metals.

1.1 Weyl metals

Weyl metals are a well-known example of metallic topological materials. As it was first pointed out in [19], it is possible that band structure may have degeneracy points (so called Weyl points), such that Berry curvature around them has the same structure, as electromagnetic field around a monopole, i.e. non-trivial flux around a closed surface surrounding it. The presence of such flux makes these points topologically protected. Furthermore, simple arguments lead to conclusion, that such Weyl metals possess *Fermi arcs* - surface states connecting the Weyl points. The existence of such states is protected topologically: at fixed momentum component along the separation of Weyl points, they can be viewed as topological surface states, analogous to edge states in a Chern insulator.

Soon after the initial prediction [19], extensive studying of the Weyl metals began. Before they were realized experimentally, it was proposed that Weyl metal phase can be created in a model

of topological/normal insulator multilayer [25]. This scenario has never been realized in practice, but this simple toy model, containing just one pair of Weyl points separated in momentum space within the Brillouin zone, was widely used as a theoretical tool to predict various phenomena. For example, within the first years after its invention, the model of topological/normal insulator multilayer made it possible to find out that Weyl metals have universal magnitude of their anomalous Hall conductivity, proportional to separation between the Weyl points [26]. In addition, through this model, it was found, that Weyl metals host a phenomenon described by the same equations as *chiral anomaly*, known from particle physics: in the presence of electric and magnetic fields, electrons get transferred from one Weyl node to another, and if they are assigned chiral charge - opposite for the opposite nodes - its non-conservation has exactly same form as non-conservation of chiral charge in particle physics [27]. It was found, that this phenomenon results in quadratic negative magnetoresistance. [27, 28]. The model of topological/normal insulator multilayer was generalized to describe topological nodal line metal, where degeneracies between two bands form closed lines, rather than points [29].

Numerous attempts were made to predict superconducting properties in Weyl metals. The first attempt was made in the work [30], where normal insulator in the topological/normal insulator multilayer was replaced with a superconductor. A few spectacular properties were found: the resulting Bogoliubov quasiparticle dispersion contains two pairs of Weyl points, i.e. each Weyl point gets split into two, and, in addition, the spectrum can host Majorana fermions localized at superconducting vortices. Soon after, intrinsic superconductivity in Weyl metal was explored [31, 32], and it was found that it can exhibit exotic phases, such as, e.g. FFLO state, where electrons form Cooper pairs with finite momentum. This was an interesting result, because FFLO state was first suggested in the mid 60-s [33, 34], but almost never realized experimentally. Motivated by this, we also decided to explore superconducting properties in Weyl metal. We found that zero momentum BCS state has lower energy than finite momentum FFLO phase [1], but it is unconventional due to spin-momentum locking. Similarly to the Ref. [30], we found that each Weyl cone gets split into two. We also found that Fermi arcs, a unique property of Weyl metal, persist in the presence of supercon-

ductivity. In addition, we computed anomalous Hall conductivity in the superconducting Weyl metal, and found that, as long as the band spectrum can be approximated as linear, its value is unaffected by the superconducting order parameter [2].

Weyl metal was first experimentally discovered in the material TaAs, and also in TaP and NbAs [35, 36, 37, 38]. Soon after, it was found, that TaAs does not become superconducting at low temperatures, but TaP may be superconducting at or after applying high pressure [39]. It is believed, that, at high pressure, TaP undergoes structural phase transition, where it gets converted into another Weyl metal with a different space group. [39]. At the same time, in the Ref. [40], it was suggested, that in TaAs, superconductivity can be induced by tip, and there was presented evidence, that such superconductivity may be unconventional. Similar work was done in the Ref. [41]: it was shown that silver tip can induce superconductivity in TaAs despite that none of them separately is superconducting. In [41], it was also confirmed that TaAs possesses spin polarized surface states, as we expected. In addition, in the Ref. [42], it was shown that superconductivity in NbAs can be induced by enriching its surface with Nb. This happens because pure Nb is superconducting, and therefore doping NbAs surface with pure Nb can be viewed as creation of extrinsic superconductivity. Finally, superconductivity has been observed in type II Weyl metal $MoTe_2$ [43] ('type II' refers to Weyl metals, which Weyl cones are tilted, so that the Fermi surfaces have the shape of pockets instead of spheres). It was also found to appear at high pressure, and it was confirmed that it has s-wave superconducting order parameter, dependent on polar angle around the Fermi surface.

The concept of Weyl metals was also generalized to multi-Weyl metals [24] - metals, possessing Weyl points with charges higher than one. Such Weyl points can happen, for example, if several usual Weyl points are merged into one. To prevent them from splitting, one has to impose additional protection. In [24] it was shown than such protection can be realized due to additional discrete rotational symmetry: a multi-Weyl point can exist along a rotation axis, as a degeneracy between two bands with different rotational eigenvalues. One can show, that in such scenario, it is impossible to split a multi-Weyl point into single ones.

1.2 Non-topological semimetals

The study of non-topological semimetals goes back to the 1950-s, when Luttinger model [44] describing the most general kp Hamiltonian with four degrees of freedom, satisfying cubic symmetry, was proposed. This model contains two double degenerate bands, touching each other at the origin of the Brillouin zone. Since then, the Luttinger model has been studied for a very long time. For example, only at 2002, its anomalous Hall conductivity in the presence of ferromagnetic impurities [45] was studied: indeed it was a good 'toy' example demonstrating that AHC can be expressed in terms of Berry curvature. A few years later, the Luttinger model was studied as a candidate for probing spin Hall effect [46]. Perhaps, the most notable property of the Luttinger model, relevant to our work, is that under Zeeman magnetic field, its quadratic band touching can split into several Weyl points [47, 48]. In the simplest scenario, there appear two single and two double Weyl points, but, generally speaking, there is plenty of possible scenarios including single and double Weyl points, as well as nodal rings. During the last few years, this concept was believed to be realized in pyrochlore iridates with general formula XIr_2O_7 [47, 49, 50]. In this work, we have also studied the Luttinger model: explored its phases and surface states. We have found that, the Luttinger model can possess critical points, where a lot of states become degenerate, though we are still not familiar with possible routes of realizing them.

Another notable example of non-topological semimetals is Dirac metal: a material, whose band structure possess Dirac points, near which, their dispersion can be described by four-component Dirac equation. In the simplest case, Dirac metal emerges, as a critical point between a topological and normal insulator. This scenario, indeed, has been realized experimentally [13]. However, later on, it became clear that a Dirac point can also be stabilized by rotational symmetry [51]. Furthermore, the presence of discrete rotational symmetry, along with time reversal and inversion (the latter are necessary to ensure double degeneracy of the bands) made it possible to perform full classification of possible Dirac Hamiltonians [52]. It was found that Dirac metals can be classified into two possible classes: in the first class, Dirac metal possess a pair of Dirac points along rotational axis, whereas in the second class, Dirac metal con-

tains a single Dirac point located at the origin of the Brillouin zone. Within the first class, two materials were discovered experimentally: Na_3Bi [53, 54, 55] and Cd_3As_2 [56, 57, 58, 59]. Dirac materials of the second class have never been discovered experimentally, but there exist a similar material $ZrTe_5$ [60]: it hosts a single Dirac point in the origin of the Brillouin zone, but it is not protected by rotational symmetry. It is believed that its Dirac point has a gap, which accidentally happens to be very small.

An interesting question to ask, is whether Dirac metal with a pair of spatially separated Dirac points possess topological Fermi arcs, similarly to Weyl metal. Indeed, such Fermi arcs have been discovered experimentally [61, 62]. Initially, they were believed to be topologically stable[61], as in Weyl metal, since each Dirac point can be viewed as two copies of Weyl points. However, in this picture, two Weyl points composing Dirac point, have the opposite charges: indeed the Dirac points are protected not topologically, but only by discrete rotational symmetry. This, in turn, implies that Fermi arcs in Dirac metal are, as well, not protected topologically [63]: Fermi arcs from each copy of the Weyl metal can, in general, mix with each other. In this work, we have shown, that, despite being not protected topologically, surface states in Dirac metal are similar to Weyl metal in a sense, that they still terminate at Dirac points. In other words, we have shown that mixing of the Fermi arcs may lead to their gapping, but it does not lead to their disappearance.

Chapter 2

Basic notions of topological band theory

2.1 Berry connection

In this work, we set a goal to derive the concept of topological metals from the basic notions of band theory. We would like to start from showing, that bands in solids can possess topological properties. To do it, we first introduce the concept of Berry phase (for a more detailed explanation, see e.g. [64]).

Suppose that an arbitrary wavefunction depends on certain parameters. In the case, when this wavefunction describes a band in a solid, such parameters can be Brillouin zone momenta. It is known, that any wavefunction $\psi(\vec{k})$ is defined up to a phase rotation, and therefore, in the case when the former is a function of parameters $\vec{k}$, phase rotation can be performed at every point $\vec{k}$:

$$\psi(\vec{k}) \sim e^{i\xi(\vec{k})}\psi(\vec{k}). \tag{2.1}$$

From this fact, one can suggest that phase rotations can be viewed as a gauge symmetry. Indeed, gauge symmetry is an internal symmetry, which can be performed separately at every point of the space.

Once we conclude, that wavefunction contains gauge symmetry, we can ask, if there exists gauge field. The answer is positive. Indeed, one can define the gauge field as:

$$\mathcal{A}_i(\vec{k}) = -i\langle\psi(\vec{k})|\frac{\partial}{\partial k_i}\psi(\vec{k})\rangle. \tag{2.2}$$

Such field is called Berry connection. Indeed, one can check that under the gauge transformations (Eq. 2.1), it transforms as a conventional gauge field:

$$\mathcal{A}(\vec{k})_i \to \mathcal{A}(\vec{k})_i + \frac{\partial \xi(\vec{k})}{\partial k_i}.$$

Once we have defined the Berry connection, which has exactly same properties as a gauge vector field, it is natural to define Berry curvature as:

$$\mathcal{F}_{ij}(\vec{k}) = \frac{\mathcal{A}_j(\vec{k})}{\partial k_i} - \frac{\mathcal{A}_i(\vec{k})}{\partial k_j}. \tag{2.3}$$

Indeed, one can check that the Berry curvature is gauge-invariant.

Finally, we would like to note that if we apply the definition of Berry connection (2.2) to the last equation, we can obtain expression for Berry curvature in terms of the wave-function:

$$\mathcal{F}_{ij} = -i \left(\langle \frac{\partial \psi}{\partial k_i} | \frac{\partial \psi}{\partial j} \rangle - \langle \frac{\partial \psi}{\partial k_j} | \frac{\partial \psi}{\partial i} \rangle \right).$$

We will use it in the future.

2.2 Magnetic monopoles

In the last section, we have defined the Berry connection and Berry curvature, according to the Eqs. 2.2, 2.3. As we mentioned, the Berry connection can be viewed as an analog of electromagnetic vector potential, and the Berry curvature can be viewed as an analog of magnetic field. If we assume that both quantities are regular and smooth, it follows that the effective magnetic field is divergence-free:

$$\epsilon_{ijk} \partial_i \mathcal{F}_{jk} = 0.$$

Due to Stokes theorem, the last equation is equivalent to the statement, that the flux of magnetic field over a closed surface is zero:

$$\oint \epsilon_{ijk} \mathcal{F}_{ij} dS_k = 0. \tag{2.4}$$

The statement that divergence of the effective magnetic field is zero, essentially means absence of magnetic monopoles.

However, one can construct special examples of singular vector potentials, which do contain magnetic monopoles. In this section, we present a familiar textbook example (see e.g. [65, 66]), Dirac monopole.

Specifically, let us consider the vector potential of the following configuration. We describe the physical space in spherical coordinates, and assume that only A_ϕ is non-zero. We write its expression as:

$$A_\phi = \frac{1}{4\pi r \sin\theta} \left(1 - \cos\theta\right). \tag{2.5}$$

One can see, that such vector potential is well-defined everywhere. except an axis $\theta = 0$. However, one can gauge-transform it using the gauge function $\xi = \frac{\phi}{2\pi}$, and obtain another expression for the vector potential:

$$\tilde{A}_\phi = \frac{1}{4\pi r \sin\theta} \left(-1 - \cos\theta\right).$$

This expression is well-defined everywhere except special axis $\theta = \pi$. Both of these configurations have magnetic field with the only radial non-zero component:

$$B_r = \frac{1}{4\pi r^2}. \tag{2.6}$$

In other words, we have obtained that singular expressions for the vector potential can, in principle, lead to regular configurations of the magnetic field.

In our case, the magnetic field is regular everywhere except just one point $r = 0$. However, the presence of just one such singular point makes the Eq. (2.4) inapplicable. Indeed, one can check that the magnetic field configuration of the form (2.6) has the total flux equal to one. Thus, we conclude that the magnetic field configuration of the form (2.6) describes a monopole, located at the point $r = 0$.

If we imagine that out electromagnetic field interacts with another field, e.g. fermions, we can derive Dirac quantization condition for the monopole. Indeed, for a monopole to have an arbitrary charge g, it is necessary to have vector potential of the form:

$$A_\phi = \frac{g}{4\pi r \sin\theta} \left(1 - \cos\theta\right),$$

which in turn results in the gauge function of the form:

$$\xi = \frac{g\phi}{2\pi}. \tag{2.7}$$

However, fermionic field transforms under the same gauge function as:

$$\psi \to e^{ie\xi}\psi.$$

. If we use the explicit form of ξ (2.7), and the fact that it has to be smooth: $\xi(\phi = 0) = \xi(2\pi)$, we arrive to a condition, that magnetic charge is discrete:

$$eg = N, \qquad N = 0, \pm 1, \pm 2 \dots$$

which is known as Dirac quantization condition.

2.3 Weyl cone as a magnetic monopole

In this section, we consider the Hamiltonian of Weyl fermions, which can exist in a solid, and show that its Berry curvature configuration contains effective magnetic monopole. This section can be used as an example of explicit calculation of the Berry curvature.

The Hamiltonian of Weyl fermions has the form:

$$H(\vec{k}) = \sigma_i k_i. \tag{2.8}$$

Here $\vec{k}$ is an electron's momentum, and σ_i are well-known Pauli matrices:

$$\sigma_1 = \begin{pmatrix} 0 & 1 \\ 1 & 0 \end{pmatrix}, \qquad \sigma_2 = \begin{pmatrix} 0 & -i \\ i & 0 \end{pmatrix}, \qquad \sigma_3 = \begin{pmatrix} 1 & 0 \\ 0 & -1 \end{pmatrix}.$$

This Hamiltonian describes two bands with linear energy spectrum:

$$E = \pm|k|.$$

These two bands cross at one singular point $\vec{k} = 0$, which is indeed called Weyl point.

Our goal is to compute the Berry connection and Berry curvature of such a system, and to see explicitly that it describes a magnetic

monopole. The easiest way of doing it, is to introduce spherical coordinates in momentum space, thus rewriting the Hamiltonian as:

$$H = k \begin{pmatrix} \cos\theta & \sin\theta e^{-i\phi} \\ \sin\theta e^{i\phi} & -\cos\theta \end{pmatrix}.$$

One can easily verify that it has expected eigenvalues $\pm k$, and the corresponding eigenvectors:

$$\psi_{\pm} = \frac{1}{\sqrt{2(1 \pm \cos\theta)}} \begin{pmatrix} \cos\theta \pm 1 \\ \sin\theta e^{i\phi} \end{pmatrix}.$$

From these eigenvectors, one can compute the components of Berry connection $\bar{\mathcal{A}}$. It is easy to see, that $\mathcal{A}_r = 0$ and $\mathcal{A}_\theta$ depends only on θ, and thus does not contribute to Berry curvature. We compute $\mathcal{A}_\phi$ in spherical coordinates as:

$$\mathcal{A}_\phi = \frac{-i}{k\sin\theta}\langle\psi|\partial_\phi\psi\rangle.$$

Here we have introduced an extra factor of $1/(k\sin\theta)$ to make the resulting vector have physical scale. This is similar to introducing the same factor into the definition of gradient. Explicitly, $\mathcal{A}_\phi$ in our case has the form:

$$\mathcal{A}_\phi = \frac{1 \mp \cos\theta}{2k\sin\theta}.$$

This equation exactly coincides with the field of magnetic monopole (Eq. 2.5). Explicitly, we can obtain the Berry curvature by taking the rotor in spherical coordinates:

$$\mathcal{F}_{\theta\phi} = \frac{1}{k\sin\theta}\left(\frac{\partial}{\partial\theta}(\sin\theta A_\phi) - \frac{\partial A_\theta}{\phi}\right),$$

which explicitly evaluates as:

$$\mathcal{F}_{\theta\phi} = \frac{1}{2k^2},$$

which is exactly the same as magnetic field of a monopole 2.6. Thus, we come to the conclusion, that Weyl point is a magnetic monopole in momentum space. However we would like to note, that

in this derivation, we assumed that, away from the Weyl point, Dirac Hamiltonian can (2.8) can be viewed as continuum, and extending along the whole space of vectors $\bar{k}$. Strictly speaking, the Brillouin zone is periodic, and at certain cases, contributions from its ends can be comparable to the contribution near its origin. We will return to this question later.

2.4 Quantum Hall conductivity as an integral of Berry curvature

2.4.1 Basics of linear response theory

In this section, we would like to show that quantum Hall conductivity can be expressed as a two-dimensional integral of Berry curvature, which is a topological invariant. This fact explains why quantum Hall conductivity is proportional to integer numbers, and not affected by any perturbations.

A simple definition of Hall conductivity is a proportionality coefficient between electric field and current flowing *perpendicularly* to the field. Mathematically speaking, Hall conductivity can be viewed as antisymmetric part of conductivity tensor σ_{xy}, which relates electric current and field:

$$j_i = \sigma_{ij} E_j. \tag{2.9}$$

In quantum mechanical systems, Hall conductivity, similarly to many other quantities, is calculated by using linear response theory. Specifically, one has to write quantum mechanical partition function of the system:

$$\mathcal{Z} = \sum_n \langle n|e^{-\beta H}|n\rangle, \tag{2.10}$$

introduce the electromagnetic field in it as a perturbation, and compute quantum mechanical average current in the leading order over the field.

The partition function (2.10) has to be rewritten as a path integral, and the electromagnetic field is introduced into it via coupling with current:

$$Z[A] = \int D\bar{\psi} D\psi e^{-S + \int d\tau d^3x \vec{J}(x)\vec{A}(x)}.$$

From this equation, it immediately follows that quantum mechanical average current can be expressed as a variation of the partition function over the field:

$$\langle J_i(x)\rangle = \frac{1}{\mathcal{Z}}\frac{\delta \mathcal{Z}}{\delta A_i(x)} = \frac{\delta \log \mathcal{Z}}{\delta A_i(x)}. \tag{2.11}$$

However, as we know from the definition of conductivity (2.9), the right-hand side of the last equation is itself a function of the electromagnetic field.

From the Eq. 2.11, it seems natural to write the current as a functional:

$$\langle J_i(x_1)\rangle = \int dx_2 \sigma_{ij}(x_1, x_2) E_j(x_2) \tag{2.12}$$

so that the conductivity is written as:

$$\sigma_{ij}(x_1, x_2) = \frac{\delta^2 \log \mathcal{Z}}{\delta A_i(x_1)\delta E_j(x_2)}.$$

However, further it is more convenient to work in momentum representation, because the momentum is a conserved quantity, which makes it possible to get rid of extra integrals. Specifically, the Eq. 2.12 can be rewritten in momentum representation as:

$$\langle J_i(k, w)\rangle = \sigma_{ij}(k, w) E_j(k, w). \tag{2.13}$$

If we further focus only on x, y components and choose the gauge $A_t = 0$, we can rewrite the Eq. (2.13) as:

$$\langle J_i(k, w)\rangle = \sigma_{ij}(k, w) iw A_j(k, w). \tag{2.14}$$

In total, this results in Kubo formula:

$$\sigma_{ij}(k, w) = \frac{\partial^2 \log \mathcal{Z}}{iw\partial A_i(k, w)\partial A_j(k, w)}, \tag{2.15}$$

and given that we consider *linear* response, i.e. take into account only linear order in the Eq. (2.14), we can assume that we are computing the derivatives in Eq. (2.16) at $\vec{A} = 0$. Since at zero electromagnetic potential, the current (2.11) is also zero, we can rewrite the Eq. (2.16) as:

$$\sigma_{ij}(k, w) = \frac{\partial^2 \mathcal{Z}}{iw\mathcal{Z}\partial A_i(k, w)\partial A_j(k, w)}, \tag{2.16}$$

2.4.2 Calculation of the quantum Hall conductivity

To compute any quantity using linear response theory, e.g. Eq. (2.16), we can write partition function of the free system as a path integral:

$$\mathcal{Z} = \int D\bar{\psi} D\psi \exp\left\{ \int_0^\beta d\tau \int \frac{d^3k}{(2\pi)^3} \psi^+ \left[\partial_\tau - H\right] \psi \right\}. \qquad (2.17)$$

To proceed, we have to include the coupling between current and vector potential. However, since the latter has non-zero momentum, we rewrite the partition function as:

$$\mathcal{Z} = \int D\bar{\psi} D\psi \exp\left\{ \int_0^\beta d\tau \sum_{k,q} \psi_k^+ \left[\delta_{k,q}\partial_\tau - \delta_{k,q} H(k) + \beta^{-1/2} \vec{J}\vec{A}_{k-q}\right] \psi_q \right\} \qquad (2.18)$$

For clarity, in the last equation, we also have discretized the momentum.

To proceed, it is convenient to Fourier-transform our fermionic fields over the τ variable. Since τ runs from 0 to β, the new variable has to be discrete. This variable runs through values called Matsubara frequencies, which are proportional to half-integer numbers, because the fermionic field in the partition function satisfies antiperiodic boundary conditions (for more details, see [67]). We also view the square brackets in Eq. (2.18) as an operator acting both in frequency-momentum and spin space.

Conventionally, we proceed with the calculation by integrating out the fermion fields, thus rewriting the partition function as:

$$\mathcal{Z} = \det\left[\delta_{k,q}(iw - H) + \beta^{-1/2}\vec{J}\vec{A}_{k-q}\right],$$

which in turn can be rewritten as:

$$\mathcal{Z} = \exp\left\{\log\det\left[\delta_{k,q}(iw - H) + \beta^{-1/2}\vec{J}\vec{A}_{k-q}\right]\right\},$$

or equivalently as:

$$\mathcal{Z} = \exp\left\{\mathrm{tr}\log\left[\delta_{k,q}(iw - H) + \beta^{-1/2}\vec{J}\vec{A}_{k-q}\right]\right\}.$$

Since, eventually, we need to take the second derivative of the partition function $\mathcal{Z}$, we can expand it up to the second order over the

vector potential A. Before doing it, it is convenient to introduce Green function as:

$$G(k,w) = (iw - H)^{-1}\,.$$

Using it, we can rewrite the partition function after the expansion as:

$$\mathcal{Z} = \exp\left\{\mathrm{tr}\left[\log G^{-1} + \beta^{-1/2} G \circ \vec{J}\vec{A} - \frac{1}{2\beta} G \circ \vec{J}\vec{A} \circ G \circ \vec{J}\vec{A}\right]\right\}.$$

We remind, that here we view each term inside the square brackets as an operator both in frequency-momentum and spin space. However, since the Green function acts non-trivially only in the spin space, whereas in momentum space it is proportional to identity operator, we can rewrite the partition function in terms of operators acting only in spin space. If we leave only the interaction terms, it looks as:

$$\begin{aligned}\mathcal{Z} \;\; = \;\; \exp\Bigg\{\mathrm{tr}\Bigg[&\sum_{k,w} G(k,w)\beta^{-1/2}\vec{J}\vec{A}(k,w) \\ &-\frac{1}{2\beta}\sum_{k,q,w} G(q,w)\vec{J}\vec{A}_{q-k}G(k,w)\vec{J}\vec{A}_{k-q}\Bigg]\Bigg\}.\end{aligned}$$

This expression leads to the conductivity tensor of the form:

$$\sigma_{ij} = -\lim_{w\to 0}\frac{1}{i\Omega\beta}\mathrm{tr}\sum_{k,q,w} G(q,w+\Omega)\vec{J}_i G(k,w)\vec{J}_j. \tag{2.19}$$

We also would like to remind, that to compute Hall conductivity, we have to take the antisymmetric part of σ_{ij}. In addition, to obtain physical Hall conductivity, we will have to transform the Eq. 2.19 from imaginary to real frequencies, i.e. perform analytical continuation.

2.4.3 Quantum Hall conductivity vs. Berry curvature

Now we are interested in general expression of the quantum Hall conductivity in terms of Berry curvature. To start its derivation, we would like to write the matrix expression of the Green function. Indeed, since the Green function, as an operator is defined as $G =$

$(iw-H)^{-1}$, we can write its matrix expression in terms of projectors to eigenstates of the Hamiltonian:

$$G = \sum_n \frac{|n\rangle\langle n|}{iw - E_n}.$$

Also we would like to note, that since current can be expressed as a variation of the Hamiltonian with respect to the vector potential:

$$\vec{J} = \frac{\delta H}{\delta \vec{A}},$$

and the vector potential, in turn, is introduced via Pierls substitution:

$$\vec{k} \to \vec{k} - e\vec{A},$$

we can write the current as a derivative of the Hamiltonian over momentum:

$$\vec{J} = -e\frac{\partial H}{\partial k}.$$

Now we can use the last equations in order to rewrite the expression for the conductivity tensor at zero external momentum in terms of matrix elements between eigenvectors of the Hamiltonian:

$$\begin{aligned} &\frac{1}{\beta}\mathrm{tr}\sum_{k,w} G(k, w+\Omega)\vec{J}_i G(k,w)\vec{J}_j \\ &= \frac{-e^2}{\beta}\sum_{k,w} \frac{\langle m|\frac{\partial H}{\partial k_i}|n\rangle\langle n|\frac{\partial H}{\partial k_j}|m\rangle}{(i(w+\Omega) - E_m)(iw - E_n)}. \end{aligned} \tag{2.20}$$

Our next step is to perform the summation over Matsubara frequencies. To do it, we use the fact that our frequencies, are multiples of half-integers:

$$w_n = \frac{2\pi}{\beta}(n + \frac{1}{2}). \tag{2.21}$$

These numbers are precisely the poles of the Fermi distribution function:

$$n_F(z) = \frac{1}{e^{\beta z} + 1}.$$

By expanding it around the poles, one can obtain that their residues are equal to $-1/\beta$.

Thus, to compute the sum (2.20), we consider an integral:

$$\oint \frac{dz}{2\pi i} \frac{n_F(z)}{(z + i\Omega - E_m)(z - E_n)} \tag{2.22}$$

Since the function is regular at $z \to \infty$, the integral taken around very large contour has to be equal to zero. On the other hand, this integral can be written as a sum over all residues of the subintegral function. More precisely, there exist two kinds of residues: the ones of the Fermi function, as determined by the Eq. (2.21), and zeros of the denominator (2.22). Since, as we have mentioned, the sum over both of them is zero, we can write the equation between the sum over the Matsubara frequencies, and the zeros of the denominator of the Eq. (2.22), thus obtaining:

$$\begin{aligned} &\frac{1}{\beta} \sum_{w_n} \frac{1}{(iw_n + i\Omega - E_m)(iw_n - E_n)} \\ &= \frac{n_F(-i\Omega + E_m)}{-i\Omega + E_m - E_n} + \frac{n_F(E_n)}{E_n + i\Omega - E_m}. \end{aligned}$$

We can recall that Ω is the difference between two fermionic frequencies, and therefore its presence does not affect the value of the Fermi function: $n_F(E + i\Omega) = n_F(E)$. Thus we can rewrite the last equation as:

$$\frac{1}{\beta} \sum_{w_n} \frac{1}{(iw_n + i\Omega - E_m)(iw_n - E_n)} = \frac{n_F(E_n) - n_F(E_m)}{i\Omega + E_n - E_m}.$$

This equation, in turn, can be substituted into the expression for the conductivity (2.20), which takes the form:

$$\begin{aligned} &\frac{1}{\beta} \mathrm{tr} \sum_{k,w} G(k, w + \Omega) \vec{J}_i G(k, w) \vec{J}_j \\ &= -e^2 \sum_k \frac{\langle m|\frac{\partial H}{\partial k_i}|n\rangle\langle n|\frac{\partial H}{\partial k_j}|m\rangle \left[n_F(E_n) - n_F(E_m)\right]}{i\Omega + E_n - E_m} \end{aligned} \tag{2.23}$$

Now we would like to use the fact, that Hall conductivity is an antisymmetric part of the conductivity tensor. If we take the anti-

symmetric part of the eq. 2.23, we obtain:

$$\frac{1}{\beta}\mathrm{tr}\sum_{k,w} G(k,w+\Omega)\vec{J}_i G(k,w)\vec{J}_j$$
$$= i\Omega e^2 \sum_{k,w} \frac{\langle m|\frac{\partial H}{\partial k_i}|n\rangle\langle n|\frac{\partial H}{\partial k_j}|m\rangle\left[n_F(E_n)-n_F(E_m)\right]}{\Omega^2+(E_n-E_m)^2} \qquad (2.24)$$

Naively, we would like to take the limit simply by substituting $\Omega = 0$ into the denominator. However, we have to take into account, that the conductivity σ_{ij} is a dynamical quantity, i.e. it is defined for a partition function as an integral over both space and time variables. To account for it, we have to take analytic continuation over Ω, which results in an extra factor of i.

In the case of zero temperature, the Fermi distribution becomes trivial: $n_F(E) = \theta(-E)$, or in other words,

$$n_F(E_n) = \begin{cases} 1 & \text{if the state } n \text{ is filled} \\ 0 & n \text{ is empty} \end{cases}$$

By using this, we can split the summation over filled and empty states, and thus to rewrite the quantum Hall conductivity as:

$$\frac{1}{\beta}\mathrm{tr}\sum_{k,w} G(k,w+\Omega)\vec{J}_i G(k,w)\vec{J}_j$$
$$= \Omega e^2 \sum_{\substack{n-filled \\ m-empty}} \sum_k \frac{\langle m|\frac{\partial H}{\partial k_i}|n\rangle\langle n|\frac{\partial H}{\partial k_j}|m\rangle - \langle m|\frac{\partial H}{\partial k_j}|n\rangle\langle n|\frac{\partial H}{\partial k_i}|m\rangle}{(E_n-E_m)^2}. \qquad (2.25)$$

If we use the Kubo formula, which relates conductivity and trace of Green functions (2.19), we can rewrite the last equation in terms of the conductivity:

$$\sigma_{ij} = ie^2 \sum_{\substack{n-filled \\ m-empty}} \sum_k \frac{\langle m|\frac{\partial H}{\partial k_i}|n\rangle\langle n|\frac{\partial H}{\partial k_j}|m\rangle - \langle m|\frac{\partial H}{\partial k_j}|n\rangle\langle n|\frac{\partial H}{\partial k_i}|m\rangle}{(E_n-E_m)^2} \qquad (2.26)$$

This equation is known as TKNN (Thouless-Kohmoto-Nightingale-den Nijs) formula.

Finally, we can simplify the above expression by using the fact that $|n\rangle$ are the eigenvectors of the Hamiltonian. To do it, we notice

that:

$$\begin{aligned}\langle m|\frac{\partial H}{\partial k_i}|n\rangle &= \langle m|\frac{\partial}{\partial k_i}\left(H|n\rangle\right) - \langle m|H\frac{\partial|n\rangle}{\partial k_i} \\ &= \frac{\partial E_n}{\partial k_i}\langle m|n\rangle + (E_n - E_m)\langle m|\frac{\partial}{\partial k_i}|n\rangle.\end{aligned}$$

If we use the fact, that the states m and n are always different (since one of them is filled, but the other is empty), and substitute the above identity into the expression for quantum Hall conductivity (2.26), we obtain:

$$\sigma_{ij} = ie^2 \sum_{\substack{n-filled \\ m-empty}} \sum_k \left(\langle \frac{\partial m}{\partial k_i}|n\rangle\langle n|\frac{\partial m}{\partial k_j}\rangle - \langle \frac{\partial m}{\partial k_j}|n\rangle\langle n|\frac{\partial m}{\partial k_i}\rangle \right) \quad (2.27)$$

The last equation can be transformed by using the identity:

$$\sum_{filled} |n\rangle\langle n| = 1 - \sum_{empty} |n\rangle\langle n|,$$

and the fact that, since the product of two states is a constant: $\langle m|n\rangle = \delta_{mn}$, we can flip the derivatives as:

$$\langle \frac{\partial m}{\partial k_i}|n\rangle = -\langle m|\frac{\partial n}{\partial k_i}\rangle.$$

Using these identities, we can derive that the quantum Hall conductivity can be written as:

$$\sigma_{ij} = -ie^2 \sum_{n-filled} \sum_k \left(\langle \frac{\partial n}{\partial k_i}|\frac{\partial n}{\partial k_j}\rangle - \langle \frac{\partial n}{\partial k_j}|\frac{\partial n}{\partial k_i}\rangle \right) \quad (2.28)$$

The bracket in the last equation is precisely the Berry curvature, and thus we arrive to our main conclusion: quantum Hall conductivity is proportional to the integral of Berry curvature over the Brillouin zone.

Chapter 3

Basic concepts of topological phases of matter

It is known, that in most real solids, electrons can be described as effectively free, and in such case, they are characterized by electronic band structure, i.e. their spectrum as a function of the Brillouin zone momentum $E(\vec{k})$. One of the main recent achievements of the modern condensed matter physics is that electronic structure can be characterized by its topological properties. Simply speaking, topological properties are properties, which do not change under continuous deformations, but may change under 'large' discrete ones. In the everyday life, examples of topological phases include, for example, a rope with fixed ends reeled up a rod. If we can not move the end of the rope, we are free to make smooth deformations of the rope, but we are not able to change the number of times it reels up the rope. Another example is a knot: if we are not allowed to move the ends of the rope, we cannot untie the knot, but can only make small continuous movements of the rope. In mathematics, topological properties are characterized by discrete topological invariants: numbers, which remain invariant under any continuous deformations. We saw one example of such number in sec 2: a Chern number, or a monopole charge. These are functions of electromagnetic field (or Berry connection), which takes discrete values, invariant under any continuous deformations of the vector field. We would like to demonstrate, how Chern numbers describe topological phases of matter.

3.1 Berry connection vs. time reversal and inversion symmetries

It is known, that many solids are invariant under time-reversal and inversion symmetry. In such case, their electronic structure obeys Kramers theorem, which states that, in the presence of both time-reversal and inversion symmetries, bands are doubly degenerate. We would like to briefly demonstrate it.

Inversion symmetry is a symmetry, which inverts coordinates:

$$x \to -x, \qquad t \to t.$$

It follows that it also inverts momentum, but does not invert spin (because it behaves as angular momentum:

$$k \to -k \qquad s \to s.$$

This is simply because, classically, momentum behaves as velocity $k \sim \frac{dx}{dt}$, and spin behaves as angular momentum: $\vec{s} \sim \vec{L} = \vec{x} \times \vec{p}$. Thus inversion symmetry P transforms quantum mechanical state $|\psi_\uparrow(k)\rangle$ to a state with opposite momentum, but the same spin:

$$P|\psi_s(k)\rangle = |\psi_s(-k)\rangle. \tag{3.1}$$

In contrast, time-reversal symmetry T is a symmetry, which inverts time:

$$x \to x, \qquad t \to -t.$$

It also inverts velocity/momentum, and angular momentum/spin:

$$p \to -p, \qquad s_i \to \epsilon_{ij} s_j.$$

We also note, that time evolution of wave function requires time-reversal to be antiunitary operator:

$$Te^{iHt}|\psi\rangle = e^{-iHt}T|\psi\rangle.$$

By writing the last equation, we essentially said: if we take wave-function $|\psi\rangle$, and let it evolve for the period t, and after it apply time-reversal operator, we should obtain the same wave function acted by time-reversal operator in the beginning, and evolved in the opposite direction of time. The fact that the operator applied to the

vector multiplied by number gives operator applied to the vector, and after it multiplied by the conjugate number, is the definition of antilinear operator. Since the operator T also preserves the norm, we can say that it is antiunitary.

Conventional matrix representation of the time-reversal operator, satisfying these properties is:

$$T\psi_i(k) = i\epsilon_{ij}\psi_j^*(-k)$$

We would like to note, that if a band possesses time-reversal invariance, its Berry connections changes sign under the T transformation:

$$\mathcal{A}(-k) = -\mathcal{A}(k).$$

This fact, in turn, means that in a time-reversal invariant system, Hall conductivity is zero.

We conclude, that non-trivial Hall conductivity arises in system with broken TR. The simplest system with non-zero Hall conductivity without external magnetic field is a Chern insulator. Due to broken time reversal symmetry, its bands have non-zero Chern numbers, and the fact that it is an insulator implies, that they are fully filled. That, in turn, means that Hall conductivity, which is an integral over the filled states, is in fact an integral over the whole Brillouin zone. Thus, in two-dimensional Chern insulator, Hall conductivity is proportional to an integer number.

3.2 Surface states in a Chern insulator

Topologically non-trivial systems obey *bulk-boundary correspondence*, which states that presence of non-trivial topology results in existence of protected surface states. Bulk-boundary correspondence can be viewed as an analog of index theorem. We do not describe it in details here (for detailed, but complicated explanation, see e.g. [68, 69, 70]), but one of its consequences is that the number of zero modes of Dirac operator is related to the topological properties of external field, where the Dirac operator acts. Analogously, Chern number of Brillouin zone is related to the number of protected surface states, which cross the energy gap.

The most simple way to interpret the existence of surface states follows from the fact that anomalous Hall conductivity is non-zero

for a Chern insulator. Generally, insulator is a solid, whose bands are either fully filled, or fully empty, i.e. it does not have a Fermi surface. However, electric current may appear, if electrons are excited near the Fermi surface. Therefore the only way to create non-zero current in an insulator is to allow that, separately from the bulk, there exist Fermi surface on the surface of the sample.

There is known heuristic Laughlin argument [5] about the existence of surface states. Consider a sample having a shape of cylinder, so that y is the coordinate along it, and x is the coordinate across it (see Fig. 3.1). In other words, the system is periodic in y direction, but open in x direction. Now imagine, that magnetic flux is inserted through the cylinder. Following high-school physics, it would result in electric field along the cylinder:

$$\vec{E} = -\frac{d\Phi}{L_y dt},$$

which would accelerate the electrons in the sample:

$$\vec{a} = -\frac{e}{m}\vec{E}.$$

Thus, the magnetic flux insertion would result in momentum change of the electrons:

$$\Delta k_y = \frac{e\Phi}{L_y}.$$

In particular, we call the flux a unit flux, if the momentum changes at one unit:

$$\Delta k_y = \frac{2\pi}{L_y},$$

which implies that the unit flux is equal to:

$$\Phi = \frac{2\pi}{e}.$$

Now let us look at the system quantum-mechanically. It is described by Hamiltonian $H(k)$, and when the flux is inserted, the Hamiltonian takes the form: $H(k - \frac{e\Phi}{L_y})$. Let us write quantum mechanical expression for the current density, in terms of the Hamilto-

nian density $\mathcal{H}$:

$$\langle j_y \rangle = e\langle\psi|\frac{\partial \mathcal{H}}{\partial k_y}|\psi\rangle = L_y\langle\psi|\frac{\partial \mathcal{H}}{\partial \Phi}|\psi\rangle$$
$$= L_y\left(\frac{\partial}{\partial\Phi}\langle\psi|\mathcal{H}|\psi\rangle - \langle\frac{\partial}{\partial\Phi}\psi|\mathcal{H}|\psi\rangle - \langle\psi|\mathcal{H}|\frac{\partial}{\partial\Phi}\psi\rangle\right).$$

The last two terms in this equation cancel out, because ψ has constant norm. Thus we can write:

$$\langle j_y \rangle = L_y\frac{\partial\langle\mathcal{E}\rangle}{\partial\Phi} \approx L_y\frac{\Delta\langle\mathcal{E}\rangle}{\Delta\Phi}.$$

In particular, if the flux is unit, the last equation is rewritten as:

$$\langle j_y \rangle = \frac{eL_y\Delta\langle\mathcal{E}\rangle}{2\pi}.$$

The factor L_y disappears, if we replace the current density with the total current, and the energy density with the total energy:

$$\langle J_y \rangle = \frac{e\Delta\langle E\rangle}{2\pi}. \tag{3.2}$$

Thus we conclude that the existence of current along the cylinder is related to change in energy of the electrons. Since the band structure is insulating, this change of energy can occur only due to change of occupation numbers of the surface states. In particular, if the unit flux is inserted, one filled surface state at one of the edges becomes empty, and vice versa.

Now, we can relate energy change of the system to the change in the voltage across it:

$$\Delta\langle E\rangle = NeV,$$

where N is the total number of electrons transferred to the boundary. Thus we can rewrite the Eq. (3.2) as:

$$\langle j_y \rangle = \frac{Ne^2V}{2\pi},$$

which, in turn, results in Hall conductivity being equal to:

$$\sigma_{xy} = \frac{Ne^2}{2\pi}.$$

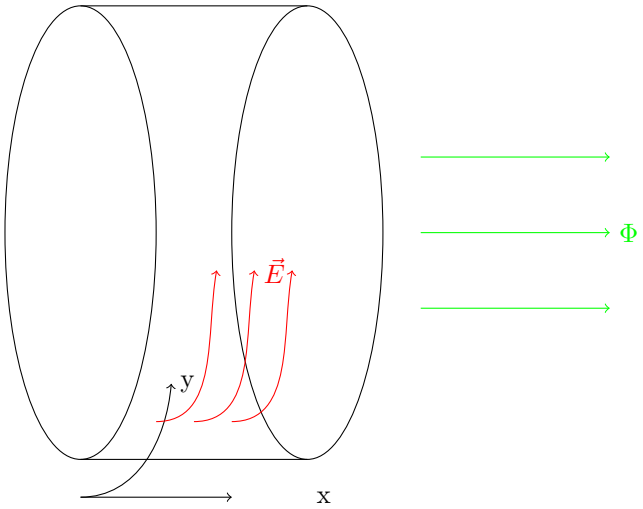

Figure 3.1: Schematic picture of the system considered in Laughlin argument. The conductor is open in x direction and periodic in y direction, or in other words, it forms a cylinder. Magnetic flux is inserted into it, which results in electric field, and consequently redistribution of electric charges along the edges due to Hall conductivity.

As we mentioned, N here is an integer number equal to the number of electrons transferred to the boundary. Since, under unit flux insertion, states can only get repopulated, one empty edge state becomes filled and vice versa. Saying it in different words, along the boundary in x direction, there exist a set of edge states with different k_y, and one of them changes its population for each of the surface bands. Therefore, we can say that N here is a number of the surface bands.

Thus we obtain, the main result of this section: Hall conductivity is proportional to Chern number of the Brillouin zone, which, in turn, is equal to the number of surface bands.

3.3 Explicit calculation of the surface states

In this section, we present an example, demonstrating analytical computation of the surface states [14, 71]. We consider the simplest possible Hamiltonian of two-dimensional Chern insulator:

$$H = k_x\sigma_x + k_y\sigma_y + m\sigma_z. \tag{3.3}$$

This Hamiltonian describes two-band model of Chern insulator, which may exist in 2D. It also has smallest - linear powers of momentum. We note, that this Hamiltonian may, as well, describe 3D material, if m is allowed to be a function of k_z.

However, let us, for simplicity, study the model (3.3) in 2D. Consistently with all symmetries, we can allow m to be dependent on the in-plane momentum:

$$m = M - B(k_x^2 + k_y^2).$$

We will see shortly, that the presence of such momentum-dependent term is necessary to obtain analytical expression for the surface states.

The Hamiltonian (3.3) is written in momentum representation, which is obtained from coordinate representation by Fourier transformation. In the case, when we are interested in bulk states, we can simply assume that the coordinate space is infinite, and therefore the momentum space is continuum. In other words, we can say, that in coordinate representation, bulk states form plane waves. However, we are interested now in surface states. Therefore, we have to view our coordinate space not as infinite, but as half-infinite. For example, we can assume that our sample is located at $x > 0$. Next, we have to account for the presence of such boundary. In general, it is difficult to do it accurately, but the simplest hand-waving way of accounting for it, is implementing fixed boundary condition, e.g.

$$\Psi(x = 0) = 0. \tag{3.4}$$

In this case, the bulk states would be proportional to $\sin(k_x x)$, but the surface states have to be localized near $x = 0$. Thus, to find them explicitly, we have to go back to the coordinate representation in x direction, i.e. to write the Hamiltonian as:

$$H = -i\partial_x \sigma_x + k_y \sigma_y + (M - Bk_y^2 + B\partial_x^2)\sigma_z. \tag{3.5}$$

Since its bulk states are obtained by Fourier transforming, it is natural to search the solution for the surface states in a form, similar to Fourier transforming, but accounting for the fact, that they are localized. Indeed, we can search for the states in the form:

$$\Psi = e^{-\lambda x}\psi, \qquad x > 0. \tag{3.6}$$

This solution differs from the bulk solution simply by replacement $k_x \to i\lambda$, and thus λ can be described as 'imaginary momentum'. This solution rapidly decreases, as x becomes positive. Now, our goal is to find the explicit expression for the wavefunction ψ, and the corresponding energy spectrum $E(\lambda, k_y)$.

If we substitute our ansatz (3.6) into the Schrodinger equation with the Hamiltonian (3.5), we can write it as:

$$E\psi = \left(i\lambda\sigma_x + k_y\sigma_y + (M - Bk_y^2 + B\lambda^2)\sigma_z\right)\psi. \tag{3.7}$$

Since we have to account for the Dirichlet boundary condition (3.4), we need to obtain a solution, which is superposition of two exponents, canceling out each other at the boundary. Thus we write our full ansatz as:

$$\Psi = \left(e^{-\lambda_1 x} - e^{-\lambda_2 x}\right)\psi, \qquad x > 0. \tag{3.8}$$

From this ansatz, it is evident, why we have to include quadratic terms in our Hamiltonian (3.3): we need to obtain two different values $\lambda_{1,2}$ having the same energy and the same wavefunction. This is possible, if $\lambda_{1,2}$ are roots of a quadratic equation, but not possible for a linear equation.

Since our total eigenstate (3.8) is a superposition of two exponents, they both have to be eigenvectors of the Hamiltonian (3.7) with the same energies: $E(\lambda_1, k_y) = E(\lambda_2, k_y)$. Let us try to find out, what this condition means. We can write the equation (3.7) for each value of λ, and to subtract the equations for λ_1 and λ_2. That would result in an equation:

$$0 = \left(i(\lambda_1 - \lambda_2)\sigma_x + B(\lambda_1^2 - \lambda_2^2)\sigma_z\right)\psi.$$

It is straightforward to simplify it by dividing both parts by $\lambda_1 - \lambda_2$, and multiplying by $-i\sigma_x$, thus obtaining:

$$0 = \left(1 - B(\lambda_1 + \lambda_2)\sigma_y\right)\psi.$$

This equation is solved straightforwardly: if ψ is an eigenvector of σ_2 with an eigenvalue ± 1, then the sum $\lambda_1 + \lambda_2$ has the form:

$$\lambda_1 + \lambda_2 = \pm 1/B \tag{3.9}$$

At this point we have to account for the fact that we are looking for the solution, decaying at positive x, or, equivalently, with both

positive $\lambda_{1,2}$. If, without loss of generality, we assume that B is positive, then we have to select only the + sign in the last equations. In contrast, if we were looking for the solution decaying at negative x, we had to select only the negative sign. This is indeed an important conclusion: it implies, that states localized at our boundary $x = 0$ have fixed spin in y direction. If the boundary is at one side of the sample, the spin has one direction, but if the boundary is on the other side, then spin has the opposite direction.

Now let us go back to the main Schrodinger equation (3.7), and try to use the fact that our solution has spin directed along y coordinate. In particular, we use the condition $\psi = \sigma_y\psi$, which is, in turn equivalent to $i\sigma_x\psi = -\sigma_z\psi$. We can rewrite the equation (3.7) as:

$$E\psi = \left(-\lambda\sigma_z + k_y + (M - Bk_y^2 + B\lambda^2)\sigma_z\right)\psi. \tag{3.10}$$

Since we already know the explicit form of ψ - it is an eigenvector of σ_y, but not an eigenvector of σ_z, we can decouple the equation (3.10) into two:

$$\begin{cases} E = k_y \\ -\lambda + M - Bk_y^2 + B\lambda^2 = 0 \end{cases} \tag{3.11}$$

Here the first equation is the answer for the energy spectrum, we were looking for. We have found that energy is linear over the momentum component along the edge k_y. Notably for a given value of k_y there exist only one value of energy (in contrast to two values in bulk spectrum). Thus we can say that our surface band has a fixed handedness. In the considered case, it is right-handed. In contrast, if we were considering states localized in the opposite boundary, we would obtain an expression for the energy with opposite sign: $E = -k_y$. Such band would be called left-handed. Furthermore, we obtained, that, along given boundary, state with fixed momentum has fixed spin direction (it is positive y direction in our case). Such state is called chiral. One can check that states localized at opposite boundaries have opposite chiralities.

Finally, we need to discuss the second equation in the system (3.11). This is a quadratic equation for λ entering the exponents (3.8), i.e. penetration depth. We can solve it easily and obtain:

$$\lambda_{1,2} = \frac{1 \pm \sqrt{1 - 4MB}}{2B}. \tag{3.12}$$

Thus we have found two different values of λ, which in sum give the Eq. (3.9). As we mentioned previously, we needed two different values of λ to satisfy the boundary conditions, and the second equation in the system (3.11) demonstrates that we had to include the quadratic terms in momentum.

Finally, we need to ensure that both values of λ, defined by the Eq. (3.12), have positive real parts. It is necessary, since our solution (3.8) has to decay inside the sample, i.e. at $x > 0$. The condition of both $\mathcal{R}e\lambda_{1,2} > 0$ leads to inequality:

$$M > 0 \tag{3.13}$$

Its left part has obvious meaning: surface states exist only at positive M, which is the range of M, where the model is a topological insulator. As M becomes negative, the system becomes a normal insulator, and its surface states disappear.

We note, that $\lambda_{1,2}$ can exist in two different regimes. In the case, when $M < 1/(4B)$, both $\lambda_{1,2}$ are real and positive, whereas in the case $M > 1/(4B)$, they become complex, but still retain positive real parts. Thus, in our model, surface states exist any any positive M. However, we remark, that if try to include the lattice effects, i.e. periodicity of the Brillouin zone, the model will acquire additional phases, and at the point $M = 1/(4B)$ there will appear an additional transition. We will discuss this issue in Chapter (4).

3.4 Topological phase transitions

In the previous sections, we described the concept of two dimensional Chern insulator: it has bands with non-zero Chern numbers. Now we would like to discuss possible transitions between different topological phases. As mentioned before, topological phases are characterized by topological invariants (in our case Chern numbers), which are discrete functions of the bands. Thus a system cannot change its topological phase under any smooth deformations of the electronic structure. However, can there exist a non-smooth transformation, which does change the topological invariant? The answer is that topological invariants can change if the system undergoes a phase transition, which can occur if the gap gets closed.

One example of such transition was proposed in Ref. [12]: it is a topological phase transition in HgTe quantum well. Such two di-

mensional system can be described by a massive Dirac Hamiltonian, which consists of two copies of Weyl Hamiltonians:

$$H = \begin{pmatrix} h(k) & 0 \\ 0 & h^*(-k) \end{pmatrix}, \tag{3.14}$$

where h is defined in exactly the same way, as in the Eq. (3.3).

Now let us consider, how each copy with the Hamiltonian h evolves, as m changes. If we imagine, that our model lives in a fictitious three-dimensional space k_x, k_y, m, we can say, that the point $k_x = k_y = m = 0$ is a magnetic monopole, i.e. integral of Berry curvature over a surface surrounding this point is equal to the magnetic charge. This, in turn, is equivalent to saying, that Chern number of such model, as an integral of Berry curvature over the (k_x, k_y) changes by unit number, as m changes sign. Thus, we can conclude, that the point $m = 0$ is a point of topological phase transition in the model with the Hamiltonian h. It is also consistent with the fact, that in the point $m = 0$, gap closing occurs. At $m = 0$, the system is gapless, whereas at any non-zero m, either positive or negative, the system is gapped. At positive m, the system with Hamiltonian h is Chern insulator, but at negative m the system is a normal insulator.

However, the full model of the HgTe quantum well (3.14) includes two copies of h. Their presence is necessary to ensure that the model possesses time reversal and inversion symmetries. Indeed, as we discussed previously, non-zero Chern number are possible only if the time reversal symmetry is broken, which indeed occurs in the subsystem with Hamiltonian h. One can check, that one copy of the subsystem transforms under time reversal to the other. Thus the total system is time reversal invariant, and it is also easy to check, that, consistently with Kramers theorem, its bands are doubly degenerate. This is simply because bands of the two copies of h have equal energies.

Since the system (3.14) consists of two copies of Hamiltonians h, which, in turn, undergo topological phase transition at $m = 0$, we can say that the whole system undergoes topological phase transition at $m = 0$. As we said, the gap closes at this point, and the total system consist of two copies of two-dimensional Weyl Hamiltonians. This is, in turn, equivalent to saying that the whole model realizes Dirac point at $m = 0$. This is our main conclusion: Dirac point can arise as a critical point between two different topological phases.

Finally, for completeness, we note that the two copies of h have the opposite Chern numbers. We also note, that in this particular model, each copy of h corresponds to a fixed direction of spin, whereas 2×2 components of each h act in the space of orbital degrees of freedom. Thus, at the topological phase, the system has a given value of anomalous Hall conductivity for one spin, and the opposite of it for the other spin. Such kind of systems is called *spin Hall insulator*.

3.5 Weyl metal

In the previous section, we discussed that studying a phase transition between two different topological phases leads to a new state of matter: Dirac metal. That is a gapless system, whose spectrum can be described by Dirac equation. We also mentioned that Dirac equation, written in terms of four component matrices, can be viewed as two copies of Weyl equations, and the two copies necessarily arise due to presence of both inversion and time reversal symmetries. Now, we are interested, if it is possible to obtain these Weyl cones separately. To achieve it, we simply need to remove the Kramers degeneracy, which can be done by breaking either time-reversal, or inversion symmetry. In such case, the bands are no longer doubly degenerate, and therefore, the Weyl cones are free to move in momentum space under any perturbations.

Once two Weyl cones become separated, they can not be gapped under any small perturbations. This is because each Weyl cone is a magnetic monopole of Berry curvature. The latter is non-zero due to the presence of the Weyl point, which is a singularity, but it would always be zero for any kind of gapped system. Thus, we can say that Weyl points are protected topologically. Our conclusion is that, under symmetry breaking, Dirac points can be deformed into either normal insulator, or a topological insulator, or a Weyl metal - a material with spatially separated Dirac points (this scenario was discussed in a large number of specific models, e.g. in [25]). Therefore, we can expect the Weyl points to be very common in the nature. Indeed, they have been detected experimentally in a large number of materials (see e.g. [35, 37, 36, 38]).

As we have just said, Weyl points possess non-zero topological charge: integral of Berry curvature around closed surfaces surround-

ing them is non-zero. Equivalently, integral of Berry curvature over Brillouin zone cross-section from one side of the Weyl point differs from the integral on the other side. Therefore, it is convenient to view Weyl metal as a 'stack' of Chern insulators in momentum space. As an example, let us imagine that a Weyl metal possess a single pair of Weyl points at the momenta $(0, 0, \pm Q)$. We can view it as a stack of Chern insulators in z direction, such that the integral of Berry curvature over xy plane is zero outside the Weyl points, i.e. at $|k_z| > Q$, and equals to 1 between them, i.e. at $|k_z| < Q$.

After these making considerations, we arrive to the simplest possible Hamiltonian describing a model of Weyl metal:

$$H = k_z\sigma_x + k_y\sigma_y + m(k_z)\sigma_z, \tag{3.15}$$

This Hamiltonian is just a superposition of 2D Hamiltonians (3.3) at fixed values of k_z. We assume, that m is positive at $|k_z| < Q$, and negative at $|k_z| > Q$. Points, where $m = 0$ are the Weyl points. Using the results from the previous sections, we can see that its Chern number at fixed k_z behaves as expected: it is equal to 1 between the Weyl points, and zero outside them.

We note, that in this model, Weyl points have opposite topological charges. It is consistent with the fact, that the topological charges have to cancel out, if the Weyl points merge into one Dirac point. We also note, that such model is possible only under breaking of time reversal symmetry, since electrons with opposite momenta have opposite spins. If, instead, the inversion symmetry were broken, the states with opposite momenta would have the same spin, and thus the Weyl points would have the same topological charges. Therefore, a minimal model of Weyl metal had to include at least four Weyl points.

Finally, we discuss the structure of surface states in a Weyl metal. As we have just discussed, Weyl metal is a Chern insulator at $k_z < |Q|$ and a normal insulator at $k_z > |Q|$. Therefore, for each value of k_z its surface states have to look exactly as surface states of a Chern/normal insulator. If we recover the properties of the surface states, that we obtained in Sec. 3.3, we obtain that Weyl metal possesses chiral surface states with dispersion $E = k_y$ at $|k_z| < Q$, but does not possess surface states at $|k_z| > Q$ (see Fig. 3.2). In other words, if we look at the surface states spectrum at fixed energy, e.g. at $E = 0$, we will see a branch of surface states connecting

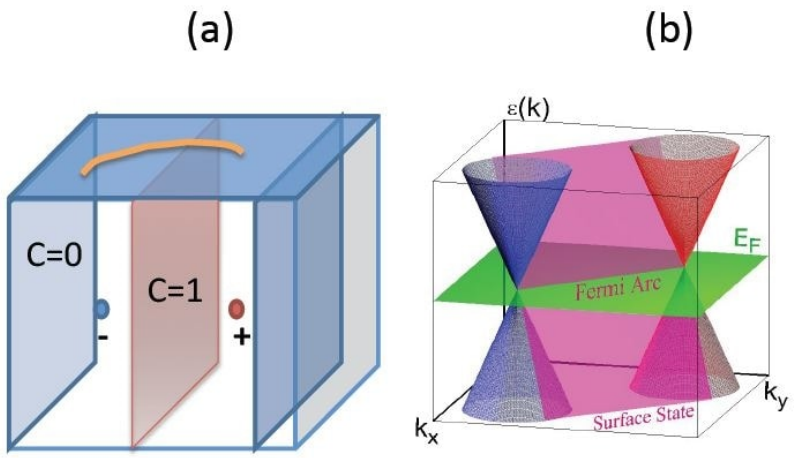

Figure 3.2: Schematic view of Weyl points in a Weyl metal, and integrals of Berry curvature over different cross-sections of the Brillouin zone (left). Dispersion structure in the bulk has two Weyl cones, whereas dispersion structure along the surface is linear; surface states exist between the Weyl points (right). This figure is reprinted from `http://phyx.readthedocs.io/en/latest/TI/Weyl_semi-metal.html` and distributed under Creative Commons License.

the Weyl points. Such branch is called a *Fermi arc*. Since the dispersions are opposite on the opposite surfaces ($E = +k_y$ on one surface, and $E = -k_y$ on the other one), there are two different Fermi arcs connecting the Weyl points: one on each surface.

3.6 A model of Weyl metal in a topological/normal insulator multilayer

In this section, we present the first theoretically proposed model of Weyl metal: a topological normal insulator multilayer [25]. We note, that this model has never been realized experimentally, but it attracted a lot of attention, because it was the first proposed model, and also because this model is the simplest, i.e. it contains only one pair of Weyl points, but includes the effect of their spatial separation, which makes it convenient to analyze as a toy model.

In the Sec. (3.5), we have said that the simplest way to imagine

Weyl metal is to view it as a stack of Chern insulators in z direction. We have also said, that at fixed k_z, Chern insulator can be described by a gapped Weyl Hamiltonian (3.15). There is a widely known example, where two-dimensional fermions with linear dispersion exist: surface states in a $3D$ topological insulator (strictly speaking, it is $\mathtt{Z}_2$ topological insulator, which is different from Chern insulators considered in this work) are described by Dirac equation. The most natural way to make them three-dimensional, but not to alter their properties along xy plane, is to create a multilayer in z direction. In this case, the fermions become effectively three-dimensional due to tunneling between the different layers.

However, we need one additional ingredient. In the Sec. (3.5) we mentioned, that Weyl metal can be realized, if time reversal or inversion symmetry is broken. $\mathtt{Z}_2$ topological insulator does not break it, and therefore, we need to break it separately, which is easy to do, for example, by adding magnetization to our multilayer. It is natural to add it in the same direction, as the multilayer growth, i.e. in z direction.

In total, we can write the Hamiltonian of the multilayer model in the following form:

$$H = \sum_{i,j,k} \quad \Big\{ v_F \tau_z (\sigma_x k_y - \sigma_y k_x)\delta_{i,j} + b\sigma_z \delta_{i,j} + \Delta_S \tau_x \delta i, j + \frac{\Delta_D \tau^+}{2} \delta j, i+1 + \frac{\Delta_D \tau^-}{2} \delta_{j,i-1} \Big\}. \tag{3.16}$$

Here we numerate the layers by indices i, j. We also have to distinguish between the surfaces on the left and on the right side of the topological insulator, which we achieve by introducing an additional flavor: τ matrices act in the space of this new flavor. In particular, the term proportional to Δ_S describes tunneling between two edges of one topological insulator layer, whereas the terms proportional to Δ_D describe tunneling between different topological insulator layers. In contrast, σ matrices act in usual spin space: each τ_z block in the first two terms of the Hamiltonian describes surface states of a one topological normal insulator interface, but the states from the opposite surfaces have the opposite chiralities. The time reversal symmetry breaking magnetization is encoded in the third term

$b\sigma_z$, which describes interaction of spin 1/2 electrons with Zeeman magnetic field.

To find the electronic structure of this model, one has to diagonalize the Hamiltonian (5.13), and to find its eigenenergies as functions of momentum. We start doing it from a standard step: we perform Fourier transformation in z direction, in order to obtain the Hamiltonian in momentum space in all three directions. This step is commonly done in many lattice models, because it straightforwardly helps to get rid of the matrix elements between the different sites (in our case the terms proportional to Δ_D).

However, we also perform another trick: a canonical transformation of the matrices entering the Hamiltonian: $\sigma^{\pm} \to \sigma^{\pm}\tau^z, \tau^{\pm} \to \sigma_z\tau^{\pm}$. It is straightforward to see, that this transformation leaves the commutation relation between the matrices unchanged, and one can also check that this transformation is, in fact, unitary transformation of the Hamiltonian $H \to UHU^+$ with the matrix $U = \frac{1+\tau_z}{2} + \frac{(1-\tau_z)\sigma_z}{2}$.

After performing these two steps, the Hamiltonian can be written as:

$$H = v_F(\sigma_1 k_2 - \sigma_2 k_1) + b\sigma_z + \left(\Delta_s\tau_x + \frac{\Delta_D\tau^+}{2}e^{ik_z d} + \frac{\Delta_D\tau^-}{2}e^{-ik_z d}\right)\sigma_z. \tag{3.17}$$

Afterwards, the Hamiltonian is easy to diagonalize. Indeed, nontrivial τ matrices enter it only inside the large bracket. Thus we can immediately diagonalize it in τ space. In particular, eigenvalues of the large bracket are equal to $\pm\Delta$, which we define as:

$$\Delta = \sqrt{\Delta_S^2 + \Delta_D^2 + 2\Delta_S\Delta_D\cos(k_z d)}.$$

To parametrize the $\pm$ sign, we introduce a new variable t, which takes values ± 1. In total, after diagonalization in τ space, the Hamiltonian (3.17) decouples into two copies for each of the signs of t. These copies are explicitly written as:

$$H = v_F(\sigma_1 k_2 - \sigma_2 k_1) + (b + t\Delta(k_z))\,\sigma_z.$$

Now, for each of the copies, we can introduce $m = b + t\Delta(k_z)$, and the connection to the Weyl metal (see Eq. 3.15) becomes straightforward. Indeed, we obtain two copies of Hamiltonians with different

m for each case of the t sign. One can check, that it is possible to find a range of parameters, such that m in the case of negative t sign behaves as in a Weyl metal, i.e. change its sign at two values of k_z. We write these values of $k_z = Q$ explicitly:

$$Q = \frac{1}{d}\text{acos}\left(\frac{b^2 - \Delta_S^2 - \Delta_D^2}{2\Delta_S\Delta_D}\right). \tag{3.18}$$

The parameters b, Δ_S, Δ_D has to be chosen, in such a way, that the acos is well-defined, which is indeed possible.

In contrast, the block with $t = +1$ never changes its sign, and furthermore, its energies lie in a different range from the energies of the block with $t = -1$ sign. Thus, the model of topological/normal insulator multilayer (5.13) contains, in total, four bands. Two of them may cross each other, forming a single pair of Weyl points, whereas the other two are separated from the former by energy gap. Hence, we can further consider the Hamiltonian of Weyl metal in the simple form (3.15), which indeed refers to the topological/normal insulator multilayer.

Finally, we note, that our multilayer model (5.13) can, in principle be modified in many different ways. For example, one may consider the situation, where both time reversal and inversion symmetries are broken [72]. The latter can be accounted simply by adding an additional term: $H_\lambda = \lambda\tau_y$.This leads to new kinds of contributions anomalous Hall conductivity and longitudinal magnetoresistance in these models [27, 28]. Also, one may consider different directions of magnetization in the multilayer, which would to a richer phase diagram: one may obtain not only Weyl metal, but also nodal line metal [29].

Chapter 4

Lattice model of Chern insulator and Weyl metal

4.1 Introduction to lattice models

In this section, we would like to place the model of Weyl metal (3.15) on a lattice. We need to do it, because only in case of the lattice, Chern number as an integral of Berry curvature, becomes integer. We can see it in the following way. In sec. 2.3 we found, that magnetic charge, which can be viewed as an integral of Berry curvature over the surface surrounding the monopole, is quantized. However, if instead of a closed surface, we consider an open surface, e.g. a part of the closed surface, its integral of Berry curvature is no longer quantized. The continuum model (3.15) is indeed defined on an open surface: k_x, k_y run from $-\infty$ to ∞, and therefore an integral of Berry curvature over the whole plane k_x, k_y is not integer. However, it will become integer, if instead of the full plane, we consider a torus $|k_{x,y}| < \pi$, because in the latter case, we can derive quantization conditions in the same way, as we did for a sphere.

Indeed every solid is known to be a lattice of atoms, and therefore, an electron's wavefunction can be viewed as a wavefunction inside an atom multiplied by plane wave as a function of discrete atomic coordinate (this statement is known as Bloch theorem). Thus, momentum in a solid conventionally refers to crystal momentum, i.e. momentum obtained by Fourier transformation over discrete lattice coordinate. However, if a variable is discreet, its Fourier transform is periodic. Thus crystal momentum is periodic: it is known that is

forms a periodic Brillouin zone.

Now let us build the simplest possible extension of the model (3.15) accounting for the periodicity of the Brillouin zone. The most straightforward way of doing it, is to replace every momentum component with its sin function: $k_{x,y} \to \sin k_{x,y}$. Such function is periodic, and in the limit of small momentum it becomes equal to the momentum component itself. This is consistent with the fact, that small momenta correspond to large distances, but at large distances, lattice can be viewed as approximately continuum.

This approach has a drawback. The Hamiltonian $H = \sigma_x \sin k_x + \sigma_y \sin k_y$ has several degeneracy points. It is degenerate not only at the point $k_x = k_y = 0$, as it would be in the continuum case, but also at the points $k_{x,y} = \pi$. However, we would like to talk about topological phase transitions occurring at the degeneracy points, and extra such points would bring extra complications for us. Thus we would like to remove such 'copies', and the easiest way to do it, is to introduce quadratic terms in the Hamiltonian, as we already did, when we were discussing surface states (see Sec. 3.3). When we switch from continuum model to the lattice, we replace our quadratic terms as: $k_{x,y}^2 \to 2(1 - \cos k_{x,y})$ - this function is periodic and has limit, consistent with the continuum model.

Thus, the proper Hamiltonian for Chern insulator on a lattice has the form:

$$H = \sigma_x \sin k_x + \sigma_y \sin k_y + \sigma_z \left(M - 2B(2 - \cos k_x - \cos k_y)\right). \quad (4.1)$$

In the following sections we compute its Chern number, and surface states.

4.2 Analytical computation of Chern number

In this section, we demonstrate how Chern number can be computed analytically on a lattice. As we discussed previously, Chern number is defined as an integral of Berry curvature over the Brillouin zone. If one computes the Berry curvature explicitly for the Hamiltonian (4.1), its expression becomes complicated, and it seems hard to take its integral analytically. However, there exists a way compute it exactly, and we would like to demonstrate it.

First, integral of Berry curvature over the Brillouin zone can be rewritten as an integral of Berry connection over its boundary:

$\int\limits_M \mathcal{F} = \int\limits_{\partial M} \mathcal{A}$. In our case, the Brillouin zone is bounded by four lines $k_{x,y} = \pm\pi$. Thus, we can write the Chern number as:

$$\begin{aligned} C &= \frac{1}{2\pi} \oint \vec{\mathcal{A}} d\vec{l} \\ &= \frac{1}{2\pi} \left(\int\limits_{-\pi}^{\pi} A_y dk_y \mid_{k_x=\pi} - \int\limits_{-\pi}^{\pi} A_x dk_x \mid_{k_y=\pi} \right. \\ &\quad \left. - \int\limits_{-\pi}^{\pi} A_y dk_y \mid_{k_x=-\pi} + \int\limits_{\pi}^{\pi} A_x dk_x \mid_{k_y=\pi} \right). \end{aligned} \tag{4.2}$$

We note, that our contour of integration is periodic, and thus the integrals at the opposite edges of the Brillouin zone $\int A_y k_y \mid_{k_x=\pm\pi}$ or $\int A_x k_x \mid_{k_y=\pm\pi}$ are almost identical. The only source of difference between them comes from the fact, that there can be singularities along the boundary of the Brillouin zone, and the integral contours have to go around them in different directions. This fact is similar to the sec. (2.2): there we also have obtained that integral of Berry curvature over a closed surface is non-zero solely due to presence of singularities of the Berry connection.

Thus, to compute the integral (4.2) we have to find all singularities of the Berry connection. To make our equations shorter, we consider a general Hamiltonian:

$$H = d_i \sigma_i. \tag{4.3}$$

Its eigenvector corresponding to the filled state has the form:

$$\psi = \frac{1}{\sqrt{2d(d+d_3)}} \begin{pmatrix} d_1 - id_2 \\ -d - d_3 \end{pmatrix}. \tag{4.4}$$

The corresponding Berry connection has an expression:

$$\mathcal{A}_i = \frac{d_1 \partial_i d_2 - d_2 \partial_i d_1}{2d(d+d_3)}.$$

It is easy to see, that its singularities may occur only if either $d = 0$, or $d + d_3 = 0$. The first case corresponds to the point $M = 0$, i.e.

the point of topological phase transition. The second case can be realized, when $d_1 = d_2 = 0$, i.e. $k_{x,y} = 0, \pm\pi$, and, in addition, $d_3 < 0$. Further analysis depends on specific details of the system.

If we choose the Hamiltonian in accordance to the Eq. (4.1), there are several possible cases. For simplicity, let us fix B to be positive and consider different possible values of M.

We start from the simplest case of $M > 8B$. The term $d_3 = M - 2B(2 - \cos k_x - \cos k_y)$ is always positive at the whole Brillouin zone, and therefore, Berry connections does not have any singularities. As a result, its integral (4.2) is zero. We will understand its meaning soon.

Singularities appear, as M becomes less than $8B$. Particularly, in the range $4B < M < 8B$, singularities appear at $k_x = k_y = \pi$. Thus the integral (4.2) is in fact an integral over a contour, which is going around the point $k_x = k_y = \pi$:

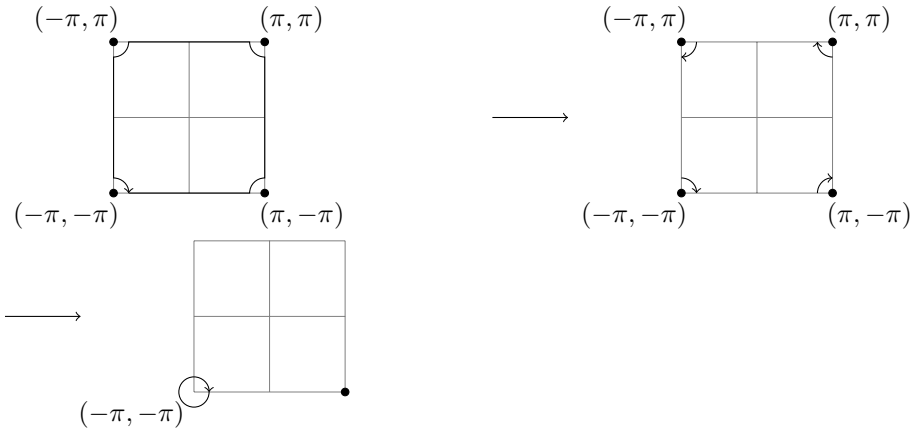

Figure 4.1: Integration contour for $\vec{\mathcal{A}}$ in the plane (k_x, k_z) in the model defined by H_+ (Eq. 7.5). in the case $4B < M < 8B$.

On this picture 4.1, we have shown that the integral over the boundary of the Brillouin zone can be transformed to the integral around the singularity. Since we can take the contour surrounding the singularity to be infinitely small, we can expand the values of $d_{1,2,3}$ entering the Eq. 4.1 around this singularity, i.e. around the point $k_x = k_y = \pm\pi$. Explicitly, we can write $k_{x,y} = \pi + q_{x,y}$, where q is very small, and make the expansion: $\sin k_{x,y} = \sin(\pi + q_{x,y}) \approx -q_{x,y}$. Since we are interested in the integral around closed contour,

it is convenient to write it in polar coordinates: $q_x = q\cos\varphi$, $q_y = q\sin\varphi$. Using them, we can write the wavefunction (4.4) as:

$$\psi = \frac{1}{\sqrt{2d(d+d_3)}} \begin{pmatrix} -qe^{-i\varphi} \\ -d-d_3 \end{pmatrix}. \tag{4.5}$$

Indeed, in the polar coordinates we need only one component of Berry connection, i.e. $\mathcal{A}_\varphi$, and it is simply equals to -1. By integrating it over φ, we obtain the answer: in the range $4B < M < 8B$, the Chern number is equal to -1.

The other cases are considered in a similar way, so let us describe them briefly. In the case $0 < M < 4B$, there two new poles appear: one at $k_x = 0, k_y = \pm\pi$, and the other at $k_x = \pm\pi, k_y = 0$. One can perform integral of Berry connection over the contours surrounding them in a similar way, and obtain that each integral is equal to 1, and thus the Chern number as a sum of all integrals is equal to $-1+1+1=1$. It has the opposite sign from the previous case. Finally, in the case $M < 0$, the point $k_{x,y} = 0$ also becomes a pole, and therefore the expression (4.2) has to be modified: since integral of Berry curvature is equal to the integral of Berry connection around the boundary of the surface, assuming there are no singularities in the surface, we have to write the integral of Berry curvature as an integral of Berry connection over the boundary of the Brillouin zone plus an integral surrounding the pole. If we perform all calculations, we obtain that the total integral, and hence Chern number is equal to zero.

Thus we derived, that the model (4.1) has in total four topological phases: trivial phases at $M < 0$ and at $M > 8B$, a phase with Chern number 1 at $0 < M < 4B$, and also a phase with Chern number -1 at $4B < M < 8B$. As we discussed in Sec. 3.4, between different topological phases, gap closing must occur. Indeed, in our model, the energy gap closes at $M = 0$, $k_x = k_y = 0$. At $M = 4B$, the gap closes at two points: $k_x = 0, k_y = \pi$ and $k_x = \pi, k_y = 0$. Finally, the gap also closes at $M = 8B$ and $k_x = k_y = \pi$. Thus, we conclude that lattice model has more topological phases, than its continuum limit.

4.3 Numerical calculation of Chern number

In this section, we would like to present a possible way of numerical computation of Chern number on a lattice. From the first sight, this problem seems to be straightforward. Chern number is defined as an integral of Berry curvature over the Brillouin zone:

$$C = \frac{1}{2\pi} \int dS\mathcal{F}, \tag{4.6}$$

and to compute it on a lattice, we have to discretize it. This, generally, can be problematic: for example, if our lattice size is Δk, then Berry connection can be computed on a lattice with the accuracy $O(\Delta k)$, but when we compute Berry curvature, we have to divide the variation of Berry connection by Δk again, which can lead to large uncertainties.

In this section we present the proper way [73, 74] of discretizing the integral (4.6), which empirically has small uncertainties. The method is inspired by lattice gauge theory, which we briefly revise here.

Berry connection is a vector field, which describes evolution of wavefunction along a given contour. It describes, how wavefunction is varied under infinitely small shifts:

$$-i\vec{\mathcal{A}}(k)d\vec{k} = \langle\psi(\vec{k})|\psi(\vec{k}+d\vec{k})\rangle - \langle\psi(\vec{k})|\psi(\vec{k})\rangle.$$

In the case of finite shifts, i.e. on a lattice, this equation can be replaced by:

$$\langle\psi(\vec{k})|\psi(\vec{k}+\Delta\vec{k})\rangle = e^{-i\int\limits_0^{\Delta k}\vec{\mathcal{A}}(k)d\vec{k}}. \tag{4.7}$$

We are assuming here, that the wavefunction is normalized: $\langle\psi(\vec{k})|\psi(\vec{k})\rangle = 1$.

Berry curvature can be defined by considering integral of Berry connection along a closed contour. For example, we can consider a small square with the sides $\Delta k_x, \Delta k_y$, and in such case, the wave-

function will evolve by a factor of:

$$\exp\left(-i\int_0^{\Delta k_x}\mathcal{A}_x(k_x,0)dk_x - i\int_0^{\Delta k_y}\mathcal{A}_y(\Delta k_x,k_y)dk_y \right.$$
$$\left. +i\int_0^{\Delta k_x}\mathcal{A}_x(k_x,\Delta k_y)dk_x + i\int_0^{\Delta y}\mathcal{A}_y(0,k_y)dk_y\right)$$

It is easy to check, that in the continuum limit, when Δk_x, Δk_y become infinitely small, this integral gets reduced to the integral of Berry curvature over the small square:

$$\exp\left(-i\mathcal{F}_{xy}\Delta k_x\Delta k_y\right) \tag{4.8}$$

Now we have to construct the numerical method, which makes it possible to compute Chern number in a lattice model. We do it, by implementing the equations (4.7 - 4.8). Suppose, we have a lattice model of fermions, which, for example, can be a model described by the Hamiltonian (4.1). To perform the numerical computation, we have to discretize the momentum. After doing it, we obtain a grid $(k_x(i), k_y(j))$. Then, we compute matrix elements, similarly to the Eq. 4.7:

$$\begin{aligned}
A_1 &= \langle\psi(k_x,k_y)|\psi(k_x+\Delta k_x,k_y)\rangle,\\
A_2 &= \langle\psi(k_x+\Delta k_x,k_y)|\psi(k_x+\Delta k_x,k_y+\Delta k_y)\rangle,\\
A_3 &= \langle\psi(k_x+\Delta k_x,k_y+\Delta k_y)|\psi(k_x+\Delta k_x,k_y+\Delta k_y)\rangle,\\
A_4 &= \langle\psi(k_x,k_y+\Delta k_y)|\psi(k_x+\Delta k_x,k_y)\rangle.
\end{aligned}$$

After it, we compute lattice approximation of the Berry curvature as:

$$\Delta\mathcal{F}_{xy} = \mathrm{Im}\log(A_1A_2A_3A_4),$$

and then obtain the approximate Chern number by summing it over the grid:

$$C = \frac{1}{2\pi}\sum_{k_x,K_y}\Delta\mathcal{F}_{xy}$$

We introduced here imaginary part of the logarithm of matrix elements to select the imaginary part under the exponent in Eq. (4.7):

strictly speaking, the matrix element also has a real part, which has a higher order of Δk, and which we are not interested.

We checked explicitly, that this method converges very quickly: it gives a very good approximation for the lattice size of just about $\sim 20 \times 20$ sites.

4.4 Numerical computation of surface states

In this section, we would like to demonstrate, that the lattice model can be used to compute numerically energy spectrum, and, particularly, surface states. As an example, let us consider the model (4.1).

In Sec. 3.3, we discussed, that pure momentum representation can only be used to analyze bulk properties of a given model. To analyze the surface properties, and in particular to find the surface states, it is essential to consider model in coordinate representation. On the other hand, the model (4.1) is, in fact, a lattice model, i.e. it corresponds to discretized coordinates. We can write such discrete coordinate representation in x direction, while leaving momentum representation in y direction. In other words, we perform Fourier-transformation of the model (4.1) in x direction. If we numerate the lattice sites by indices i, j, this is equivalent to the replacement:

$$\begin{aligned} 1 &\rightarrow \delta_{i,j}, \\ \cos(k_x) &\rightarrow \frac{\delta_{i+1,j} + \delta_{i,j+1}}{2}, \\ \sin(k_x) &\rightarrow \frac{\delta_{i+1,j} - \delta_{i,j+1}}{2i}. \end{aligned}$$

Thus, we can write the model Hamiltonian in coordinate representation as:

$$H = \mathcal{M}\delta_{i,j} + \mathcal{T}\delta_{i+1,j} + \mathcal{T}^{+}\delta_{i,j+1}. \tag{4.9}$$

We are assuming here, that since a Hamiltonian is a Hermit operator, its matrix elements in front of $\delta_{i+1,j}$ and $\delta_{i,j+1}$ have to be Hermit conjugate to each other. In the case of the model with the Hamiltonian (4.1), the matrix elements have the form:

$$\begin{aligned} \mathcal{M} &= \sigma_y k_y + \sigma_z (M - 2B(2 - \cos k_y)), \\ \mathcal{T} &= \frac{\sigma_x}{2i} + \sigma_z B. \end{aligned}$$

Now we can imagine, that our sample is finite in the x direction - we need it to find the surface states. In other words, we assume, that the indices i, j run through a finite range of values, e.g. from 1 to N. In this case, we can write the Hamiltonian (4.9) as a matrix in coordinate space:

$$H = \begin{pmatrix} \mathcal{M} & \mathcal{T}^+ & 0 & \dots & 0 \\ \mathcal{T} & \mathcal{M} & \mathcal{T}^+ & \dots & 0 \\ 0 & \mathcal{T} & \mathcal{M} & & 0 \\ \vdots & & & & \vdots \\ 0 & \dots & & \mathcal{T} & \mathcal{M} \end{pmatrix} \tag{4.10}$$

We remind, that, in this Hamiltonian, each element $\mathcal{M}, \mathcal{T}$ is, in addition, a matrix in momentum space.

To compute the eigenstates of this Hamiltonian, we need to code explicitly the Eq.(4.10), and then to diagonalize it numerically. This method is called *exact diagonalization*, because it is exact after placing the model on the lattice, and does not involve any further approximations, contrary to other numerical methods, such as e.g. DMRG.

Once we performed the diagonalization, we need to split between the bulk and surface states. We find both kinds of states as eigenvectors of the Hamiltonian (4.10), but the difference between two of them is that surface states are localized on a surface: on a large lattice, only a few components of the eigenvectors are significantly different from zero, whereas others are very small. In contrast, bulk states are distributed in a bulk, i.e. many of their components within the whole range of coordinates have magnitude of roughly the same order.

If an eigenvector has components v_i, we can distinguish, whether it is a bulk, or a surface state by computing *participation ratio*:

$$\sum_i v_i^4.$$

For a normalized bulk state with total N components, each component has roughly an order $1/\sqrt{N}$, and thus participation ratio has an order of $1/N$. In contrast, a surface state has a few components of order 1, and therefore its participation ratio has also an order of 1 . Thus, bulk and surface states can be distinguished from each other by computing their participation ratio.

Finally, for surface states, it may be of interest to distinguish, whether they are localized on the left, or on the right edge. This can be done very easily: one just has to take a certain number of components (e.g. $N/3$) on the left, and the same amount of components on the right, and to compare their contribution to the norm.

Chapter 5

More complicated examples of topological materials

5.1 Double Weyl metal

In this section, we consider a slight modification of a Weyl metal described in Sec. 3.5 - a double Weyl metal. Its difference from a simple Weyl metal is that it contains Weyl points with topological charge ± 2 (as we discussed before, topological charge of conventional Weyl points is equal to ± 1). As previously, we can write the simplest Hamiltonian of a double Weyl metal, which contains just one pair of the Weyl points. It happens to be quite similar to the model studied in the Sec. 3.5:

$$H = \begin{pmatrix} M(k_z) - B(k_x^2 + k_y^2) & (k_x - ik_y)^2 \\ (k_x + ik_y)^2 & -M(k_z) + B(k_x^2 + k_y^2). \end{pmatrix}. \quad (5.1)$$

The main difference from simple Weyl metal is that the non-diagonal terms are quadratic over momentum, in contrast to the linear terms in the former. As previously, the Weyl points have monopole charge, and, because of that, they cannot be gapped out by an arbitrary perturbation. However, there, in principle, exists a perturbation, which can destroy the double Weyl points without breaking the monopole charge - that is a perturbation, which splits each double Weyl point into to simple Weyl points with charge ± 1. Thus, to create a double Weyl metal, we need an additional protection from splitting.

It happens, that such protection can arise from discrete rotational

symmetry. More precisely, in the Eq. (5.1), we are assuming, that the double Weyl points are located along z axis. Now let us suppose, that the solid with the double Weyl points possesses rotational symmetry along the z axis [1]. From the basics of crystallography, it is known, that rotational symmetry in a crystal is always discrete, and it can be only $2, 3, 4, 6$ -fold. Let us also suppose, that, along the z axis, i.e. at $k_x = k_y = 0$, eigenstates of the Hamiltonian (5.1) are also eigenvectors of the rotational symmetry operator, and their eigenvalues are equal to $J_{A,B}$. Obviously, along the z axis, the Hamiltonian (5.1) is diagonal, but suppose, that we added to it a non-diagonal perturbation Δ, thus writing it as:

$$H_0 = \begin{pmatrix} m & \Delta \\ \Delta & -m \end{pmatrix}.$$

Now let us transform it under the rotational symmetry:

$$H_0 \to \begin{pmatrix} e^{-iJ_a} & 0 \\ 0 & e^{-iJ_b} \end{pmatrix} \begin{pmatrix} m & \Delta \\ \Delta & -m \end{pmatrix} \begin{pmatrix} e^{iJ_a} & 0 \\ 0 & e^{iJ_b} \end{pmatrix} = \begin{pmatrix} m & \Delta e^{-i(J_a - J_b)} \\ \Delta e^{i(J_a - J_b)} & -m \end{pmatrix}.$$

From the last equation, it is evident that, at $J_a \neq J_b$, such non-diagonal term would break the rotational symmetry. Thus, we arrive to our conclusion: double Weyl metal can be realized, if it is protected by discrete rotational symmetry, i.e. its eigenstates along the rotation axis are rotational eigenvectors with different eigenvalues.

As we mentioned, while discussing simple Weyl metals, m entering the Hamiltonian (in our case 5.1), is a function of k_z, which is positive between the Weyl points, and negative outside. The Weyl points exist, where m changes its sign, i.e. becomes equal to zero. For this reason, it is convenient to view Weyl metal as a 'stack' of $2D$ topological insulators in momentum space, i.e. we consider the Hamiltonian for a fixed k_z as effectively two-dimensional Hamiltonian. In the next subsections, we compute Chern number in the model (5.1) at fixed k_z, to verify that its Weyl points, indeed have charge ± 2, and we also compute its surface states.

[1] Strictly speaking, the Hamiltonians for both simple 3.15 and double Weyl metals 5.1 are invariant under continuous rotational symmetry along z axis. However, this symmetry can, in principle, be violated by higher-order corrections to the Hamiltonians, which, as we know, do not affect the Weyl points

5.1.1 Chern number in double Weyl metal

In this subsection, we compute Chern number in model (5.1) at fixed k_z. Its derivation is very similar to the case of simple Weyl metal, discussed in Sec. (4.2).

If we formally try to compute the Chern number, as an integral of Berry curvature, in the continuum model (5.1), i.e. without placing it on the lattice, we obtain:

$$C = \frac{1}{2\pi}\int d^2k \mathcal{F}_{xy} = \frac{B}{\sqrt{1+B^2}} + \text{sign}(M).$$

We can see, that the Chern number changes by 2 at the point, where M changes sign, but in general it is not integer. Thus, the continuum model makes it possible to correctly find the point of phase transition, but does not make it possible to describe each topological phase.

If we place the model on the lattice, our Hamiltonian can be written as a linear superposition of Pauli matrices: $H = d_i\sigma_i$, with the coefficients equal to:

$$\begin{aligned} d_1 &= 2(\cos(k_y) - \cos(k_x)), \\ d_2 &= 2\sin(k_x)\sin(k_y), \\ d_3 &= M - 2B(2 - \cos(k_x) - \cos(k_y)). \end{aligned}$$

As in the case of usual Weyl metal, we introduced here quadratic corrections to the M term, to remove copies of the Weyl point at the edges of the Brillouin zone.

If we perform the same calculation as in the Sec. (4.2), we obtain that there are three possible cases with different behavior of the Berry connection $\mathcal{A}$:

$M > 8B$ In this case d_3 is positive everywhere. Therefore, $\vec{\mathcal{A}}$ is well-defined and periodic everywhere, which results in $C = 0$.

$0 < M < 8B$ In this range of points $\vec{\mathcal{A}}$ has singularities at $(k_x, k_y) = (\pm\pi, \pm\pi), (\pm\pi, \mp\pi)$. Therefore, the integral over the boundary of the BZ can be transformed to the integral around the point (π, π), as it is shown on the picture:

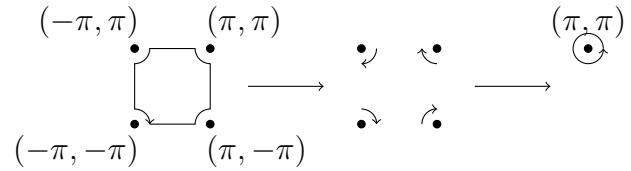

The radius of the contour of integration can be taken infinitely small, therefore we can expand the momentum around the the singular point: $k_{x,y} = \pi + p_{x,y}$ and, after that, rewrite it in polar "coordinates": $p_x \pm ip_y = pe^{\pm i\phi}$. After using these notations, we can obtain $\vec{\mathcal{A}}_\phi = -2$, which results in $C = 2$.

$m < 0$ In this case, the Brillouin zone contains two singular points: $(k_x, k_y) = (\pi, \pi)$ and $(0, 0$, therefore the Chern number has to be written as an integral over two contours:

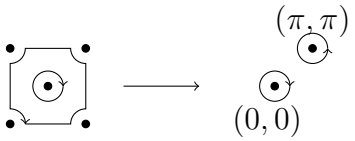

By using the same method as previously, one can check that the contributions from these two points exactly cancel each other, which means that the total Chern number is zero.

Summarizing our results, we obtain that the Chern number is equal to 2 in the range $0 < M < 8B$, and zero otherwise. This is consistent with the fact, that, in the Hamiltonian (5.1), the gap closes at the points $M = 0$ and $M = 8B$.

5.1.2 Surface states

In this subsection, we present the structure of surface states in the model (5.1). Since, in the range $0 < M < 8B$, Chern number is equal to 2, we expect two surface states of the same handedness on each surface. To compute them explicitly, we follow the same method, as in Sec. 3.3.

As in the case of usual Weyl Hamiltonian, we consider our model in the half-space $x > 0$ and look for the solution Ψ satisfying the boundary conditions $\Psi\,|_{x=0} = 0$ and $\Psi\,|_{x\to\infty} = 0$. This implies that the eigenstate of the Hamiltonian has to have the form:

$$\Psi = \left(e^{-\lambda_1 x} - e^{-\lambda_2 x}\right)\psi(k_y, \lambda_1, \lambda_2), \tag{5.2}$$

which, in turn, implies the condition:

$$(H(\lambda_1) - H(\lambda_2))\,\Psi = 0.$$

By applying this condition to the Hamiltonian (5.1), we obtain the constraint on $\lambda_1 + \lambda_2$ and the form of eigenvector:

$$\frac{\lambda_1 + \lambda_2}{2} = \frac{|k_y|}{\sqrt{1+B^2}}$$
$$\Psi = \begin{pmatrix} \frac{\lambda_1+\lambda_2}{2} - k_y \\ B\frac{(\lambda_2+\lambda_2)}{2} \end{pmatrix}$$

This state is an eigenstate of the Hamiltonian (5.1) if $\lambda_{1,2}$ has an expression:

$$\lambda_{1,2} = \frac{|k_y| \pm \sqrt{B(k_y^2 B - M)}}{\sqrt{1+B^2}},$$

which, in turn, means that the state has the form:

$$\Psi = \begin{pmatrix} 1 - \mathrm{sign}(k_y)\sqrt{1+B^2} \\ B \end{pmatrix}$$

and its energy is:

$$E = \mathrm{sign}(k_y)\frac{(2k_y^2 B - M)}{\sqrt{1+B^2}}.$$

One can try to analyze the range of the parameters M, B, k_y, when the solution is well-defined. Indeed, the solution has to satisfy the conditions $\mathcal{R}e\lambda_{1,2} > 0$, which implies that the solution does *not* exist, when $B(k_y^2 B - M) > k_y^2$, which, in turn, means that the solution is *not* well-defined when:

$$\begin{cases} |B| > 1 \\ k_y^2 > \dfrac{mB}{B^2-1} \end{cases}$$
$$\begin{cases} |B| < 1 \\ k_y^2 < \dfrac{-mB}{1-B^2} \end{cases}$$

These conditions result the energy spectrum have one of the forms showed on the Fig. 5.1. The edge spectrum always contains two

branches, one of which emerges from the valence band and the other emerges from the conduction band. One can also see that configurations at M having different signs are topologically distinct, i.e. they cannot be smoothly deformed one into another. If one asks, whether the edge modes are topologically stable, the answer is positive in the cases of $M > 0$, $B > 1$ and $M < 0$, $B < -1$: the states are topologically stable because they connect bands separated by energy gap. However, the answer is not clear in the other cases: our analysis of the model shows that the arcs can emerge from one band and not cross the other, but strictly speaking, the picture may change if one includes higher powers of momentum in the Hamiltonian (5.1). Indeed, the corrections can shift the arc to make it either topological (connect two bands) or non-topological (connect two points within one band).

Thus, we conclude that the continuum model makes it possible to determine the number of surface states, their handedness, and the points, where they emerge. However, the continuum model does not make it possible to determine, whether the surface states are actually topological, i.e. if they connect the different bands. For this reason, we also analyze our model in a different way. Specifically, we use the results of the Ref. [75] about general conditions on existence of surface states in a lattice model. When we use these conditions, we write them separately in the cases of small and large B. Also, to get more clear picture, we compute the surface states numerically on the lattice model (5.12), using the method described in Sec. 4.4. Our results look as following:

$|B| < 1$ In this case, the surface states must satisfy the condition:

$$-1 + \frac{B(M - 8B)}{2(1 - B^2)} < \cos(k_y) < 1 + \frac{MB}{2(1 - B^2)}, \qquad (5.3)$$

which at positive B does not constrain k_y, if $0 < M < 8B$. In other words, in the range of parameters where the Chern number is non-zero, edge state exists at any k_y. By computing them numerically (see Fig. 5.2a), one can see that there are precisely two edge states at each side of the sample, which are topological and cross the energy gap, thus confirming that the number of topological edge states is equal to the Chern number. At $M = 0$ or $M = 8B$ the bulk gap closes, and the topological phase transition occurs. Outside of the range of parameters

with non-zero Chern number, the edge states still may exist. However, numerical calculation demonstrates that they are no more topological, which is again consistent with the fact that the Chern number is zero. An example of such state is shown on the Fig. 5.2b. These states disappear at $M = -\frac{4(1-B^2)}{B}$ and $M = 8B + \frac{4(1-B^2)}{B}$, and since they are non-topological, they disappear without phase transition.

$|B| > 1$ In this case, the edge states exist if

$$\frac{2B^2 - 2 - MB}{2(B^2-1)} < \cos(k_y) < \frac{6B^2 + 2 - MB}{2(B^2-1)}.$$

This implies that, in the "topological" range of parameters, edge states exist at any k_y, when:

$$\frac{4(B^2-1)}{B} < M < \frac{4(B^2+1)}{B}.$$

Outside this range, the topological edge states still connect two bands, but they range not through all values of k_y (see Fig. 5.2c). After passing the "critical values" $M = 0, 8B$, the edge states disappear.

Thus, we showed that the lattice model (5.12) has two regimes: topological at $0 < M < 8B$, and non-topological otherwise. In the topological regime, the model's Chern number is 2, and it always possesses two topological edge states connecting two bands through the gap, which is consistent with Laughlin argument (see Sec.3.2). In the non-topological regime, the model's Chern number is zero. It may not possess edge states, or it may possess edge states, which are not topological and do not pass through the energy gap, thus having no effect on Hall conductivity, if the Fermi level lies within the gap.

We note, that the structure of edge states in the lattice model is consistent with the continuum model (Eq. 5.1), assuming that the latter holds only at small k_y. In conclusion, we obtain that double Weyl point separates areas with trivial and non-trivial topological properties, and analysis near the WP makes it possible to show topological phase transition between them. However, to establish the topological nature of each area, it is not sufficient to analize

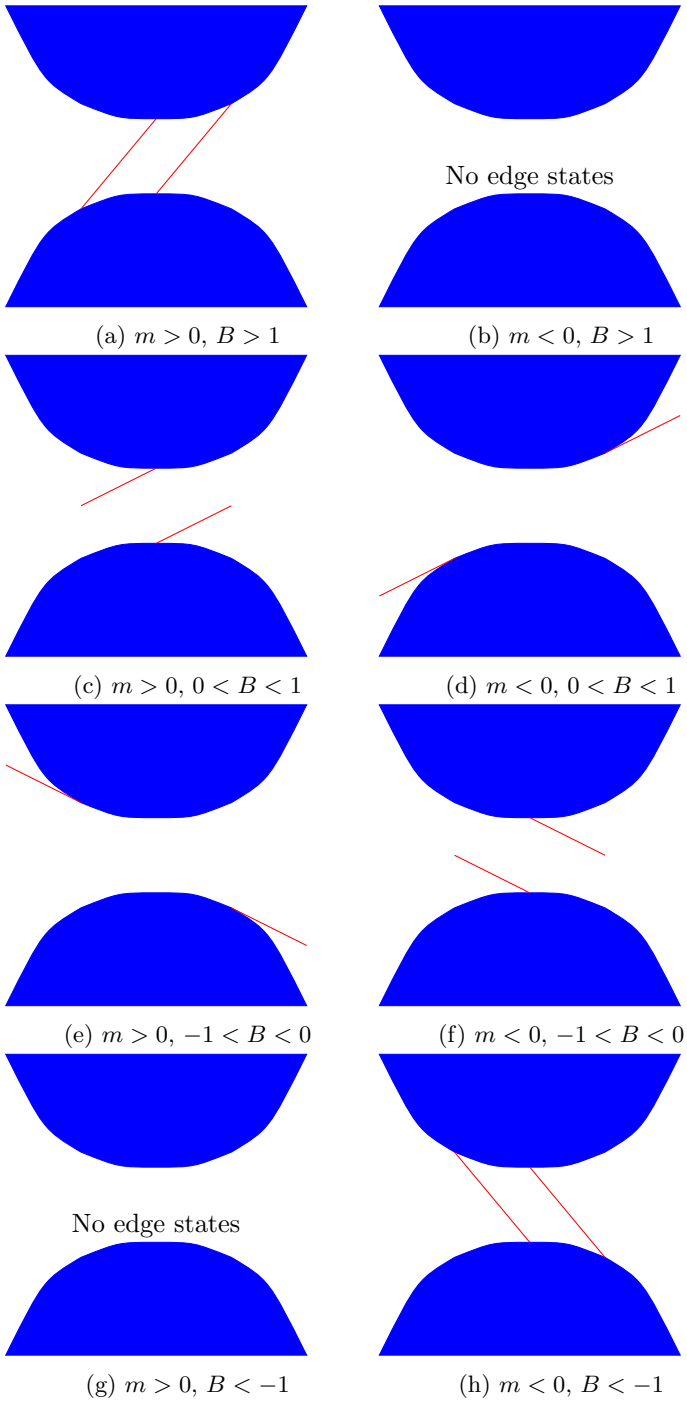

Figure 5.1: Sketches of possible energy spectra of the Hamiltonian 5.1. Bulk states are showed by blue, and edge states at $x > 0$ are showed by red.

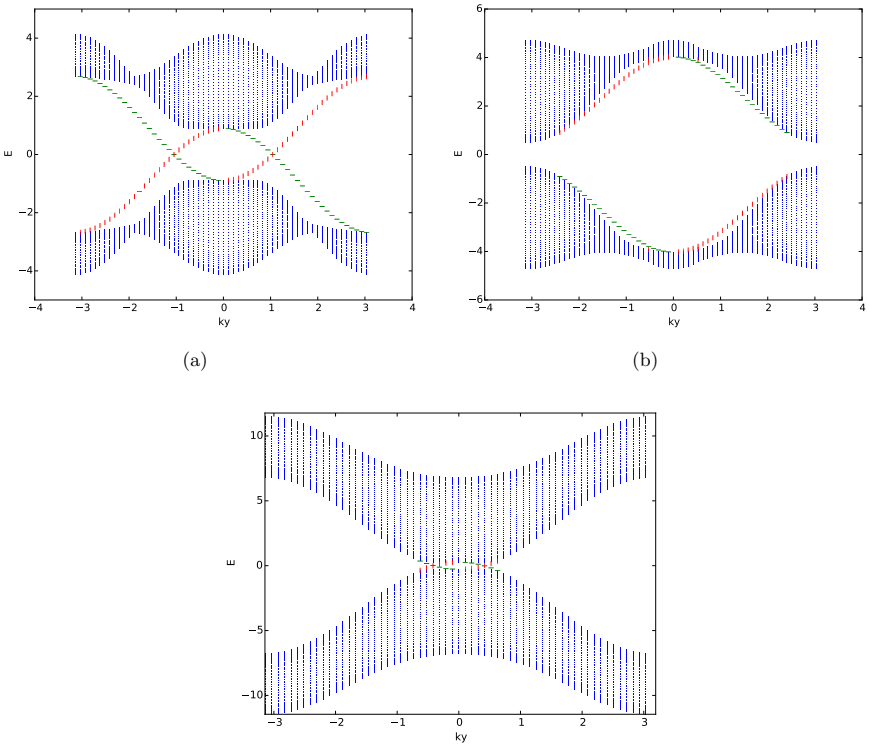

Figure 5.2: An example of the band structure with topological (left) and non-topological (right) edge states. The parameters are: $m = 1.0$, $B = 0.5$ (top left); $m = 4.5$, $B = 0.5$ (top right); $m = 0.5$, $B = 1.5$ (bottom left).

only surrounding of the WP: one has to take into account the full periodic BZ.

5.2 Luttinger model

In this section, we consider a more complicated example, where we can compute surface states analytically. We consider *Luttinger model*, which was introduced a long time ago [44] in the context of physics of semiconductors. The Luttinger model is quite general, and it is used to describe electrons in cubic lattices. Specifically, it takes into account three symmetries: time reversal, inversion and cubic crystalline symmetry. The former two of them result in double degeneracy. Luttinger model describes two different bands: conduction, and valence, and thus it has in total, four degrees of freedom. In general, the conduction and valence band can be decoupled from each other, but the purpose of Luttinger model is to include irreducible representations of the cubic group. It turns out [44], that the most general quadratic Hamiltonian satisfying these symmetries contains just a few kinds of terms:

$$\begin{aligned} H &= \frac{\gamma_1 k^2}{2m} + E\left(k_y k_z \Gamma_1 + k_x k_z \Gamma_2 + k_x k_y \Gamma_3\right) \\ &\quad + C\left((k_x^2 - k_y^2)\Gamma_4 + \frac{1}{\sqrt{3}}(2k_z^2 - k_x^2 - k_y^2)\Gamma_5\right). \end{aligned} \tag{5.4}$$

This Hamiltonian describes an electron with spin 3/2, For this reason, it is convenient to introduce spin operators:

$$\begin{aligned} S_x &= \begin{pmatrix} 0 & \sqrt{3}/2 & 0 & 0 \\ \sqrt{3}/2 & 0 & 1 & 0 \\ 0 & 1 & 0 & \sqrt{3}/2 \\ 0 & 0 & \sqrt{3}/2 & 0 \end{pmatrix}, \\ S_y &= \begin{pmatrix} 0 & -i\sqrt{3}/2 & 0 & 0 \\ i\sqrt{3}/2 & 0 & -i & 0 \\ 0 & i & 0 & -i\sqrt{3}/2 \\ 0 & 0 & i\sqrt{3}/2 & 0 \end{pmatrix}, \\ S_z &= \begin{pmatrix} 3/2 & 0 & 0 & 0 \\ 0 & 1/2 & 0 & 0 \\ 0 & 0 & -1/2 & 0 \\ 0 & 0 & 0 & -3/2 \end{pmatrix}, \end{aligned} \tag{5.5}$$

and write the Γ matrices [46] in terms of them:

$$\begin{aligned}\Gamma_1 &= \frac{1}{\sqrt{3}}(S_yS_z + S_zS_y),\\ \Gamma_2 &= \frac{1}{\sqrt{3}}(S_zS_x + S_xS_z),\\ \Gamma_3 &= \frac{1}{\sqrt{3}}(S_xS_y + S_yS_x),\end{aligned}$$

$$\begin{aligned}\Gamma_4 &= \frac{1}{\sqrt{3}}(S_x^2 - S_y^2),\\ \Gamma_5 &= S_z^2 - \frac{5}{4}.\end{aligned}$$

One can check, that the Γ matrices written is this way, indeed satisfy the correct commutation relations $\{\Gamma_i, \Gamma_j\} = 2\delta_{ij}$. This fact makes it possible to immediately write the energy spectrum of the Luttinger model :

$$\mathcal{E} = \frac{\gamma_1 k^2}{2m} \pm \sqrt{\frac{4C^2}{3}\left(k_x^4 + k_y^4 + k_z^4\right) + \left(E^2 - \frac{4C^2}{3}\right)\left(k_y^2k_z^2 + k_x^2k_z^2 + k_x^2k_y^2\right)}.$$

Due to time reversal and inversion symmetries, each band is double degenerate, and thus the total spectrum of the four component model contains two energy levels.

In the special case $2C = \pm E$, the Luttinger model becomes isotropic: it is invariant not only under cubic symmetry, but also under continuous rotational symmetry. Two cases of $\pm$ signs are equivalent: they are obtained from each other through change of signs of the Γ matrices, and therefore, they can be canonically transformed into each other. In the isotropic Luttinger model, it is convenient to switch the notations by introducing:

$$\gamma_2 = \frac{2Cm}{\sqrt{3}}.$$

This makes it possible to write the Luttinger Hamiltonian as:

$$H = \frac{\gamma_1 k^2}{2m} + \frac{\gamma_2}{m} d_a \Gamma_a, \tag{5.6}$$

where d_a are five d-wave functions in momentum space [46]:

$$\begin{aligned} d_1 &= \pm\sqrt{3}k_y k_z, \\ d_2 &= \pm\sqrt{3}k_x k_z, \\ d_3 &= \pm\sqrt{3}k_x k_y, \\ d_4 &= \frac{\sqrt{3}}{2}(k_x^2 - k_y^2), \\ d_5 &= \frac{1}{2}(2k_z^2 - k_x - k_y^2). \end{aligned}$$

The expression for its energies becomes very simple:

$$\mathcal{E} = \frac{(\gamma_1 \pm 2\gamma_2)k^2}{2m}. \tag{5.7}$$

Thus, the Luttinger model contains two double degenerate bands, which both have quadratic dispersion. The bands 'touch' each other at the point $k = 0$. In the case $\gamma_1 > 2\gamma_2$, both bands disperse in the same direction, and the band with the $-$ sign has larger effective mass. For this reason, the lower band is sometimes called as 'heavy hole', whereas the higher is called 'light hole'.

5.2.1 Luttinger model in magnetic field

It is interesting to study Luttinger model in the presence of Zeeman magnetic field [48]. Physically, this situation may occur, for example, in magnetically doped semiconductors [45]. More recently, there were attempts to use Luttinger model to describe other materials, such as e.g. pyrochlore iridates [47, 49].

The simplest way to study the effect of magnetic field on the Luttinger model, is to introduce Zeeman field in z direction:

$$H_1 = -bS_z. \tag{5.8}$$

Here S_z is a spin matrix in z direction, as it was introduced in Eq. (5.5). Evidently, such Zeeman field breaks time reversal symmetry, and thus splits double degeneracy of the bands. General analytical solution of the total Hamiltonian containing both the terms (5.4) and (5.8) is unknown, but it can be easily solved in the special case along the z direction, i.e. at $k_x = k_y = 0$. Indeed, in the latter case,

the Hamiltonian just becomes diagonal:

$$H(k_x = k_y = 0) = \begin{pmatrix} \frac{(\gamma_1+2\gamma_2)k_z^2}{2m} - \frac{3b}{2} & 0 & 0 & 0 \\ 0 & \frac{(\gamma_1-2\gamma_2)k_z^2}{2m} - \frac{b}{2} & 0 & 0 \\ 0 & 0 & \frac{(\gamma_1-2\gamma_2)k_z^2}{2m} + \frac{b}{2} & 0 \\ 0 & 0 & 0 & \frac{(\gamma_1+2\gamma_2)k_z^2}{2m} + \frac{3b}{2} \end{pmatrix}. \tag{5.9}$$

Schematic plot of its bands is shown on the Fig. 5.3. Indeed, there are four non-degenerate bands, which cross each other. By computing perturbation to the Hamiltonian (5.9) at small transverse momenta, one can see, that these crossings are, indeed, Weyl points. In total, the model has four Weyl points: two of them are simple, and the other two are double. We checked the Chern numbers of each band by computing them numerically. They proved to be consistent with the charges of the Weyl points, and their values are also shown on the Fig. 5.3.

It is interesting to note, that our model model has two regimes, which depend on the relative sign of C and E in the Eq. (5.4). In both of them, the simple (or linear) Weyl points have the same charges, but the double (or quadratic) Weyl points have the charges of opposite signs.

5.2.2 Surface states in Luttinger model

In this section, we compute surface states in the Luttinger model. As we mentioned previously, the Luttinger model (without magnetic field) possesses two double degenerate bands with the spectrum satisfying the Eq. 5.7. If we consider the simplest example, when γ_1 is positive, there are two possible cases. In the case $\gamma_1 > 2|\gamma_2|$, both bands disperse in the same direction, whereas in the case $\gamma_1 < 2|\gamma_2|$, the bands disperse in the opposite directions. Since, due to double degeneracy, the bands in free Luttinger model do not have nontrivial Chern invariants, we expect the surface states to be nontopological. However, we find that they exist exactly in the case, when the bands disperse in the opposite directions. We think that simple way of explaining it, is that surface states connect the gap,

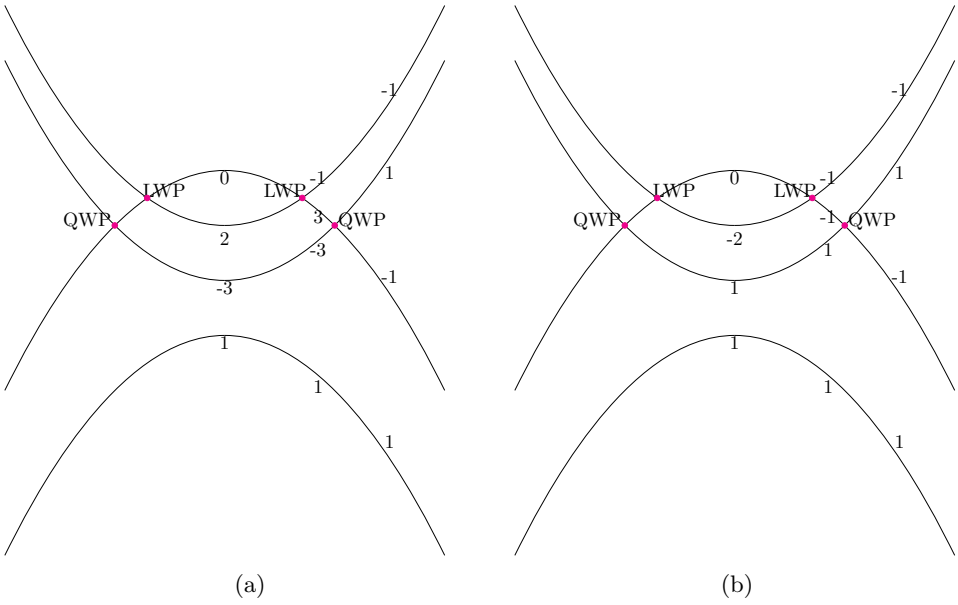

Figure 5.3: Band structure of the Luttinger model with Zeeman field: schematic view of the bands at $k_x = k_y = 0$ and $C = -\frac{\sqrt{3}}{4}$, $b = 0.5$. $E = -\sqrt{3}/2$ (left) and $E = \sqrt{3}/2$ (right)). The numbers shown on the left picture, are Chern numbers of each band.

which exist at $k \neq 0$, when the bands disperse in the opposite directions, whereas in the opposite case, there is no energy gap present.

We managed to compute the surface states in the Luttinger model analytically, by using the method from Sec. 3.3. The calculation is very long, but we just mention, that we performed it by making change of variables:

$$\begin{aligned} x &= \sqrt{\frac{2\gamma_2 - \gamma_1}{2\gamma_2 + \gamma_1}}, \\ y &= \frac{k_y}{\sqrt{k_y^2 + k_z^2}}, \\ z &= \frac{\gamma_2(k_y^2 + k_z^2)}{m} \\ \mu &= \frac{\lambda}{\sqrt{k_y^2 + k_z^2}}. \end{aligned}$$

After long, but straightforward calculations, we found the following results. The expressions for the surface states (we parametrize them by $\pm$) are:

$$v(\pm) = \frac{1}{2\sqrt{2(x^2+1)}} \begin{pmatrix} i\sqrt{1 \pm y}(2y - \sqrt{3}x \mp 1) \\ \mp\sqrt{1 \mp y}(-2\sqrt{3}y + x \mp \sqrt{3}) \\ i\sqrt{1 \pm y}(2\sqrt{3}y + x \mp \sqrt{3}) \\ \pm\sqrt{1 \mp y}(2y + \sqrt{3}x \pm 1) \end{pmatrix}. \tag{5.10}$$

Their energies are:

$$E_\pm = \frac{k^2\sqrt{3}}{4m}\left(\sqrt{3}\gamma_1 \mp \sqrt{4\gamma_2^2 - \gamma_1^2}\right)$$

and penetration depth parameters λ_1, λ_2 are:

$$\begin{aligned} \lambda_1 &= \frac{\sqrt{k_y^2 + k_z^2}}{2}\left(\sqrt{\frac{3(2\gamma_2 - \gamma_1)}{2\gamma_2 + \gamma_1}} \pm 1\right), \\ \lambda_2 &= \frac{\sqrt{k_y^2 + k_z^2}}{2}\left(\sqrt{\frac{3(2\gamma_2 + \gamma_1)}{2\gamma_2 - \gamma_1}} \mp 1\right). \end{aligned}$$

By analyzing them, one can find that the model has edge states, if $2|\gamma_2| > |\gamma_1|$, i.e. when there exist energy gap between bulk bands. More specifically, there are three cases:

$\gamma_2 < \gamma_1 < 2\gamma_2$ Only $v(+)$ is well-defined and has positive energy.

$-\gamma_2 < \gamma_1 < \gamma_2$ Both $v(\pm)$ are well-defined. $v(+)$ has negative energy and $v(-)$ has positive energy.

$-2\gamma_2 < \gamma_1 < \gamma_2$ Only $v(-)$ is well-defined and its energy is negative.

Thus, we have found, that the Luttinger model has two transitions: one of them is at $\gamma_1 = \pm 2\gamma_2$, where one of the bulk bands changes its curvature, and simultaneously, one surface band appears. The other transition occurs at $\gamma_1 = \pm\gamma_2$, where the second surface band appears as flat. We note, that, to best of our understanding, surface states in the Luttinger model without magnetic field are not topologically protected.

We have also repeated the same calculation numerically on the lattice, and we obtained a very similar picture. We present it on the Fig. 5.4.

Finally, we note that while writing this manuscript, we became aware of the work [76], where surface states in Luttinger model have also been computed. Contrary to our view, that work presented an argument, that the surface states may be topological in a different sense from our reasoning. We are interested in exploring this question further.

5.2.3 Surface states in Luttinger model with magnetic field

In the presence of Zeeman magnetic field, the band structure of the Luttinger model changes. As we discussed in Sec. 5.2.1, there appears four non-degenerate bands, which contain two pairs of Weyl points: one pair has the charge ± 1, and the other ± 2.

In general, at non-zero magnetic field, the energy spectrum cannot be found analytically, and so are the surface states. However, there exists an interesting special case, when the surface states can be found analytically, which is $k_z = 0$. In this special case, the Luttinger Hamiltonian (5.6) decouples into two 2×2 Hamiltonians describing the $S_z = 3/2, -1/2$ and $S_z = 1/2, -3/2$ bands, which

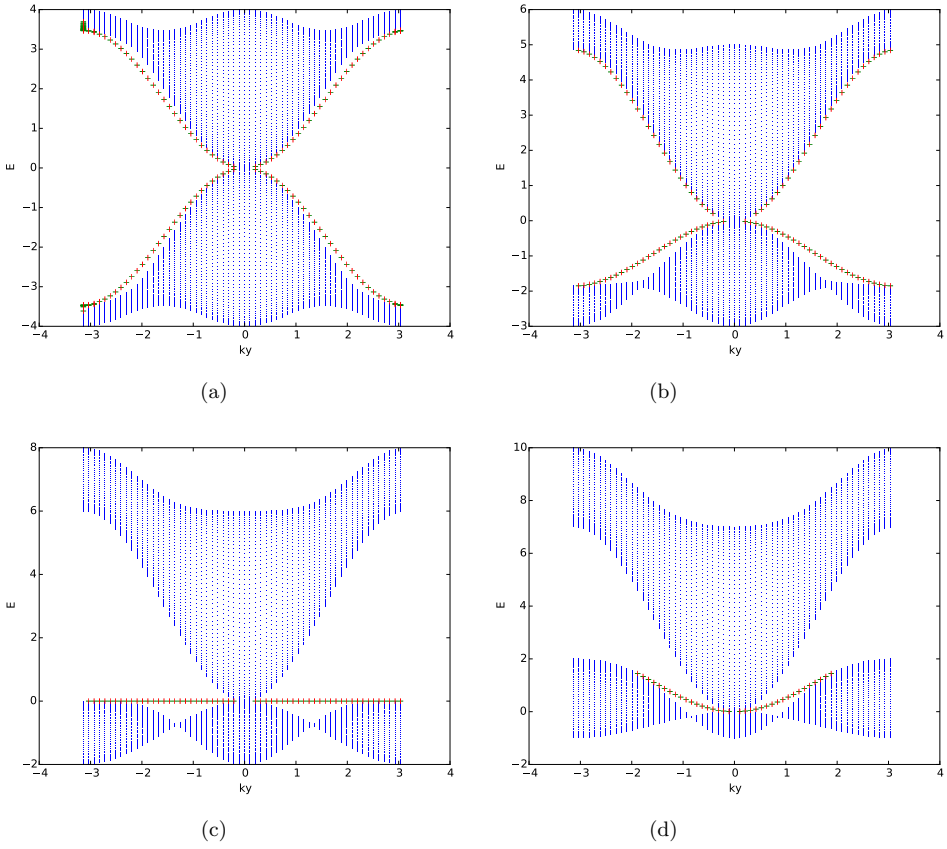

Figure 5.4: Dispersion structure of the Luttinger model at zero magnetic field. The parameters are $\gamma_2 = 1.0$, $m = 1.0$, $k_z = 0.0$. The values of γ_1 are: 0.0 (5.4a); 0.5 (5.4b); 1.0 (5.4c); 1.5 (5.4d).

have the following form:

$$H_{3/2,-1/2} = \frac{\gamma_1 k^2}{2m} - \frac{b}{2}$$
$$+\frac{\gamma_2}{m}\left[(\frac{k_x^2+k_y^2}{2} - \frac{bm}{\gamma_2})\sigma_3 + \frac{\sqrt{3}}{2}(k_y^2-k_x^2)\sigma_x - \sqrt{3}k_xk_y\sigma_y\right],$$
$$H_{1/2,-3/2} = \frac{\gamma_1 k^2}{2m} + \frac{b}{2}$$
$$+\frac{\gamma_2}{m}\left[(-\frac{k_x^2+k_y^2}{2} - \frac{bm}{\gamma_2})\sigma_3 + \frac{\sqrt{3}}{2}(k_y^2-k_x^2)\sigma_x - \sqrt{3}k_xk_y\sigma_y\right].$$

These Hamiltonians can be viewed as "tilted" models of double Weyl points, i.e. models deformed by the term $\frac{\gamma_1 k^2}{2m}$. Their surface states can be found analytically in a similar way to the Sec. 5.1.2.

$H_{1/2,-3/2}$

We start our analysis from the Hamiltonian $H_{1/2,-3/2}$, which has two surface state solutions. The first of them has the form:

$$v(+)\mid_{y=-1} = \begin{pmatrix} x+\sqrt{3} \\ -\sqrt{3}x+1 \end{pmatrix}.$$

Its energy is equal to:

$$E = -\frac{z\sqrt{3}(x+\sqrt{3})(\sqrt{3}x-1)}{2(x^2+1)} - \frac{bx(\sqrt{3}-x)}{1+x^2}$$

and it is *not* well-defined, when

$$\begin{cases} z < -\frac{by(x+\sqrt{3})(\sqrt{3}x-1)}{(\sqrt{3}-x)(\sqrt{3}x+1)} \\ -\frac{1}{\sqrt{3}} < x < \sqrt{3} \end{cases}$$
$$\begin{cases} z > -\frac{by(x+\sqrt{3})(\sqrt{3}x-1)}{(\sqrt{3}-x)(\sqrt{3}x+1)} \\ x > \sqrt{3} \quad \text{or} \quad x < -\frac{1}{\sqrt{3}} \end{cases}$$

The second solution has the form:

$$v(-)\mid_{y=1} = \begin{pmatrix} -x+\sqrt{3} \\ \sqrt{3}x+1 \end{pmatrix},$$

its energy is:

$$E = \frac{z\sqrt{3}(\sqrt{3}x+1)(\sqrt{3}-x)}{2(x^2+1)} + \frac{bx(x+\sqrt{3})}{1+x^2}$$

and it is *not* well-defined, when

$$\begin{cases} z > -\frac{by(x-\sqrt{3})(\sqrt{3}x+1)}{(\sqrt{3}+x)(\sqrt{3}x-1)} \\ -\sqrt{3} < x < \frac{1}{\sqrt{3}} \end{cases}$$
$$\begin{cases} z < -\frac{by(x-\sqrt{3})(\sqrt{3}x+1)}{(\sqrt{3}+x)(\sqrt{3}x-1)} \\ x > \frac{1}{\sqrt{3}} \quad \text{or} \quad x < -\sqrt{3} \end{cases}$$

By analyzing these conditions, one can find that the surface states have the following behavior. In the range $-\gamma_2 < \gamma_1 < \gamma_2$, (i.e. at $1/\sqrt{3} < x < \sqrt{3}$) both solutions are well-defined. The solution at $k_y > 0$ always has positive energy and the solution at $k_y < 0$ always has negative energy. Both energies are positively inclined. In the limit $\gamma_1 \to \gamma_2$, the mode at $k_y > 0$ disappears, but the mode at $k_y < 0$ becomes flat. As γ_1 increases further, the mode at $k_y < 0$ "shrinks" until, at $\gamma_1 = 2\gamma_2$, it disappears. One can find numerically, that the bands have zero CN, and therefore the surface states are expected to be non-topological. This can be confirmed by numerical calculation (since the analytical calculation captures only the behavior at small k_y!), which results are shown on Fig. 5.5.

$H_{3/2,-1/2}$

The Hamiltonian $H_{3/2,-1/2}$ also has two surface state solutions, similarly to $H_{1/2,-3/2}$. The first of them has the form:

$$v(+) \mid_{y=1} = \begin{pmatrix} 1-\sqrt{3}x \\ \sqrt{3}+x \end{pmatrix}$$

and energy

$$E = -\frac{z\sqrt{3}(x+\sqrt{3})(\sqrt{3}x-1)}{2(x^2+1)} + \frac{bx(\sqrt{3}-x)}{x^2+1}.$$

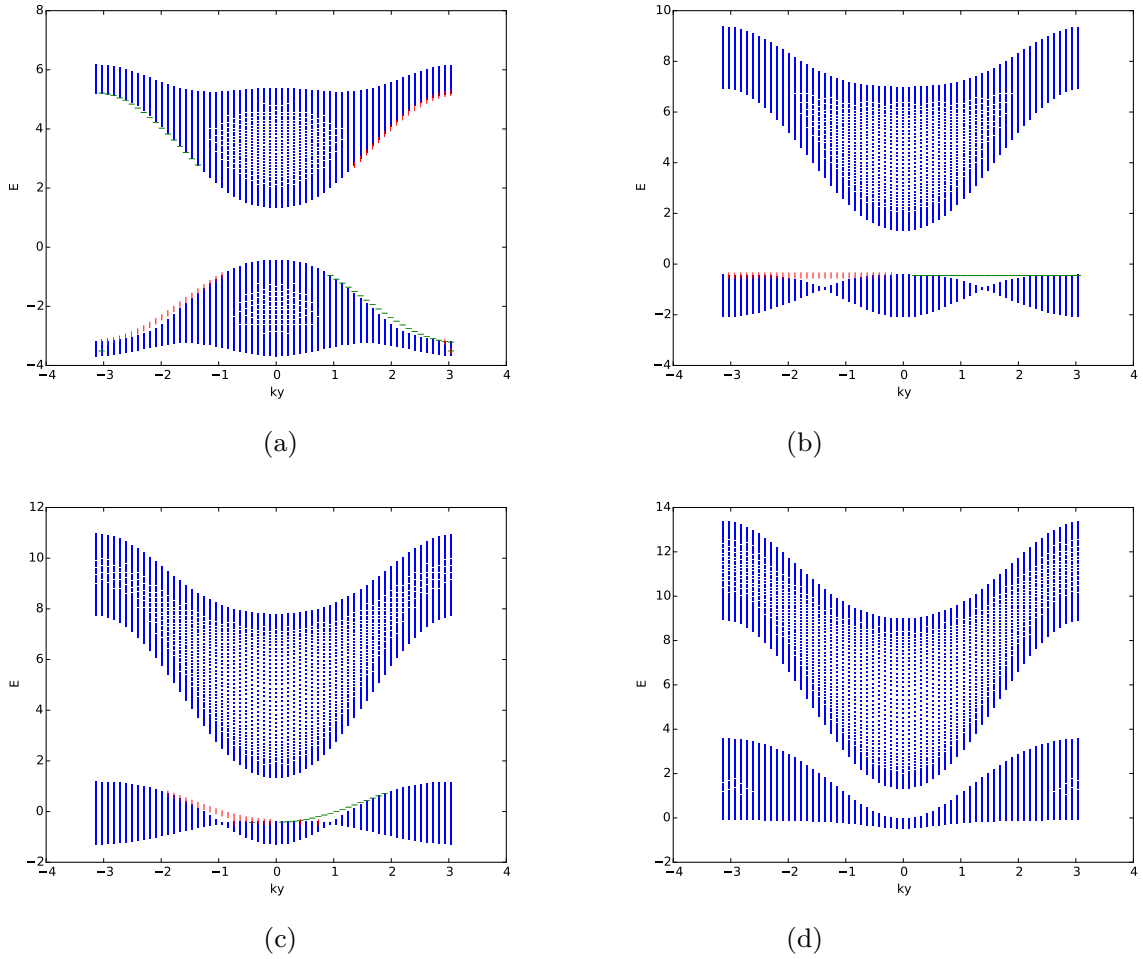

Figure 5.5: A few examples of non-topological edge states of $H_{1/2,-3/2}$. The parameters are $\gamma_2 = 1.0$, $m = 1.0$, $b = 0.9$. The values of γ_1 are: 0.2 (5.5a); 1.0 (5.5b); 1.4 (5.5c); 2.0 (5.5d).

It is not well-defined if:

$$\begin{cases} z < -\frac{b(x+\sqrt{3})(\sqrt{3}x-1)}{(\sqrt{3}-x)(\sqrt{3}x+1)} \\ -\frac{1}{\sqrt{3}} < x < \sqrt{3} \end{cases}$$
$$\begin{cases} z > -\frac{b(x+\sqrt{3})(\sqrt{3}x-1)}{(\sqrt{3}-x)(\sqrt{3}x+1)} \\ x > \sqrt{3} \quad \text{or} \quad x < -\frac{1}{\sqrt{3}} \end{cases}$$

The second solution has the form:

$$v(-) \mid_{y=-1} = \begin{pmatrix} \sqrt{3}x+1 \\ -x+\sqrt{3} \end{pmatrix},$$

energy:

$$E = \frac{z\sqrt{3}(\sqrt{3}x+1)(\sqrt{3}-x)}{2(x^2+1)} - \frac{bx(x+\sqrt{3})}{x^2+1}$$

and it is not well-defined when:

$$\begin{cases} z > \frac{b(x-\sqrt{3})(\sqrt{3}x+1)}{(x+\sqrt{3})(\sqrt{3}x-1)} \\ -\sqrt{3} < x < \frac{1}{\sqrt{3}} \end{cases}$$
$$\begin{cases} z < \frac{b(x-\sqrt{3})(\sqrt{3}x+1)}{(x+\sqrt{3})(\sqrt{3}x-1)} \\ x < -\sqrt{3} \quad \text{or} \quad x > \frac{1}{\sqrt{3}} \end{cases}$$

By analyzing the conditions, when the solutions are well-defined, one can find that their behavior shares similar properties to the previous model. Indeed, at small γ_1, both modes are well-defined in the whole range of z. In the limit $\gamma_1 = \gamma_2$, the mode $v(+) \mid_{y=1}$ forms flat band, and as γ_1 increases further, the range of momenta, where the modes exist, becomes more narrow. At $\gamma_1 = 2\gamma_2$, the edge modes disappear.

However, in contrast to the model, studied in the previous section, this model is topologically non-trivial. Its CN is equal 2, and as one can confirm by the numerical calculations (see Fig. 5.6), its surface modes are topological. Therefore, an important question is: how topologically non-trivial states can disappear under smooth change of one parameter γ_1, given that CN does not change? This question becomes even more interesting if one tries to compute numerically the bulk band structure of the lattice model: the bulk gap does not close, as one can see from Fig. 5.7. The answer is that,

even though the gap in the bulk spectrum does not close, the projected bands still "touch" each other at $\gamma_1 = 2\gamma_2$, and as the modes "shrink" by approaching this limit, they can disappear. Thus we obtain an important physical result: *to "destroy" topological edge states it is not necessary to close bulk gap, it is sufficient to close gap between projected bands*. This result does not contradict Laughlin argument for existence of edge states, because even though the bulk bands are separated from each other, any Fermi level would always cross them. Therefore the system is not insulating, and thus does not require edge states to have non zero anomalous Hall conductivity.

We would like to mention, that, besides $k_z = 0$, we have found another special case, when the surface states in Luttinger model can be found analytically. That is a special condition, when

$$y = \frac{z^2(3-x^2) + b^2x^2}{2\sqrt{3}bxz}.$$

In the latter case, the solution has the form:

$$\begin{pmatrix} i\sqrt{x^2(z+b)^2 - 3z^2}((3-x^2)z - 2bx^2) \\ -\sqrt{3}\sqrt{3z^2 - x^2(z-b)^2}((3-x^2)z - 2bx^2) \\ i\sqrt{3}\sqrt{x^2(z+b)^2 - 3z^2}((3-x^2)z + 2bx^2) \\ -\sqrt{3z^2 - x^2(z-b)^2}((3-x^2)z + 2bx^2) \end{pmatrix},$$

and the penetration depth parameters are:

$$\lambda_{1,2} = \frac{1}{4xz}\left(\sqrt{3}z(x^2+1) \pm \sqrt{4b^2x^4 - z^2(x^2-3)^2}\right).$$

It also has remarkably simple expression for energy

$$E = -\frac{b^2x^2}{2z(x^2+1)} = -\frac{b^2m(2\gamma_2 - \gamma_1)}{8\gamma_2^2(k_y^2 + k_z^2)}.$$

However, we do not know the physical reasons explaining why this solution is special.

Finally, we can find the spectrum (including the surface states) in the Luttinger model numerically by placing it on the lattice, and exploring their evolution at different k_z. We plot numerically computed surface states on the Fig. 5.8. As expected, at $k_z = 0.0$ (see Fig. 5.8a), the plot for the Luttinger model is a superposition of plots for $H_{3/2,-1/2}$ and $H_{1/2,-3/2}$. One can notice that, at

$k_y = 0$, the lowest band of $H_{3/2,-1/2}$ has lower energy than the one of $H_{1/2,-3/2}$, and therefore, the topological states of $H_{3/2,-1/2}$ enter inside the bulk structure of $H_{1/2,-3/2}$. However, as k_z increases, the topological states evolve, so that, sufficiently away from $k_z = 0$, they end at the verge of the bulk band structure (see Fig. 5.8b, 5.8c). The presence of linear Weyl points does not affect the surface states, as one can see from Fig. 5.8d, 5.8e. This is expected, because the linear Weyl points are located inside the bulk spectrum: there is no energy gap in the projected band structure near them. In contrast, after passing through the quadratic Weyl points, the surface states transform from topological to non-topological (see Fig. 5.8f), which is consistent with the fact that, at quadratic Weyl point, two gapped bands touch each other.

Thus, surface state structure of the Luttinger model can be summarized as follows: it has surface states, if there exists a gap between the projected bands. At zero Zeeman field, it may have one or two pairs of surface states, which are not topologically protected. At non-zero Zeeman field, the Luttinger model still has non-topological surface states far away from the Weyl points, but between the quadratic Weyl points, it always has two pairs of topological surface states. This is consistent with the fact that the total CN of the bands lying below the energy gap is 0 outside of the quadratic Weyl points, and 2 between them. The presence of additional linear Weyl point does not affect the topological structure of the surface state spectrum, because in the projected band spectrum, the Weyl points lie inside the bulk gap.

5.3 Transitions between different topological phases

In this section, we briefly describe a few possible ideas about transitions between different topological phases. In the Sec. 3.4, we introduced one well-known example of such transition: transition between normal and topological insulator occurs through gap closing, and thus leads to the formation of a new critical phase, which is a Dirac metal. In this section, we consider examples of phase transitions between different phases involving Weyl metals.

Let us describe one possible example of such transition. Consider Weyl metal with one pair of spatially separated Weyl points. As we discussed previously, Chern number, as an integral over the plane

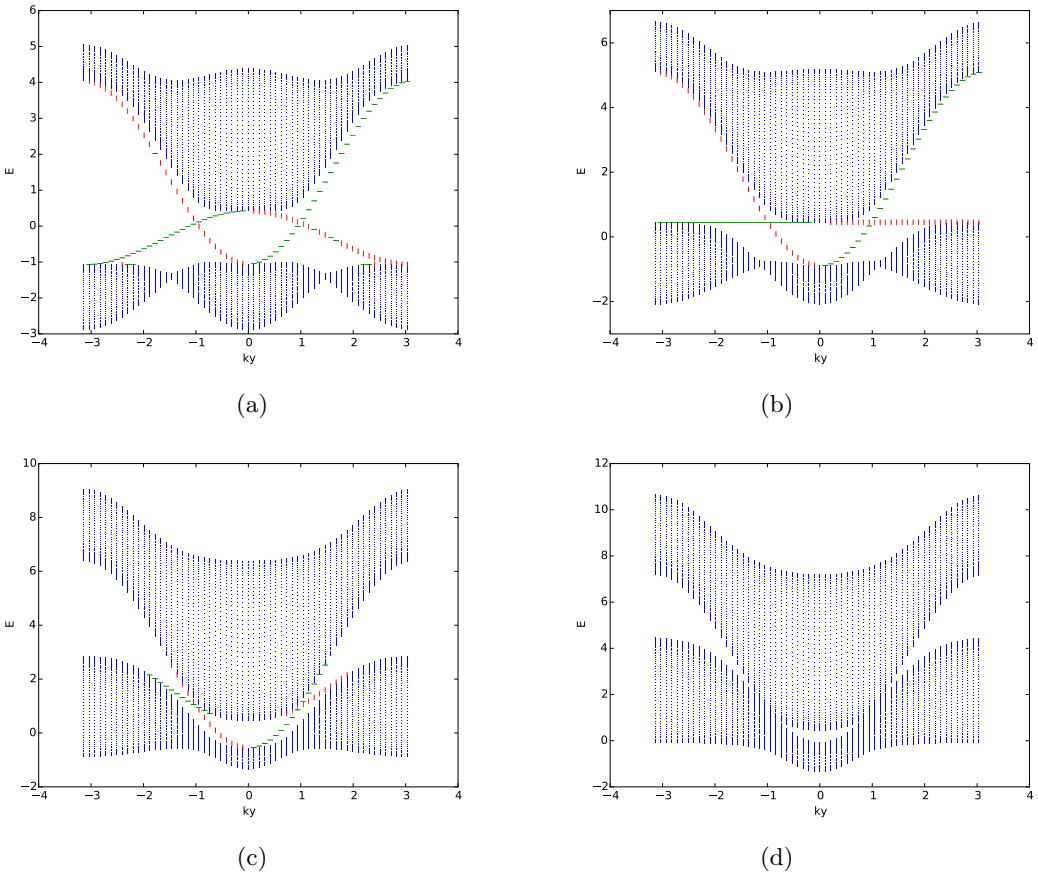

Figure 5.6: Topological edge states of $H_{3/2,-1/2}$. The parameters are $\gamma_2 = 1.0$, $m = 1.0$, $b = 0.9$. The values of γ_1 are: 0.6 (5.6a); 1.0 (5.6b); 1.6 (5.6c); 2.0 (5.6d).

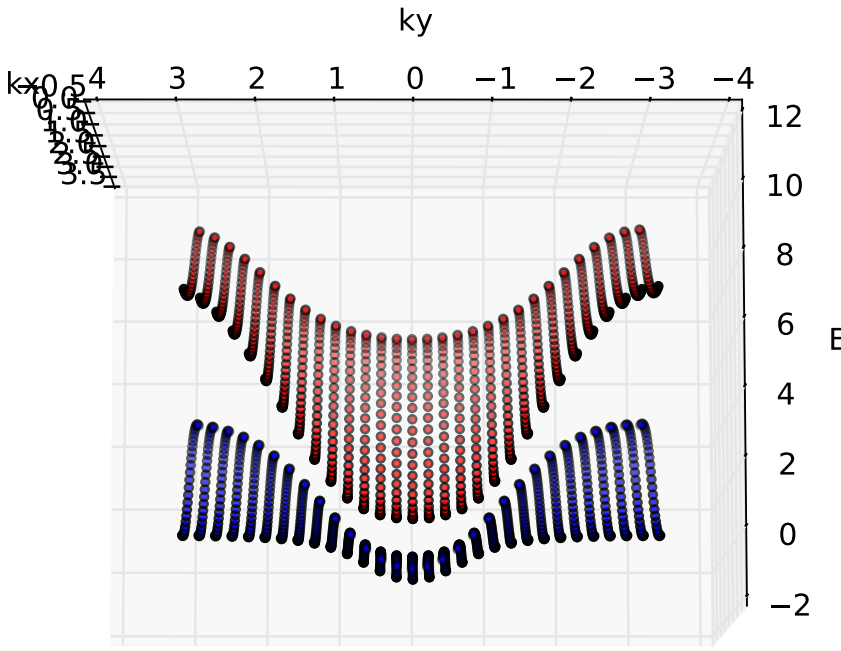

Figure 5.7: Bulk states structure of $H_{3/2,-1/2}$ (Bulk view of the states plotted on Fig. 5.6d). The parameters are $\gamma_1 = 2.0$, $\gamma_2 = 1.0$, $m = 1.0$, $b = 0.9$.

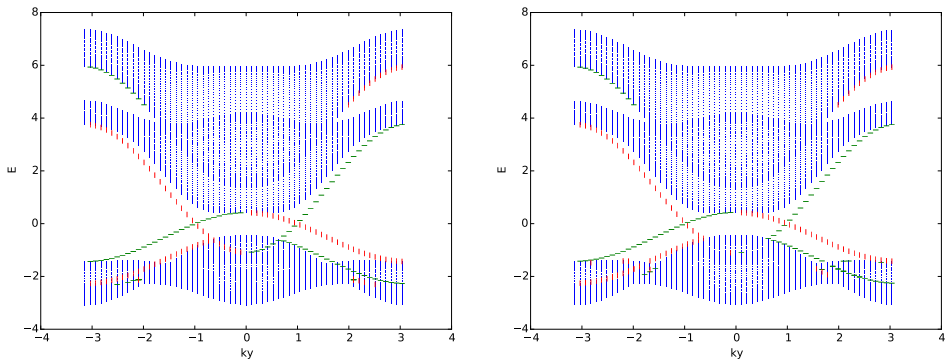

(a)

(b)

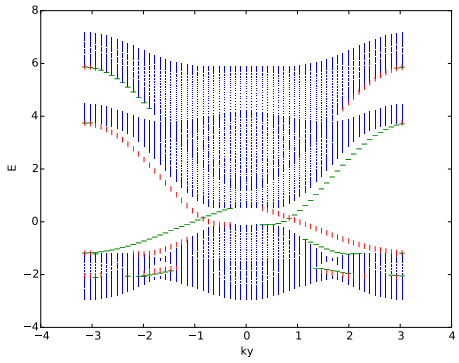

(c)

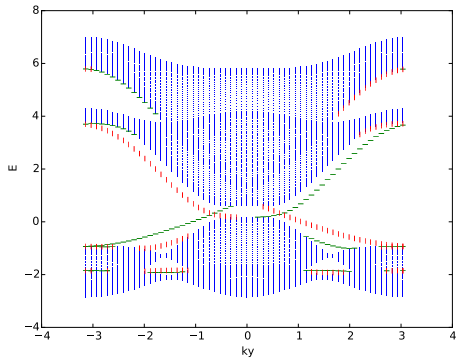

(d)

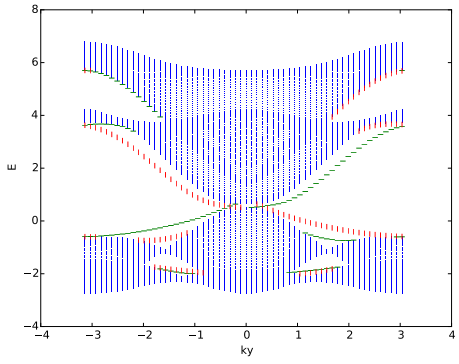

(e)

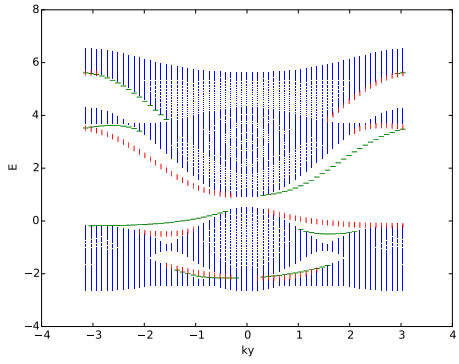

(f)

Figure 5.8: Full surface states structure of the Luttinger model with Zeeman field at $\gamma_1 = 0.5$, $\gamma_2 = 1.0$, $m = 1.0$, $b = 0.9$. The values of k_z are: 0.0 (5.8a), 0.1 (5.8a), 0.5 (5.8c), 0.7 (5.8d), 0.9 (5.8e), 1.1 (5.8a).

perpendicular to the spatial separation of the Weyl points, is equal to zero outside the WP, and a non-zero integer, if the plane lies between them. Now let us consider a smooth change of parameters, such that the Weyl points change the signs of their charges. The fact, that they change their charges implies, that the integral of Berry curvature taken between the Weyl points, also changes. As we discussed, this can occur through gap closing at every plane, where the integral of Berry curvature changes. Thus, change of signs of the Weyl points would imply gap closing in the whole range between them.

Let us show it, using one specific example of a double Weyl metal. The most general Hamiltonian of double Weyl metal has the form:

$$H = \begin{pmatrix} m(k_z, k_\perp^2) & ak_+^2 + bk_-^2 \\ ak_-^2 + bk_+^2 & -m(k_z, k_\perp^2) \end{pmatrix}, \tag{5.11}$$

where we have introduced $k_\pm = k_x \pm ik_y$. As it was pointed out in Ref. [24], this Hamiltonian describes double Weyl point with the charge $2\text{sign}(|a| - |b|)$. This means that the charge is different in the cases $|a| > |b|$ or $|a| < |b|$. Now, let us ask a question: what happens in the transition point $a = b$?

For concreteness, we place the model on the lattice, thus rewriting the effective Hamiltonian as:

$$H = \begin{pmatrix} m(k) & A^+ \\ A & -m(k) \end{pmatrix}, \tag{5.12}$$

where, for shortness of notations, we have introduced

$$m(k) = M(k_z) - 2B(2 - \cos(k_x) - \cos(k_y)),$$
$$A = 2(a+b)(\cos(k_y) - \cos(k_x)) - 2i(a-b)\sin(k_x)\sin(k_y).$$

For simplicity, we assume $M, B, a, b > 0$. The model possesses Weyl points at $(k_x, k_y, M) = (0, 0, 0)$ and $(\pi, \pi, 8B)$. Chern numbers in xy planes are zero at $M < 0$ or $M > 8B$, and are equal to ± 2 at $0 < M < 8B$. Since the Chern number changes, as $a - b$ changes sign, one can expect that, at $a = b$, energy gap has to close in the whole range $0 < M < 8B$. To see it explicitly, we write general expression for the energy:

$$\begin{aligned} \mathcal{E}^2 &= (m - 2B(2 - \cos(k_x) - \cos(k_y)))^2 \\ &\quad +4(a+b)^2(\cos(k_y) - \cos(k_x))^2 \\ &\quad +4(a-b)^2\sin^2(k_x)\sin^2(k_y) \end{aligned}$$

One can see, that in the case $a = b$, the energy gap closes at

$$\cos(k_x) = \cos(k_y) = 1 - \frac{m}{4B}.$$

Thus we conclude: *if, under smooth change of parameters, Weyl points change their charges, then, at the critical point, there exist energy crossing, which connects them.* In the considered case, this crossing has the shape of two 'glued' rings, consistently with C_4 rotational symmetry of the Hamiltonian (5.12). We note, that within our model, it is not clear, how the critical point $a = b$ can be realized physically, but, in principle, these 'tied' rings may form a new state of matter. However, there also exists a different, and more realistic model [77], where critical point between two Weyl points forms one Weyl ring.

5.3.1 Transitions between different topological phases in Luttinger model

It is interesting to study possible transitions between different topological phases in the Luttinger model. If we look at the anisotropic Luttinger model without magnetic field (see Eq. 5.4), we can see that, in general, it has two double degenerate bands, but in the special cases of $C = 0$, or $E = 0$, four-fold degeneracies appear. In particular, at $E = 0$, there are such degeneracies at $k_x^2 = k_y^2 = k_z^2$, and in the case $C = 0$, there are degeneracies at $k_x = k_y = 0$, $k_x = k_z = 0$, and $k_y = k_z = 0$.

Extra degeneracies also happen in the Luttinger model with nonzero magnetic field. Indeed, as we discussed in Sec. 5.2.1, the model possesses four Weyl points, and as C, E change their signs, the signs of monopole charges change as well. Thus, in the cases of zero C or E, the model has to have additional degeneracies. We would like to look at them at more details.

$E = 0$

In this limit, energy spectrum can be found exactly:

$$\frac{\sqrt{3}}{C}\mathcal{E}_{-1/2,3/2} = -\frac{\sqrt{3}b}{2C} \pm \sqrt{\left(2k_z^2 - k_x^2 - k_y^2 - \frac{\sqrt{3}b}{C}\right)^2 + 3\left(k_x^2 - k_y^2\right)^2},$$

$$\frac{\sqrt{3}}{C}\mathcal{E}_{-3/2,1/2} = \frac{\sqrt{3}b}{2C} \pm \sqrt{\left(2k_z^2 - k_x^2 - k_y^2 + \frac{\sqrt{3}b}{C}\right)^2 + 3\left(k_x^2 - k_y^2\right)^2}.$$

From these expressions, one can find that the degeneracies occur in the following cases:

$\mathcal{E}_{3/2} = \mathcal{E}_{1/2}$. Two-dimensional degeneracy with the equation

$$k_z^2 = \frac{k_x^2 + k_y^2 + \sqrt{(k_x^2 - k_y^2)^2 + \frac{3b^2}{4C^2}}}{2}$$

It starts at the linear Weyl point, and proceeds to the increasing k_z. Along this degeneracy, the energy is equal to:

$$\mathcal{E} = -\frac{C}{\sqrt{3}}\sqrt{4(k_x^2 - k_y^2)^2 + \frac{3b^2}{C^2}}.$$

$\mathcal{E}_{3/2} = \mathcal{E}_{-1/2}$. One-dimensional degeneracy

$$\begin{cases} k_x^2 = k_y^2 \\ k_z^2 = k_x^2 + \frac{\sqrt{3}b}{2C} \end{cases}$$

It consists of four lines emerging from the quadratic Weyl point. The energy along these lines is constant and equal to $\frac{\sqrt{3}}{C}\mathcal{E} = -\frac{\sqrt{3}b}{2C}$.

$\mathcal{E}_{1/2} = \mathcal{E}_{-3/2}$: One-dimensional degeneracy

$$\begin{cases} k_x^2 = k_y^2 \\ k_z^2 = k_x^2 - \frac{\sqrt{3}b}{2C} \end{cases}$$

Four lines emerging from the new Weyl point located at $k_x^2 = k_y^2 = \frac{\sqrt{3}b}{2C}$, $k_z = 0$. This new Weyl point exists only at $E = 0$.

$\mathcal{E}_{-3/2} = \mathcal{E}_{-1/2}$: Two-dimensional degeneracy with the equation

$$k_z^2 = \frac{k_x^2 + k_y^2 - \sqrt{(k_x^2 - k_y^2)^2 + \frac{3b^2}{4C^2}}}{2}.$$

This two-dimensional degeneracy also appears only at sufficiently large k_x, k_y and exists only at $E = 0$.

C=0

At $C = 0$, the Hamiltonian can be diagonalized analytically, and the resulting energies are:

$$\mathcal{E} = \pm\sqrt{\frac{5b^2}{4} + E^2(k_x^2k_y^2 + k_x^2k_z^2 + k_y^2k_z^2) \pm \sqrt{b^4 + b^2E^2k_x^2k_y^2 + 4b^2E^2k_z^2(k_x^2 + k_y^2)}}.$$

One can see that, in this case, the degeneracies having zero energy, occur (up to interchange $k_x \leftrightarrow k_y$) at

$$\begin{cases} |k_xk_z| = \frac{\sqrt{3}b}{2E} \\ k_y = 0 \end{cases}$$

Thus, we have shown that studying critical points between phases of different topological metals can lead to many new exotic phases with degeneracies of different dimensions. As for now, we are not familiar, how these phases can be stabilized, e.g. how C or E in the Luttinger model can be tuned to zero, but we believe that it might be of interest to explore it further.

5.4 Multilayers of Weyl metal

In this section, we would like to discuss band structure that can arise in a multilayer containing Weyl metals. To demonstrate, why it is interesting, we briefly remind an idea of topological/normal insulator (see Sec. 3.6): since each topological or normal layer is in a different topological phase, surface states appear at their interfaces. But, since, each layer is thin, these surface states can tunnel between the different interfaces, thus forming effectively three-dimensional states, which can form new states of matter.

5.4.1 Two Weyl metals with oppositely separated Weyl points

We would like to explore, what may happen, if the multilayer is made from Weyl metals. For example, it can be Weyl metal/normal insulator multilayer, or a multilayer formed from two different kinds of Weyl metals. A specific example, that we consider, is the following: suppose that the multilayer is formed from two Weyl metals, in such a way that, in each layer, the Weyl points are separated in the direction perpendicular to the growth direction. Also suppose, that the Weyl points in the neighboring layers are separated in the opposite directions (see Fig. 5.9).

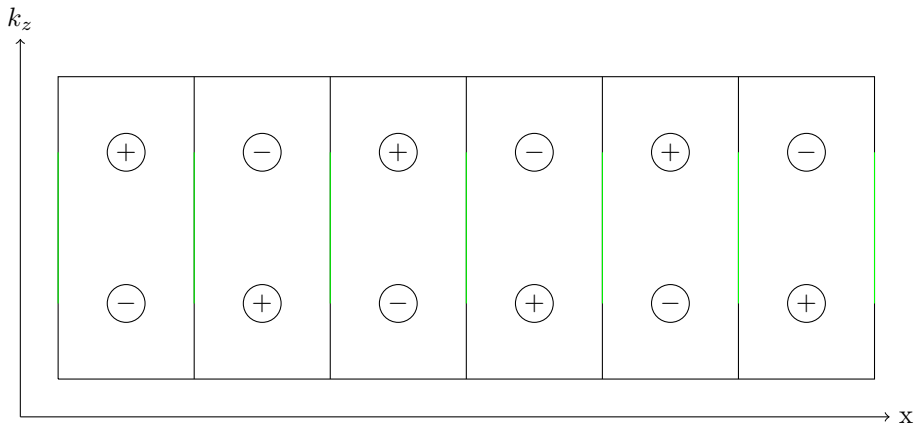

Figure 5.9: Multilayer formed by two Weyl metals. The picture is drawn in mixed representation: coordinate in the growth direction (horizontal), and momentum in the direction of Weyl points separation (vertical). Surface states are shown in green.

As we discussed before, each layer of Weyl metal contains chiral surface states, so that surface states localized on the opposite surfaces have the opposite chiralities. In this example, at each interface, surface states arising from two neighboring layers have the same chirality. However, surface states from different surfaces can tunnel between each other. Thus, we expect the resulting energy spectrum to be superposition of surface states from different surfaces.

To find the energy spectrum, we assume that the layer is grown in the x direction, but the Weyl points are separated in the z direction.

We write the Hamiltonian as:

$$H = \begin{cases} \begin{pmatrix} m(k_z) - B(\hat{k_x}^2 + k_y^2) & v_F(\hat{k_x} - ik_y) \\ v_F(\hat{k_x} + ik_y) & -m(k_z) + B(\hat{k_x}^2 + k_y^2). \end{pmatrix} & \text{odd layer} \\ \begin{pmatrix} m(k_z) - B(\hat{k_x}^2 + k_y^2) & v_F(\hat{k_x} + ik_y) \\ v_F(\hat{k_x} - ik_y) & -m(k_z) + B(\hat{k_x}^2 + k_y^2). \end{pmatrix} & \text{even layer} \end{cases}$$

Here we introduce the $\hat{}$ symbol above k_x to emphasize that it is an operator, which acts in coordinate representation, whereas $k_{y,z}$ are written in the momentum representation. This Hamiltonian accounts for the fact that the Weyl points in each layer are separated in the opposite directions, but by the same distance, exactly as shown on the Fig. 5.9.

We find spectrum of this model numerically by placing it on a lattice in x direction, and present our findings on the Fig. 5.10. We obtain two main features: first, we find surface states localized at the boundary of the whole sample, which persist in the multilayer. Second, the surface states from all other interfaces get mixed with each other, thus forming effectively bulk states. Surprisingly, we find that the dispersion spectrum of such states is significantly different from the spectrum of an isolated layer, but the main feature here, is that these states are inside the bulk gap of each layer. They look almost as if the connected the conduction and valence bands, but a more detailed calculation (the same as presented on the Fig. 5.9, but with higher resolution) shows that they are hybridized. Thus we can say that multilayer of two Weyl metals is a way to create three dimensional states with a very narrow gap, almost like Dirac electrons. For completeness, we have also plotted profiles of these in-gap states, which confirm that they are superposition of the surface states from each layer. The profiles look like a Bloch wave formed by the surface states from each interface, and we present them on the Fig. 5.11.

5.4.2 Weyl metal/normal insulator multilayer

Similarly to the previous case, we can consider a multilayer formed by Weyl metal and a normal insulator. We write the Hamiltonian in a very similar way, but with the only difference that allow m to

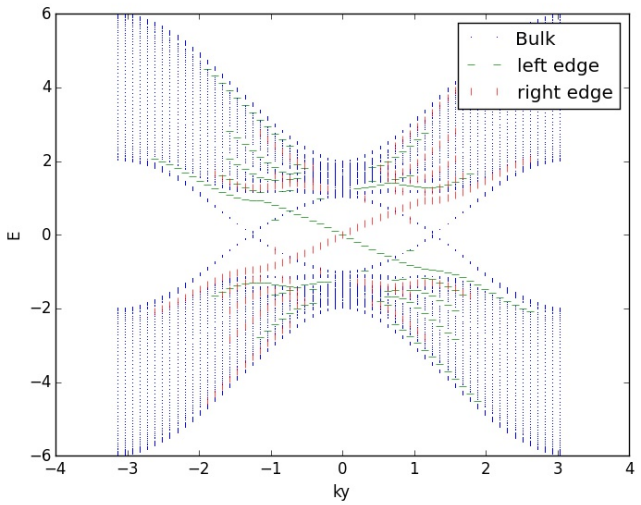

Figure 5.10: Dispersion structure in a multilayer of two Weyl metals. The parameters for both layers are: $m = 2.0$, $B = 1.0$, $v_F = 1.0$, the number of sites for each odd layer is 4, and for each even layer is 3. The number of bilayers is 8 (9 odd layers and 8 even layers). Blue color refers to bulk states; green: states localized on the left edge; red: states localized on the right edge

be different at odd/even layers:

$$H = \begin{cases} \begin{pmatrix} m_1 - B(\hat{k_x}^2 + k_y^2) & v_{F_1}(\hat{k_x} - ik_y) \\ v_{F_1}(\hat{k_x} + ik_y) & -m_1 + B(\hat{k_x}^2 + k_y^2). \end{pmatrix}, \\ \text{at} \quad -L < x < 0, \quad L < x < 2L \ldots \\ \begin{pmatrix} m_2 - B(\hat{k_x}^2 + k_y^2) & v_{F_2}(\hat{k_x} + ik_y) \\ v_{F_2}(\hat{k_x} - ik_y) & -m_2 + B(\hat{k_x}^2 + k_y^2). \end{pmatrix}, \\ \text{at} \quad 0 < x < L, \quad 2L < x < 3L \ldots \end{cases} \tag{5.13}$$

Specifically, we assume that m_1 is positive, whereas m_2 is negative. Strictly speaking, this Hamiltonian may describe WM-NI multilayer, or a multilayer formed by two Weyl metals with different separation between the Weyl points, and in the range of k_z, where the odd layers are in topologically non-trivial phase, whereas the even layers

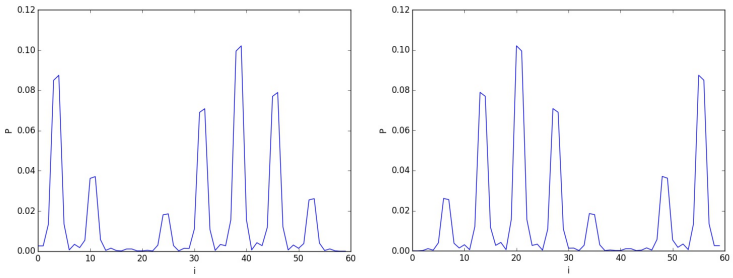

(a) State with E = -0.34527 (b) State with E = 0.345276

Figure 5.11: Profiles of two in-gap states from the Fig. 5.10 at $k_y = 1.0$

are topologically trivial.

We find that the resulting energy spectrum is somewhat simpler, than in the case, considered in Sec. 5.4.1. We present it on the Fig. 5.12. We can see, that there still exist surface states localized at the boundary of the sample, but the states localized at all other interfaces get hybridized. In contrast to the case, considered in the Sec. 5.4.1, hybridization affects the energy spectrum insignificantly: the states only obtain a tiny gap, which is not clearly visible on the Fig. 5.12. Thus, our conclusion remains: a multilayer containing Weyl metal is a way to create a material with a very narrow energy gap.

We have also plotted the profiles of the in-gap states, which confirm that they are superposition of the surface states from each interface. We plot two of them on the Fig. 5.13

Let us state again, that the model with the Hamiltonian (5.13) may describe either WM-NI multilayer, or multilayer formed by two Weyl metals with different spatial separation between the Weyl points. Since Weyl metal is characterized by Chern number at fixed momentum component k_z, we can say that the scenario shown on the Fig. 5.12 will be realized at such k_z, that one Weyl metal is in a topological phase, whereas the other is normal. In other words, if the spatial separation between Weyl points in each layer is equal to $Q_{1,2}$, then the phase shown on the Fig. is realized at $Q_1 < |k_z| < Q_2$.

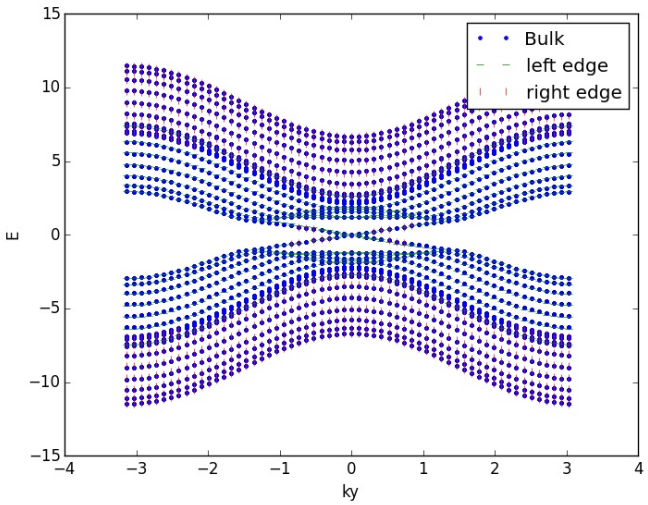

Figure 5.12: Dispersion structure in a WM-NI multilayer. The parameters for both layers are: $m_1 = 2.0$, $m_2 = -2.0$, $B = 1.2$, $v_F = 1.0$, the number of sites for each (both odd and even) layer is 8. The number of bilayers is 8 (8 odd layers and 8 even layers). Blue color refers to bulk states; green: states localized on the left edge; red: states localized on the right edge

5.4.3 Weyl metal in a spatially modulated field

In the previous section, we have established, that a multilayer formed by two Weyl metals with different spatial separation of the Weyl points can form new low-gap states. We discussed, that Weyl points can be separated in momentum space due to non-zero Zeeman field. Thus, our multilayer can be realized if the Zeeman field is spatially modulated. Following the previous sections, we could assume that the magnitude of the Zeeman field is a two-valued function (one value for odd and even layers), but in this section, we take a different approach. We assume that the Zeeman field is a smooth and periodic function along the growth direction of the multilayer:

$$b_{eff} = b + b_0 \cos\left(\frac{2\pi x}{\lambda}\right).$$

We also assume, that without the Zeeman field, our material would be a Dirac metal, but solely due to the former, Weyl points become

spatially separated. Thus, we write the Hamiltonian as:

$$\begin{aligned} H &= \gamma_1 k_x + \gamma_2 k_y + \gamma_3 k_z \\ &\quad +2B(\cos(kx) + \cos(ky) + \cos(kz) - 3)\gamma_4 + b_{eff} S_z. \end{aligned}$$

We present numerically computed energy spectrum on the Fig. 5.14. Indeed, we obtain expected results: its energy spectrum can be viewed as a superposition of the energy spectra for each of the layers. If the wavelength of the Zeeman field is large, the bulk states look almost like two bulk Weyl metals. In addition, the full spectrum includes Fermi arcs localized at the boundary of the multilayers. Since, at small k_z, all layers are in the same topological phase, there are no 'surface' states localized at each interface. However, there are hybridized surface states in the range of k_z between the smaller and the larger separation of the Weyl points. In the case of 'thick' layers, i.e. large wavelength of the Zeeman field, they form almost flat bands. Thus, we believe that Dirac metal in a spatially modulated Zeeman field is close to a new state of matter, which can be called *an open nodal line*.

We conclude, that we checked numerically, that multilayer of Weyl metals can be realized by considering Dirac or Weyl metal with a spatially modulated Zeeman field. It has very interesting properties, which include in-gap states with very low, almost zero energies. These states are almost degenerate.

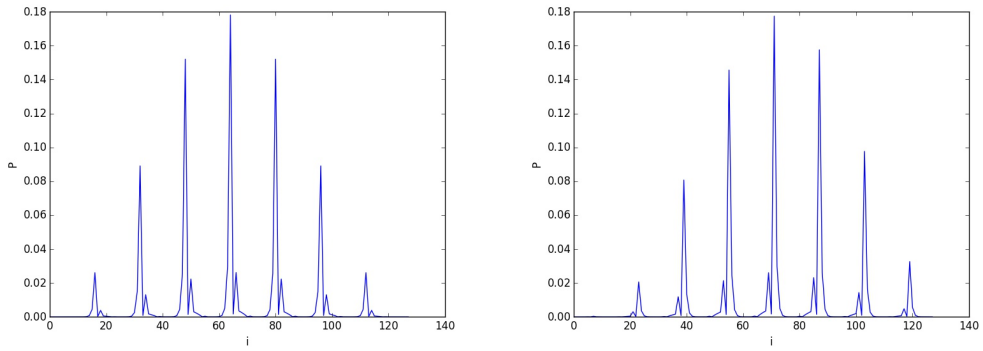

Figure 5.13: Profiles of two states from the Fig. 5.12 at $k_y = 0.2$

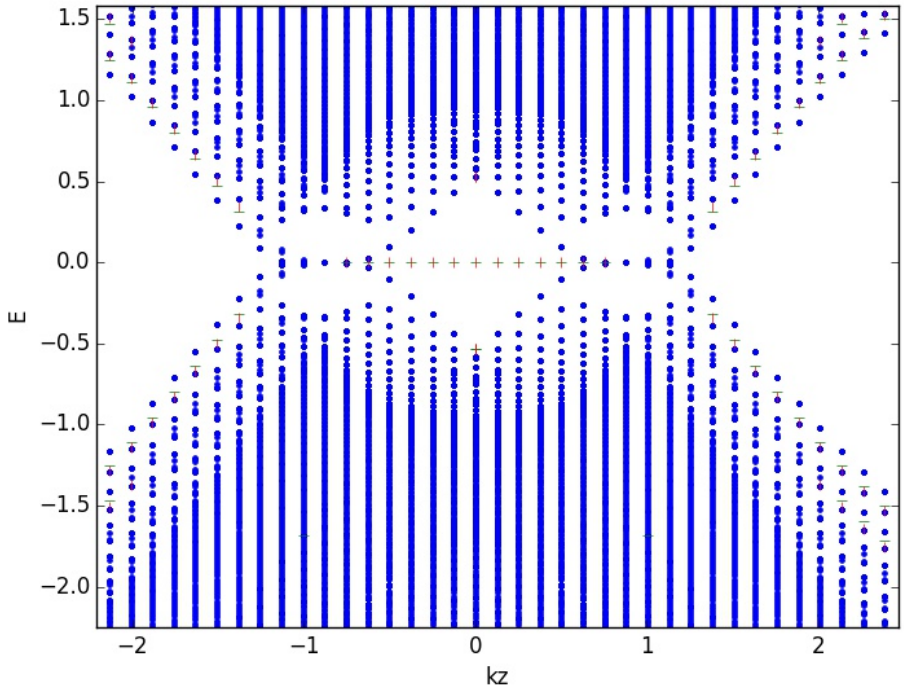

Figure 5.14: Dispersion structure in a four band Weyl metal with spatially modulated magnetic field. The parameters are: $B = 0.8$, $v_F = 1.0$, $b_0 = 0.5$, $b = 1.0$, $\lambda = 50$. The number of sites is 250.

Chapter 6

Superconductivity in Weyl metals

In this chapter, we explore possible superconducting states, that can arise in Weyl metal. We consider a model of Weyl metal in a topological/normal insulator multilayer, because it is the simplest full model of Weyl metal, which contains only one pair of Weyl points. We use this model to demonstrate our calculations of various properties related to superconductivity: free energy, critical temperature, order parameter, anomalous Hall conductivity.

6.1 Hamiltonian of superconducting state

Conventionally, superconductivity arises due to interaction between electrons, such that they form 'Cooper pairs'. The most well-known example of electron-electron interaction is Coulomb interaction, which has a Hamiltonian of the form:

$$H = e^2 \int dx_1 dx_2 \frac{\psi^+_{\sigma_1}(x_1)\psi_{\sigma_1}(x_1)\psi^+_{\sigma_2}(x_2)\psi_{\sigma_2}(x_2)}{|x_1 - x_2|}.$$

This Hamiltonian describes Coulomb repulsion between electron densities at the points x_1 and x_2. This is a very rough model, because it does not take into account a lot of additional effects, such as interaction with the lattice, impurities etc. However, we still can obtain a lot of non-trivial results by approximating it even further, i.e. assuming that the interaction is local. Specifically, the local interaction means, that its potential has a shape of delta-function,

so that the Hamiltonian is written as:

$$H = U \int dx \psi^+_{\sigma_1}(x)\psi_{\sigma_1}(x)\psi^+_{\sigma_2}(x)\psi_{\sigma_2}(x).$$

Here, we have introduced arbitrary coupling strength U. We can rewrite the Hamiltonian in momentum representation as:

$$H = U \sum_{kk'q} \psi^+_{\sigma_1,k+q}\psi_{\sigma_1,k-q}\psi^+_{\sigma_2,k'-q}\psi_{\sigma_2,k'+q}.$$

This model can host interesting strongly coupled states, when the Hamiltonian H is not small. For example, superconductivity can arise in the case of non-zero expectation $\langle\psi_{\sigma_1,k-q}\psi_{\sigma_2,k+q}\rangle$. We will see shortly the relation between this expectation and the interaction Hamiltonian. For now, we only note, that we are interested in the simplest case of singlet pairing, when the expectation is non-zero only for electrons with the opposite spins, $\langle\psi_{\uparrow,k-q}\psi_{\downarrow,k+q}\rangle$. As we will see, it results, that we have to consider only the terms in the interaction Hamiltonian of the form:

$$H = U \sum_{kk'q} \psi^+_{\uparrow,k+q}\psi^+_{\downarrow,k'-q}\psi_{\uparrow,k-q}\psi_{\downarrow,k'+q}.$$

We notice that this Hamiltonian may change its form if we transform the wavefunctions by multiplying them by a k-dependent matrix. For this reason, if we are interested in interactions, that can arise in the model of topological/normal insulator multilayer, we have to start our analysis from the full four-band Hamiltonian. Thus, we write together the initial Hamiltonian of the multilayer, and its superconducting pairing:

$$\begin{aligned} H &= H_0 + H_{sc} \\ H_0 &= c^+ \Big(v_F\tau_z(\sigma_1 k_2 - \sigma_2 k_1) + b\sigma_z \\ &\quad + \Delta_s\tau_x + \frac{\Delta_D\tau^+}{2}e^{ik_z d} + \frac{\Delta_D\tau^-}{2}e^{-ik_z d} + \lambda\tau_y\sigma_z \Big) c, \\ H_{sc} &= -\frac{U}{V}\sum_{kk'q} c^+_{k+q\uparrow}c^+_{-k+q\downarrow}c_{-k'+q\downarrow}c_{k'+q\uparrow}. \end{aligned}$$

In addition to the Hamiltonian considered in the case of topological/normal insulator without interactions (see Sec. 3.6), this model

also contains inversion symmetry breaking term, which strength is proportional to λ. We are going to neglect it while performing diagonalization, but later, account for it numerically. We will find, that it has non-trivial consequences.

As we can see, the canonical transformation $\sigma^{\pm} \to \sigma^{\pm}\tau^z, \tau^{\pm} \to \sigma_z\tau^{\pm}$ does not affect the superconducting pairing. After performing it, the Hamiltonian is rewritten as:

$$\begin{aligned} H_0 &= c^+ \left(v_F(\sigma_1 k_2 - \sigma_2 k_1) + b\sigma_z \right. \\ &\quad \left. + (\Delta_s \tau_x + \frac{\Delta_D \tau^+}{2} e^{ik_z d} + \frac{\Delta_D \tau^-}{2} e^{-ik_z d})\sigma_z + \lambda \tau_y \right) c, \\ H_{sc} &= -\frac{U}{V} \sum_{kk'q} c^+_{k+q\uparrow} c^+_{-k+q\downarrow} c_{-k'+q\downarrow} c_{k'+q\uparrow}. \end{aligned} \tag{6.1}$$

As a next step, we have to perform diagonalization in the τ space, which turns out to affect the superconducting interaction. Indeed, the matrix diagonalizing H_0 in the τ space has the form:

$$\frac{1}{\sqrt{2}} \begin{pmatrix} 1 & 1 \\ \frac{\Delta_s + \Delta_D e^{-ik_z d}}{\Delta} & -\frac{\Delta_s + \Delta_D e^{-ik_z d}}{\Delta} \end{pmatrix},$$

where $\Delta = \sqrt{\Delta_s^2 + \Delta_D^2 + 2\Delta_s \Delta_D \cos(k_z d)}$. It can be rewritten in terms of imaginary exponents as:

$$\frac{1}{\sqrt{2}} \begin{pmatrix} 1 & 1 \\ e^{-i\phi} & -e^{-i\phi} \end{pmatrix},$$

where each exponent is defined as:

$$e^{-i\phi} = \sqrt{\frac{\Delta_S + \Delta_D e^{-ikd}}{\Delta_S + \Delta_D e^{ikd}}}.$$

After diagonalization in τ space, the Hamiltonian is rewritten as:

$$\begin{aligned} H_0 &= c^+ \left(v_F(\sigma_1 k_2 - \sigma_2 k_1) + b\sigma_z + \Delta \tau_z \sigma_z \right) c, \\ H_{sc} &= -\frac{U}{4V} \sum_{kk'q\tau} U^+_{t_1\tau} U^+_{t_2\tau} U_{\tau t_3} U_{\tau t_4} c^+_{k+q\uparrow t_1} c^+_{-k+q\downarrow t_2} c_{-k'+q\downarrow t_3} c_{k'+q\uparrow t_4}. \end{aligned}$$

Its free part H_0 is a block of two 2×2 Hamiltonians with masses $b \pm \Delta$. As we showed in Sec. 3.6, only the block with negative

sign contains Weyl points, whereas the block with positive sign is separated from the former by energy gap, and thus can be neglected. As a result, we write 2×2 Hamiltonian describing the Weyl points in the form:

$$\begin{aligned} H_0 &= c^+ \left(v_F(\sigma_1 k_2 - \sigma_2 k_1) + m\sigma_3\right) c, \qquad (6.2) \\ H_{sc} &= -\frac{U}{4V} \sum_{kk'q\tau} \Xi(k,k',q) c^+_{k+q\uparrow t_1} c^+_{-k+q\downarrow t_2} c_{-k'+q\downarrow t_3} c_{k'+q\uparrow t_4}, \end{aligned}$$

where we have introduced new parameters:

$$\begin{aligned} & m = b - \Delta \\ & \Xi(k,k',q) = \\ & 1 + \frac{(\Delta_s + \Delta_D e^{i(k+q)d})(\Delta_s + \Delta_D e^{i(-k+q)d})}{\Delta(k+q)\Delta(-k+q)} \\ & \qquad \times \frac{(\Delta_s + \Delta_D e^{-i(-k'+q)d})(\Delta_s + \Delta_D e^{-i(k'+q)d})}{\Delta(-k'+q)\Delta(k'+q)} \\ & = 1 + e^{i\phi(q+k)+i\phi(q-k)-i\phi(q-k')-i\phi(q+k')}. \end{aligned}$$

We would like to emphasize, that the fact, that our initial model contained four bands, results in the factor Ξ, which would not appear, if we started considering 2×2 Hamiltonian (6.2) from the beginning. However, it is easy to see that at $q = 0$, the factor Ξ is just a constant equal to 2, and thus we can, in principle, approximate it by 2 everywhere. This approximation works at $qd << 1$, i.e. when separation between the Weyl points is small. In this section, we keep the factor Ξ for completeness, but we will neglect it further, when we will be studying anomalous Hall conductivity.

Our goal is to find possible superconducting states, which can arise in the model with Hamiltonian (6.2). It is known, that superconducting state is a condensate of Cooper pairs, created by electrons with different momenta. Thus we can make a qualitative conclusion, that superconducting state can appear only when the electron density of states is finite. In a Weyl metal, density of states is finite only at finite chemical potential, whereas if the chemical potential is zero, i.e. Fermi level is aligned with the Weyl points, the density of states vanishes. Thus, we assume that the chemical potential is finite, and not too close to the Weyl points. This, in turn means, that if we are interested in the possible superconducting

states, i.e. Fermi surface phenomena, we can further consider only one band, which crosses the Fermi level.

If we perform diagonalization of the Hamiltonian 6.2 explicitly, we obtain the following eigenvectors of H_0:

$$z_s = \frac{1}{\sqrt{2}} \begin{pmatrix} \sqrt{1+\frac{sm}{E}} \\ s\sqrt{1-\frac{sm}{E}}\frac{(k_y-ik_x)}{\sqrt{k_x^2+k_y^2}} \end{pmatrix},$$

which have energies sE, where $E = \sqrt{v_F^2 k_\perp^2 + m^2}$ is the positive eigenvalue of H_0, and $s = \pm 1$.

Without loss of generality, we can assume that the chemical potential is positive, which, in turn, means, that after diagonalizing free part of the Hamiltonian, we can leave only the band with positive energy. However, when we perform diagonalization of the free term, we also have to transform the interaction term. To do it, we introduce the factor

$$g(k,q) = \frac{1}{2}\sqrt{1-\frac{m_{q-k}}{E_{q-k}}}\sqrt{1+\frac{m_{q+k}}{E_{q+k}}}\frac{(-k_y+ik_x)}{\sqrt{k_x^2+k_y^2}}.$$

In these notations, the interaction term takes the form:

$$H_{sc} = -\frac{U}{4V}\sum_{kk'q}\Xi(k,k',q)g^+(k,q)g(k',q)c^+_{\uparrow,q+k}c^+_{\downarrow,q-k}c_{\uparrow,q-k'}c_{\downarrow,q+k'}.$$

Since each pair of creation/annihilation operator is invariant under their commutation and simultaneous change of sign of the momentum $k \leftrightarrow -k$, we antisymmetrize the factors g by introducing a new factor:

$$\begin{aligned} \gamma(k,q) &= \frac{g(k,q)-g(-k,q)}{2} \\ &= -\frac{(k_y-ik_x)}{4|k_\perp|}\left(\sqrt{1-\frac{m_{q+k}}{E_{q+k}}}\sqrt{1+\frac{m_{q-k}}{E_{q-k}}}\right. \\ &\qquad \left. +\sqrt{1-\frac{m_{q-k}}{E_{q-k}}}\sqrt{1+\frac{m_{q+k}}{E_{q+k}}}\right), \end{aligned} \tag{6.3}$$

and rewrite the interaction term (6.3) as:

$$H_{sc} = -\frac{U}{V}\sum_{kk'q}\Xi(k,k',q)\gamma^+(k,q)\gamma(k',q)c^+_{q+k}c^+_{q-k}c_{q-k'}c_{q+k'}, \tag{6.4}$$

6.2 Path integral treatment of the superconducting state. Gap equation.

In this section, we write the full quantum mechanical partition function describing superconducting Weyl metal. Its initial expression has a conventional form:

$$Z = \int Dc^+ Dc \exp\{-\int\limits_0^\beta d\tau (c^+ \partial_\tau c + H - \mu N)\}$$

and we assume here, that the Hamiltonian contains one band, describing Weyl metal near the Fermi level, which, in turn, is away from the Weyl points (see Sec. 6.1).

After Fourier-transformation of the imaginary time τ and introducing $\xi = E - \mu$, the partition function is rewritten as:

$$\begin{aligned} Z &= \int Dc^+ Dc \exp\left\{ \sum_k c_k^+ (iw - \xi_k) c_k \right. \\ &\left. + \frac{U}{4V\beta} \sum_{kk'q} \Xi(k,k',q) g^+(k,q) g(k',q) c^+_{q+k} c^+_{q-k} c_{q-k'} c_{q+k'} \right\}. \end{aligned}$$

In this equation and further, when we write sum over k, we imply sum over spatial momentum k and Matsubara frequencies w.

As we mentioned previously, we cannot assume here, that the interaction term is small. On the other hand, we have to account for the fact, that superconductivity arises, when the correlator $\langle cc \rangle$ is non-zero. When we work with the path integral, we express these two statements by performing Hubbard-Stratonovich transformation, i.e. introducing additional integration over field Δ, thus

rewriting the partition function as:

$$\begin{aligned} Z &= \int Dc^{+}DcD\bar{\Delta}D\Delta \exp\left\{\sum_{k} c_{k}^{+}(iw-\xi_{k})c_{k}\right. \\ &+\frac{U}{4V\beta}\sum_{kk'q}\Xi(k,k',q)g^{+}(k,q)g(k',q)c_{q+k}^{+}c_{q-k}^{+}c_{q-k'}c_{q+k'} \\ &-\frac{U}{4V\beta}\sum_{kk'q}\Xi(k,k',q)(g^{+}(k,q)c_{q+k}^{+}c_{q-k}^{+}-\frac{2V\beta}{UN_{k}}\bar{\Delta}) \\ &\left.\times(g(k',q)c_{q-k'}c_{q+k'}-\frac{2V\beta}{UN_{k}}\Delta)\right\}. \end{aligned}$$

Here we introduced a new variable N_k which refers to the number of wavevectors k, k'. The last equation can be simplified and rewritten as:

$$\begin{aligned} Z &= \int Dc^{+}DcD\bar{\Delta}D\Delta \\ &\exp\left\{\sum_{k} c_{k}^{+}(iw-\xi_{k})c_{k}-\frac{V\beta}{UN_{k}^{2}}\sum_{k,k',q}\Xi(k,k',q)|\Delta(2q)|^{2}\right. \\ &\left.+\sum_{kk'q}\frac{\Xi(kk'q)}{2N_{k}}\left(g^{+}(k,q)c_{q+k}^{+}c_{q-k}^{+}\Delta(2q)+g(k,q)c_{q-k}c_{q+k}\bar{\Delta}(2q)\right)\right\} \end{aligned}$$

If we also symmetrize the interaction term and introduce $\gamma(k,q)$ (see Eq. 6.3), we can rewrite the partition function as:

$$\begin{aligned} Z = &\int Dc^{+}DcD\bar{\Delta}D\Delta \exp\left\{-\frac{V\beta}{UN_{k}^{2}}\sum_{k,k',q}\Xi(k,k',q)|\Delta(2q)|^{2}\right. \\ &+\sum_{k}\frac{iw-\xi_{k}}{2} \\ &\left.+\sum_{kq}\begin{pmatrix} c_{q+k}^{+} & c_{q-k} \end{pmatrix}\begin{pmatrix} \frac{iw-\xi_{q+k}}{2} & \gamma^{+}(k,q)\Delta(2q) \\ \gamma(k,q)\bar{\Delta}(2q) & \frac{iw+\xi_{q-k}}{2} \end{pmatrix}\begin{pmatrix} c_{q+k} \\ c_{q-k}^{+} \end{pmatrix}\right\}. \end{aligned} \tag{6.5}$$

In the last sum it is assumed, that q runs over two values corresponding to the positions of the nodes, and k runs in their vicinity.

The physical meaning of non-diagonal elements in the matrix entering the Hamiltonian in Eq. 6.5 is that superconductivity mixes particles (annihilated by the operator c) and holes (annihilated by c^+).

In the last equation, we can integrate out the fermions, thus obtaining partition function of the order parameter Δ, which has the form:

$$Z = \int D\bar{\Delta} D\Delta \exp\left(-\frac{V\beta}{UN_k^2} \sum_{k,k',q} \Xi(k,k',q) |\Delta(2q)|^2 + \sum_k \frac{iw - \xi_k}{2} \right.$$
$$\left. + \sum_{kq} \log\left(\frac{(iw - \xi_{q+k})(iw + \xi_{q-k})}{4} - |\gamma(k,q)|^2 |\Delta(2q)|^2 \right) \right) \qquad (6.6)$$

We can consider its *mean field approximation*, i.e. assume that Δ is a classical well-defined field. In this case, it has to obey semiclassical field equation, which is obtained by varying the action entering the partition function over $\bar{\Delta}$. Explicitly, such gap equation has the form:

$$\frac{1}{V\beta} \sum_{k,w} \frac{4|\gamma(k,q)|^2}{(-iw + \xi_{q+k})(iw + \xi_{q-k}) + 4|\gamma|^2|\Delta|^2} = \frac{1}{UN_k^2} \sum_{kk'} \Xi(k,k',q) \qquad (6.7)$$

In the last equation the zeros of the denominator correspond to the energies of Bogoliubov quasiparticles:

$$\mathcal{E}_\pm = \pm \frac{\xi_{q+k} - \xi_{q-k}}{2} + \sqrt{\left(\frac{\xi_{q+k} + \xi_{q-k}}{2} \right)^2 + 4|\gamma|^2|\Delta|^2} \qquad (6.8)$$

By using it, one can simplify the gap equation as:

$$-\frac{1}{V\beta} \sum_{k,w} \frac{4|\gamma(k,q)|^2}{(iw - \mathcal{E}_+)(iw + \mathcal{E}_-)} = \frac{1}{UN_k^2} \sum_{kk'} \Xi(k,k',q)$$

If we perform summation over the Matsubara frequencies w, the gap equation is rewritten as:

$$\frac{1}{V} \sum_k \frac{4|\gamma|^2}{\mathcal{E}_+ + \mathcal{E}_-} \left(n_F(-\mathcal{E}_-) - n_F(\mathcal{E}_+) \right) = \frac{1}{UN_k^2} \sum_{kk'} \Xi(k,k',q) \quad (6.9)$$

Solving this equation makes it possible to obtain critical temperature, when the superconductivity appears, and magnitude of the order parameter Δ.

6.3 Equation for critical temperature

In this section, we are interested in finding *critical temperature*, i.e. temperature at which the superconductivity appears. The equation for it is obtained from the gap equation (6.7) by setting $\Delta = 0$. To simplify it, we, first replace momentum summation with integration. Next, we split the overall momentum integral into integral over energies and integral over momenta at fixed energies, thus rewriting the LHS of the equation as:

$$\frac{1}{V\beta}\sum_{k,w}\frac{4|\gamma(k,q)|^2}{(-iw+\xi_{q+k})(iw+\xi_{q-k})}$$
$$=\frac{4}{\beta}\sum_{w}\int d\xi_k\int\frac{d^3k}{(2\pi)^3}\delta(\xi_k-\bar{\xi_k})\frac{|\gamma(k,q)|^2}{(-iw+\xi_k+\xi_{q+k}-\bar{\xi_k})(iw+\xi_k+\xi_{q-k}-\bar{\xi_k})}$$

In the last equation, ξ_k is an independent integration variable, and $\bar{\xi_k}$ is expressed in terms of the momentum k.

Further, we assume that the total integral is mostly contributed near the Fermi surface. This fact makes it possible to assume, that the momentum integral at fixed energy is equal to the momentum integral at the Fermi level. Thus, we rewrite the LHS as:

$$\frac{4}{\beta}\sum_{w}\int\frac{dk}{(2\pi)^3}\delta(\bar{\xi_k})|\gamma(k,q)|^2\int\frac{d\xi_k}{(\xi_k-iw+\xi_{q+k}-\bar{\xi_k})(\xi_k+iw+\xi_{q-k}-\bar{\xi_k})}$$
$$=\frac{4}{\beta}\sum_{w>0}\int\frac{dk}{(2\pi)^3}\delta(\bar{\xi_k})|\gamma|^2 2\pi i\left(\frac{1}{2iw-\xi_{q+k}+\xi_{q-k}}+\frac{1}{2iw+\xi_{q+k}-\xi_{q-k}}\right)$$

If we recall that w are Matsubara frequencies defined by $w=\frac{2\pi(n+1/2)}{\beta}$ and perform the summation over w up to Debye frequency w_D, which we take as physical cut-off, we rewrite the LHS of the

equation for critical temperature as:

$$2\int \frac{dk}{(2\pi)^3}\delta(\bar{\xi_k})|\gamma(k,q)|^2 \times$$
$$\left(\psi(\frac{\beta w_D}{2\pi}+1+\frac{i\beta}{4\pi}(\xi_{q+k}-\xi_{q-k}))-\psi(\frac{1}{2}+\frac{i\beta}{4\pi}(\xi_{q+k}-\xi_{q-k}))\right.$$
$$\left.+\psi(\frac{\beta w_D}{2\pi}+1-\frac{i\beta}{4\pi}(\xi_{q+k}-\xi_{q-k}))-\psi(\frac{1}{2}+1-\frac{i\beta}{4\pi}(\xi_{q+k}-\xi_{q-k}))\right).$$

Here we have introduced digamma function ψ, and approximated it by logarithm in the limit $\omega_D >> T_c$. By using its asymptotic, the last expression can be rewritten as:

$$4\int \frac{dk}{(2\pi)^3}\delta(\bar{\xi_k})|\gamma(k,q)|^2 \times \left(\log\left(\frac{w_d}{2\pi T_c}\right)-\mathrm{Re}\psi\left(\frac{1}{2}+\frac{i}{4\pi T_c}(\xi_{q+k}-\xi_{q-k})\right)\right)$$

and thus the equation for critical temperature takes the form:

$$1/U = 2\int \frac{dk}{(2\pi)^3}\delta(\bar{\xi_k})|\gamma(k,q)|^2 \tag{6.10}$$
$$\times\left(\log\left(\frac{\omega_d}{2\pi T_c}\right)-\mathrm{Re}\psi\left(\frac{1}{2}+\frac{i}{4\pi T_c}(\xi_{q+k}-\xi_{q-k})\right)\right).$$

Now we use specific form of the energy spectrum of our model, i.e. the fact that energy is linear over momentum. Furthermore, we are interested in two special cases of the Cooper pair momentum q: conventional BCS pairing, where $q = 0$, and finite momentum FFLO pairing. We assume that in the latter case, Cooper pairs are created between electrons from the opposite parts of each Weyl cone, i.e. momentum of each Cooper pair is equal to the momentum of the Weyl cone center, i.e. $\pm Q$. In either case, we can assume, that $\xi_{q+k} = \xi_{q-k}$. This approximation makes it possible to find expression for the critical temperature analytically:

$$T_c = \frac{w_D}{2\pi}\exp\left\{-\psi\left(\frac{1}{2}\right)-\frac{1}{2U\int\frac{dk}{(2\pi)^3}\delta(\xi_k)|\gamma|^2}\right\}.$$

Let us estimate the critical temperature for each of the cases. In the case of FFLO pairing, i.e. at $q = Q$ we have

$$|\gamma|^2 = \frac{1}{4}$$

and the momentum integral over the Fermi surface (one node) is evaluated as:

$$\int \frac{dk}{(2\pi)^3}\delta(\xi_k) = \frac{\mu^2}{2\pi^2 v_F^2 v_z}$$

Thus the critical temperature has an expression:

$$T_c = \frac{w_D}{2\pi}\exp\left\{-\psi\left(\frac{1}{2}\right) - \frac{4\pi^2 v_F^2 v_z}{\mu^2 U}\right\} \tag{6.11}$$

In contrast, in the BCS case, i.e. at $q = 0$, we obtain:

$$|\gamma|^2 = \frac{1}{4}\left(1 - \frac{m_k^2}{E_k^2}\right)$$

and the momentum integral is evaluated as:

$$\int \frac{dk}{(2\pi)^3}\delta(\xi_k)|\gamma|^2 = \frac{\mu^2}{6\pi^2 v_F^2 v_z}.$$

As a result, the critical temperature is equal as:

$$T_c = \frac{w_D}{2\pi}\exp\left\{-\psi\left(\frac{1}{2}\right) - \frac{3\pi^2 v_F^2 v_z}{\mu^2 U}\right\}. \tag{6.12}$$

By comparing the Eqs. (6.11) and (6.12), one can find that $T_c^{(FFLO)} < T_c^{(BCS)}$, i.e. the critical temperature in the FFLO case is lower, than in the BCS case. We also note, that the difference between them becomes more significant at small coupling U. Thus we have established, that there exists temperature range, where BCS pairing is possible, whereas FFLO is not.

6.3.1 Broken inversion symmetry

Now let us explore, what happens to critical temperature, if inversion symmetry in the multilayer is broken. The simplest way of doing it is to write the energy spectrum in the form:

$$\xi_k = \sqrt{v_F^2 k_\perp^2 + m^2} - \Lambda k_z - \mu. \tag{6.13}$$

Here, the parameter Λ is obtained by transforming and taking the leading order contribution in the inversion symmetry breaking term 6.1. One can show, that it has the following expression:

$$\Lambda = \frac{\lambda \Delta_D d}{|\Delta_S + \Delta_D|}.$$

In other words, we approximate the full dispersion curve by two Dirac cones centered in the Weyl nodes. After this simplification, it is convenient to rewrite the momentum in terms of polar "coordinates" acting in each cone:

$$\begin{aligned} v_F k_\perp &= p \sin\theta, \\ v_z(k_z \pm Q) &= p \cos\theta. \end{aligned} \tag{6.14}$$

This change of variables makes it possible to compute the resulting integrals over p analytically. In particular, the equation (6.10) explicitly contains delta-function, and integration over the "radius" p removes it. As a result, we obtain equation containing only one-dimensional integrals over the polar angle θ. The equation for critical temperature (6.10) in the FFLO case, i.e. at $q = Q$ has the form:

$$\frac{1}{U} = \frac{\tilde{\mu}^2}{8\pi^2 v_F^2 v_z} \int_0^\pi \sin\theta d\theta \left\{ \log\left(\frac{\omega_D}{2\pi T_c}\right) - \mathrm{Re}\psi\left(\frac{1}{2} - \frac{i\Lambda\tilde{\mu}\cos\theta}{2\pi v_z T_c}\right)\right\}$$

with $\tilde{\mu}$ being the "effective" chemical potential at the node: $\tilde{\mu} = \mu + \Lambda Q$. Analogously, the Eq. (6.10) in the BCS case, i.e. at $q = 0$ is rewritten as:

$$\begin{aligned} \frac{1}{U} &= \frac{\mu^2}{4\pi^2 v_F^2 v_z} \int_0^\pi \sin^3\theta d\theta \\ &\times \left\{ \log\left(\frac{w_D}{2\pi T_c}\right) - \mathrm{Re}\psi\left(\frac{1}{2} - \frac{i\Lambda}{2\pi T_c}(Q + \frac{\mu}{v_z}\cos\theta)\right)\right\} \end{aligned}$$

We mention, that the integral over terms containing the radicand is taken only within the range where the latter is positive.

We solve these two equations numerically in the case of linear energy spectrum defined by the Eq. (6.13) and present our results on the Fig. 6.1a. One can see, that, in this model, the critical temperature at the inversion symmetric point, i.e. at $\lambda = 0$ is higher for the internodal pairing than for the intranodal, which implies that Cooper pairs form conventional BCS state. As the inversion asymmetry increases, both critical temperatures decrease and eventually disappear. At weak coupling, the critical temperature in the BCS phase is higher in the whole range of Λ, which means that only

the BCS superconducting state can be created. However, as the coupling increases, it is possible to realize the situation, when the critical temperature for the FFLO phase overruns the BCS. One can also see that, in the case of FFLO pairing, critical temperature is not even under change of sign of Λ. It means, that the critical temperature is different for each node, which, in turn, implies that it is possible to realize a situation, when the superconducting pairing is present only in one node, thus forming *helical state* with the order parameter having the form $\Delta(z) = \Delta e^{2iQz}$.

6.4 Order parameter

In this section, we would like to find the magnitude of superconducting order parameter at zero temperature. To do it, we have to solve the gap equation (6.9). If we take the temperature to be zero, use symmetry of the energy $\mathcal{E}_+(k) = \mathcal{E}_-(-k)$, and approximate $\Xi(k, k', q) \approx 2$, we can rewrite it as:

$$\frac{1}{U} = 2 \int \frac{dk}{(2\pi)^3} \frac{|\gamma(k,q)|^2}{\mathcal{E}_+ + \mathcal{E}_-} \left(\theta(\mathcal{E}_+) - \theta(-\mathcal{E}_-)\right). \tag{6.15}$$

If we also represent the integral over momenta as a combination of integrals over energy and the Fermi surface (similarly to the Sec. 6.3), introduce

$$\xi_{q+k} = \xi + \delta_k$$
$$\xi_{q-k} = \xi + \delta_{-k}$$

and make shift $\xi + \frac{\delta_k + \delta_{-k}}{2} \to \xi$, we can rewrite the gap equation as:

$$\frac{1}{U} = \int d\xi \int \frac{dk}{(2\pi)^3} \frac{\delta(\xi_k)|\gamma(k,q)|^2}{\sqrt{\xi^2 + 4|\gamma|^2|\Delta|^2}}$$
$$\times \left(1 - 2\theta\left(\frac{\delta_{-k} - \delta_k}{2} - \sqrt{\xi^2 + 4|\gamma|^2|\Delta|^2}\right)\right)$$

If we perform integration over the energy, we obtain:

$$\frac{1}{U} = 2 \int \frac{dk}{(2\pi)^3} \delta(\xi_k)|\gamma|^2$$
$$\times \left(\log\left(\frac{w_d}{|\gamma||\Delta|}\right) - \operatorname{arcsh}\left(\sqrt{\left(\frac{\delta_k - \delta_{-k}}{4|\gamma||\Delta|}\right)^2 - 1}\right)\right). \tag{6.16}$$

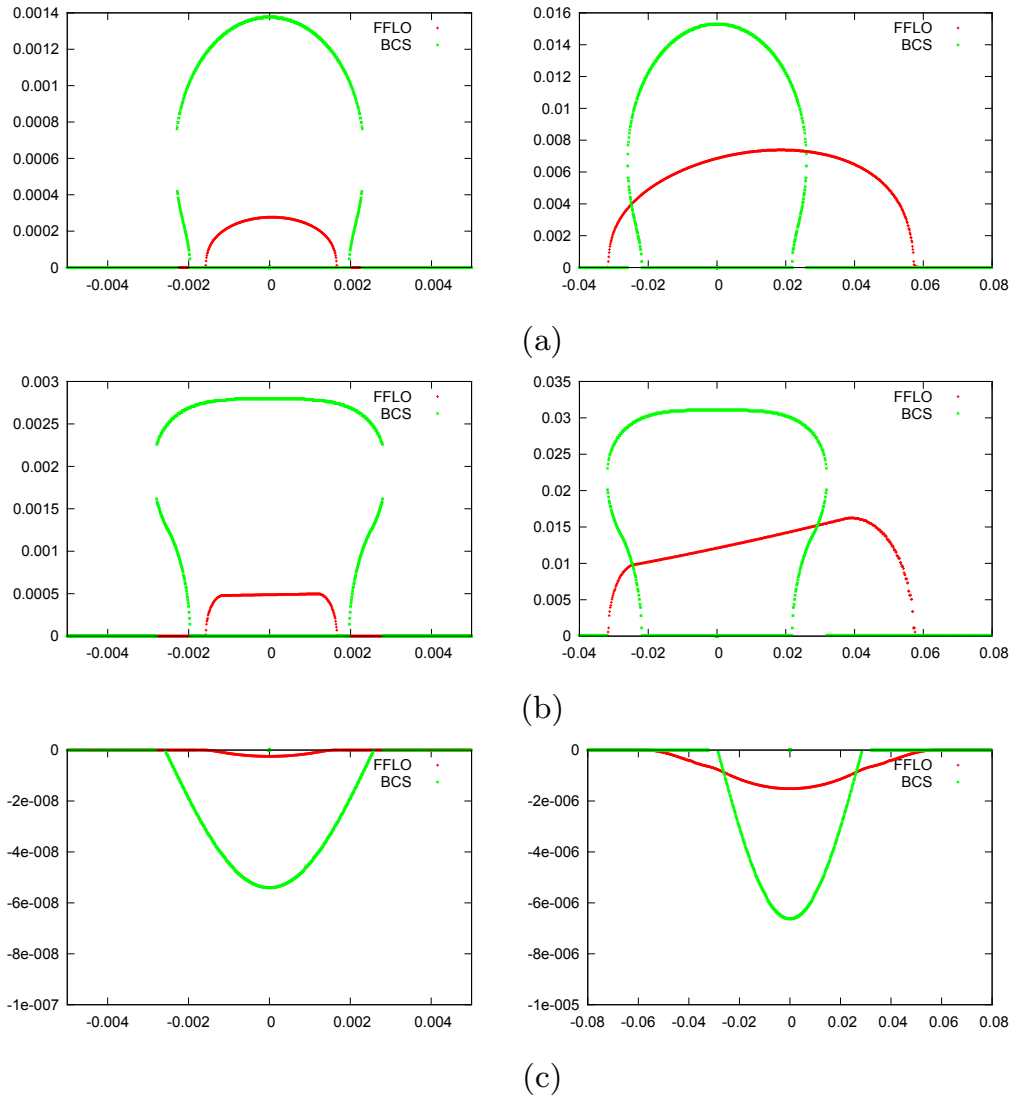

Figure 6.1: Plots for critical temperature 6.1a, order parameter 6.1b and free energy 6.1c in a superconducting Weyl metal as functions of the inversion symmetry breaking parameter λ in the cases of weak (left) and strong (right) coupling. The parameters we choose are $b = 10.0$, $\Delta_S = 7.8$, $\Delta_D = 2.6$, $\mu = 0.5$, $\omega_D = 0.15$. We choose $U = 30$ for the case weak coupling and $U = 60$ for the strong coupling. For simplicity we take $v_\perp = 1$ and $d = 1$.

In this equation the last term is present only if the expression entering the root is positive.

In the case of linear dispersion, we have $\delta_k = \delta_{-k}$, and thus we can find the expression for order parameter analytically:

$$\Delta = w_D \exp\left\{-\frac{\frac{1}{2U} + \int \frac{dk}{(2\pi)^3}\delta(\xi_k)|\gamma|^2 \log|\gamma|}{\int \frac{dk}{(2\pi)^3}\delta(\xi_k)|\gamma|^2}\right\}. \tag{6.17}$$

Similarly to the problem of critical temperature, we can compute the order parameter explicitly in the FFLO and BCS cases. Specifically, in the FFLO case, i.e. at $q = Q$, the Eq. (6.17) can be evaluated as:

$$\Delta = 2w_D \exp\left\{-\frac{4\pi^2 v_F^2 v_z}{\mu^2 U}\right\}, \tag{6.18}$$

whereas in the BCS case, the Eq.(6.17) takes the form:

$$\Delta = w_D \exp\left\{-\frac{3\pi^2 v_F^2 v_z}{\mu^2 U} + \frac{5}{6}\right\}. \tag{6.19}$$

Similarly to the critical temperature, in the case of broken inversion symmetry, the order parameter cannot be found analytically. However, we can simplify the gap equation (6.16) in a way, similar to the Sec. 6.3.1 and solve it numerically. Simplified equation in the FFLO case has the form:

$$\frac{1}{U} = \frac{(\tilde{\mu}^2}{2(2\pi)^2 v_\perp^2 v_z}\int \sin\theta d\theta \left\{\log\left(\frac{2w_D}{|\Delta|}\right) - \operatorname{arcsh}\left(\sqrt{\left(\frac{\Lambda\tilde{\mu}\cos\theta}{v_z|\Delta|}\right)^2 - 1}\right)\right\},$$

and, analogously, in the BCS case, the equation for Δ is written as:

$$\frac{1}{U} = \frac{\mu^2}{(2\pi)^2 v_\perp^2 v_z}\int \sin^3\theta d\theta \left\{\log\left(\frac{2w_D}{|\Delta||\sin\theta|}\right) - \operatorname{arcsh}\left(\sqrt{\left(\frac{\Lambda(Q + \frac{\mu}{v_z}\cos\theta)}{|\Delta|\sin\theta}\right)^2 - 1}\right)\right\}$$

Its numerical solutions are shown on the Fig. 6.1b. As in the case of critical temperature, in the presence of inversion symmetry, BCS pairing has larger magnitude than FFLO. However, at sufficient inversion symmetry breaking, and coupling strength, it is possible, that FFLO pairing exists, whereas BCS does not.

6.5 Free energy of superconducting state

In this section, we compute free energy of the possible superconducting states, that can arise in Weyl metals. This is of interest, because its expression makes it possible to figure out, which state in more favorable, and thus can be practically realized. Indeed, the more favorable is the state, which has lower free energy.

We start from a known thermodynamical relationship between free energy and partition function:

$$F = -\frac{1}{\beta}\log Z.$$

We use this equation to compute free energy in the mean field approximation, i.e. assuming that the partition function is equal to exponent of the action computed at the saddle point, i.e. at the classical field configuration. It is known, that negative exponent is mainly contributed from the point, where its argument, i.e. the action, takes the smallest possible value, which, in turn, happens on the classical field solutions.

By taking mean-field approximation of the partition function (6.6), and rewriting it in terms of energies of the Bogoliubov quasiparticles (eq. 6.8), we obtain the following expression for the free energy:

$$F(q) = -\frac{1}{\beta}\sum_k \log\left(\frac{(-iw+\mathcal{E}_+)(iw+\mathcal{E}_-)}{4}\right) + \frac{2V}{U}|\Delta(2q)|^2 - \sum_k \frac{iw-\xi_k}{2\beta}.$$

However, we are interested in change of free energy due to superconductivity. For this reason, we consider difference between free energies in superconducting and normal regimes at zero temperature, which we write as:

$$\frac{F_{sq}(q)-F_n(q)}{V} = -\int \frac{d^3kdw}{(2\pi)^4}\log\left(\frac{(-iw+\mathcal{E}_+)(iw+\mathcal{E}_-)}{(-iw+\xi_{q+k})(iw+\xi_{q-k})}\right) + \frac{2}{U}|\Delta(2q)|^2,$$

or equivalently as:

$$\begin{aligned}&\frac{F_{sq}(q)-F_n(q)}{V}\\ =\;& \frac{2}{U}|\Delta(2q)|^2 - \frac{1}{2}\int \frac{d^3kdw}{(2\pi)^4}\log\left(\frac{w^2+\mathcal{E}_+^2}{w^2+\xi_{q+k}^2}\right) - \frac{1}{2}\int \frac{d^3kdw}{(2\pi)^4}\log\left(\frac{w^2+\mathcal{E}_-^2}{w^2+\xi_{q-k}^2}\right).\end{aligned}$$

We can simplify it by integrating over the Matsubara frequency w, thus rewriting it as:

$$\frac{F_{sq}(q) - F_n(q)}{V} = \frac{2}{U}|\Delta(2q)|^2 - \frac{1}{2}\int \frac{d^3k}{(2\pi)^3}\left(|\mathcal{E}_+| + |\mathcal{E}_-| - |\xi_{q+k}| - |\xi_{q-k}|\right). \tag{6.20}$$

This equation has a clear physical meaning: the fact, that energies of Bogoliubov quasiparticles are larger than energies of free excitations, leads to the decrease of free energy. However, there is also a positive contribution due to superconducting order parameter Δ, and superconductivity appears, when the latter is smaller than the former.

We would like to compute free energy explicitly in our model. After assuming that the dispersion is linear, we can take $\xi_{q+k} \approx \xi_{q-k}$, and thus simplify the free energy as:

$$\mathcal{F}(q) = \frac{F_{sq}(q) - F_n(q)}{V} = \frac{2}{U}|\Delta(2q)|^2 - \int \frac{d^3k}{(2\pi)^3}\left(|\mathcal{E}| - |\xi|\right). \tag{6.21}$$

We can also transform it by using the gap equation (6.15), which, in the case of linear dispersion, can be simplified as:

$$\frac{1}{U} = \int \frac{dk}{(2\pi)^3}\frac{|\gamma|^2}{|\mathcal{E}|}.$$

If we substitute it into the equation for free energy (6.21), we obtain:

$$\mathcal{F}(q) = \int \frac{dk}{(2\pi)^3}\left(\frac{2|\gamma|^2|\Delta|^2}{|\mathcal{E}|} - |\mathcal{E}| + |\xi|\right).$$

By using the relation between the energies of electrons and Bogoliubov quasiparticles: $|\mathcal{E}| = \sqrt{\xi^2 + 4|\gamma|^2|\Delta|^2}$, the free energy can be simplified as:

$$\mathcal{F}(q) = -\int \frac{dk}{(2\pi)^3}\frac{(|\mathcal{E}| - |\xi|)^2}{2|\mathcal{E}|}.$$

Further, we compute the integral entering the last equation. We assume that $|\xi| < w_D << \mu$, and take the leading order over $|\xi|/\mu$. In both FFLO and BCS cases, the integral is performed over both

Fermi surfaces. We obtain that, in the FFLO case, the free energy (for the both nodes) has the form:

$$\mathcal{F} = -\frac{\mu^2}{\pi^2 v_F^2 v_z}\left(w_D\sqrt{w_D^2+\Delta^2} - w_D^2\right),$$

and its leading term over Δ/w_D is expressed as:

$$\mathcal{F} \approx -\frac{\mu^2\Delta^2}{2\pi^2 v_F^2 v_z}. \tag{6.22}$$

Similarly, in the BCS case, the free energy has the form:

$$\mathcal{F} = -\frac{2\mu^2}{(2\pi)^2 v_F^2 v_z}\left(\frac{(w_D^2+\Delta^2)w_D}{\Delta}\arctan\left(\frac{\Delta}{w_D}\right) - w_D^2\right),$$

and its expansion over Δ/w_D gives:

$$\mathcal{F} \approx -\frac{\mu^2\Delta^2}{3\pi^2 v_F^2 v_z}. \tag{6.23}$$

By substituting the previously obtained expressions for the order parameter Δ (6.18, 6.19) into the free energies (6.22, 6.23) and comparing the obtained expressions, we can see that $F_{BCS} < F_{FFLO}$. This is an important physical result, which implies that zero momentum BCS pairing is energetically more favorable than finite momentum FFLO state.

Finally, we are interested in the expression for free energy in the inversion symmetry breaking case. In this case, simplifying its expression (6.20) by using the gap equation gives the following expression:

$$\begin{aligned}\mathcal{F} = |\Delta|^2 \int \frac{d^3k}{(2\pi)^3}\frac{1}{\mathcal{E}_+ + \mathcal{E}_-}\left(1-\theta(-\mathcal{E}_-)-\theta(-\mathcal{E}_+)\right)\\ -\frac{1}{2}\int\frac{d^3k}{(2\pi)^3}\left(|\mathcal{E}_+|+|\mathcal{E}_-|-|\xi_{q-k}|-|\xi_{q+k}|\right).\end{aligned}$$

We treat it further in a similar way to the critical temperature and order parameter, considered in the Secs. 6.3.1 and 6.4. Specifically, we approximate the energy spectrum according to the Eq. 6.13, and perform integration over magnitude of the momentum.

In the FFLO case, free energy per one node can be written as:

$$\mathcal{F}(Q) = \frac{\tilde{\mu}^2}{(2\pi)^2 v_\perp^2 v_z} \int dp \sin\theta d\theta \left\{ \frac{|\Delta|^2}{2\sqrt{p^2+\Delta^2}} - \frac{|\Delta|^2}{\sqrt{p^2+\Delta^2}} \theta \left(\frac{\Lambda\tilde{\mu}\cos\theta}{v_z} - \sqrt{p^2+\Delta^2} \right) \right.$$
$$\left. - \left| -\frac{\Lambda\tilde{\mu}\cos\theta}{v_z} + \sqrt{p^2+\Delta^2} \right| + \left| p - \frac{\Lambda\tilde{\mu}\cos\theta}{v_z} \right| \right\},$$

and, after evaluation of the integrals (under assumption $\frac{|\Lambda|\mu}{v_z} < w_D$),
it takes the form:

$$\mathcal{F}(Q) = -\frac{\tilde{\mu}^2}{2\pi^2 v_\perp^2 v_z} \left(w_D \sqrt{w_D^2+\Delta^2} - w_D^2 - \frac{\Lambda^2\tilde{\mu}^2}{3v_z^2} \right), \quad \text{if} \quad \frac{|\Lambda|\mu}{v_z} < |\Delta|$$

$$\mathcal{F}(Q) = -\frac{\tilde{\mu}^2}{2\pi^2 v_\perp^2 v_z} \left(w_D \sqrt{w_D^2+\Delta^2} - w_D^2 \right.$$
$$\left. - \frac{\Lambda^2\tilde{\mu}^2}{3v_z^2} + \frac{v_z}{3|\Lambda|\mu} \left(\left(\frac{\Lambda\mu}{v_z} \right)^2 - \Delta^2 \right) \right), \quad \text{if} \quad \frac{|\Lambda|\mu}{v_z} > |\Delta|$$

In the BCS case, free energy can be written as:

$$\mathcal{F}(0) = \frac{\mu^2}{(2\pi)^2 v_\perp^2 v_z} \int dp \sin\theta d\theta \left\{ \frac{|\Delta|^2 \sin^2\theta}{\sqrt{p^2+|\Delta|^2\sin^2\theta}} \right.$$
$$\left(1 - \theta \left(\Lambda Q + \frac{\Lambda\mu}{v_z}\cos\theta - \sqrt{p^2+|\Delta|^2\sin^2\theta} \right) - \theta \left(-\Lambda Q - \frac{\Lambda\mu}{v_z}\cos\theta - \sqrt{p^2+|\Delta|^2\sin^2\theta} \right) \right)$$
$$- \left| -\Lambda Q - \frac{\Lambda\mu}{v_z}\cos\theta + \sqrt{p^2+|\Delta|^2\sin^2\theta} \right| - \left| \Lambda Q + \frac{\Lambda\mu}{v_z}\cos\theta + \sqrt{p^2+|\Delta|^2\sin^2\theta} \right|$$
$$\left. + \left| p - \Lambda Q - \frac{\Lambda\mu}{v_z}\cos\theta \right| + \left| p + \Lambda Q + \frac{\Lambda\mu}{v_z}\cos\theta \right| \right\}.$$

and after evaluating the integral over p, it takes the form:

$$\mathcal{F}(0) = -\frac{\mu^2}{2\pi^2 v_\perp^2 v_z} \int \sin\theta d\theta \left\{ w_D \sqrt{w_D^2+\Delta^2\sin^2\theta} - w_D^2 \right.$$
$$\left. - \left(\Lambda Q + \frac{\Lambda\mu}{v_z}\cos\theta \right)^2 + \left| \Lambda Q + \frac{\Lambda\mu}{v_z}\cos\theta \right| \sqrt{\left(\Lambda Q + \frac{\Lambda\mu}{v_z}\cos\theta \right)^2 - \Delta^2\sin^2\theta} \right\}.$$

We use these complicated expressions to evaluate the free energies numerically, and we present the resulting graphs on the Fig.

6.1c. Our conclusions are similar to the problem of critical temperature: at the inversion symmetric case, zero momentum BCS state is always energetically more favorable, than the FFLO. However, as the inversion symmetry gets broken, two scenarios are possible. At weak pairing, BCS state is still always energetically more favorable than FFLO, but with the growing asymmetry, it disappears. However, at sufficiently strong pairing, it is possible, that in the certain range of the inversion symmetry breaking parameter, FFLO state becomes more energetically favorable than BCS.

We note that our results have a clear physical meaning. We have obtained that BCS state is energetically more favorable, which is consistent with the fact, that electrons at opposite momenta have exactly same energies due to inversion symmetry. In contrast, electrons in the opposite sides of one Weyl cone are not forced to have equal energies, and thus it is natural to expect, that pairing between them is less favorable. Once inversion symmetry gets broken, Weyl cones shift their energies, so that electrons with opposite momenta have different energies, and thus their pairing is less favorable. After this shift, it is possible, that electrons in the opposite parts of one Weyl cone are less separated in energy space, than electrons in the different Weyl cones.

6.6 Energies of superconducting excitations

In this section, we are interested in energy spectrum of excitations above the superconducting state. From now on, we assume that the underlying normal Weyl metal is described by two-band Hamiltonian (6.2), and assume that BCS superconductivity with zero momentum of the Cooper pairs is created. We neglect the factor Ξ, and, for our purposes, it is not important, whether superconductivity is intrinsic or extrinsic.

We write the Hamiltonian of normal state in component form as:

$$H = \begin{pmatrix} m-\mu & k_2+ik_1 \\ k_2-ik_1 & -m-\mu \end{pmatrix}. \tag{6.24}$$

After we add superconducting pairing and introduce Nambu spinor:

$$\psi = \begin{pmatrix} c_{k\uparrow} & c_{k\downarrow} & c^+_{-k\downarrow} c^+_{-k\uparrow} \end{pmatrix}^T, \tag{6.25}$$

we write the total Hamiltonian as:

$$H = \begin{pmatrix} m-\mu & k_2+ik_1 & \Delta & 0 \\ k_2-ik_1 & -m-\mu & 0 & -\Delta \\ \Delta & 0 & m+\mu & k_2+ik_1 \\ 0 & -\Delta & k_2-ik_1 & -m+\mu \end{pmatrix}. \tag{6.26}$$

This Hamiltonian can be diagonalized analytically, and its four eigenstates have energies $\pm E_+$ and $\pm E_-$ defined as:

$$E_\pm = \sqrt{k^2+m^2+\mu^2+\Delta^2 \pm 2\sqrt{\Delta^2 m^2 + (k^2+m^2)\mu^2}}. \tag{6.27}$$

A special limit is zero chemical potential μ. In this case, the energies can be rewritten as:

$$E_\pm = \sqrt{k^2 + (m \pm \Delta)^2}.$$

Its physical meaning is that, in the presence of superconductivity, each Weyl cone splits into two cones, and their separation is proportional to the magnitude of the superconducting order parameter Δ.

6.7 Electromagnetic response in superconducting Weyl metal

6.7.1 Effective action

In this section, we would like to study electromagnetic response in our model of superconducting Weyl metal. Our final goal is to compute its anomalous Hall conductivity. We start from quantum mechanical partition function with the action for superconducting electrons interacting with electromagnetic field, which is written as:

$$\begin{aligned} -S &= \int d\tau c^+ \partial_\tau c - H + \mu N \\ &= \sum_k \begin{pmatrix} c^+_{k\uparrow} & c^+_{k\downarrow} \end{pmatrix} \begin{pmatrix} iw-m+\mu & -k_2-ik_1 \\ -k_2+ik_1 & iw+m+\mu \end{pmatrix} \begin{pmatrix} c_{k\uparrow} \\ c_{k\downarrow} \end{pmatrix} \\ &-e\sum_{k,p} \begin{pmatrix} c^+_{k+p\uparrow} & c^+_{k+p\downarrow} \end{pmatrix} \begin{pmatrix} iA_0 & -A_2-iA_1 \\ -A_2+iA_1 & iA_0 \end{pmatrix} \begin{pmatrix} c_{k\uparrow} \\ c_{k\downarrow} \end{pmatrix} \\ &-\Delta e^{2i\theta} \sum_k c^+_{k\uparrow} c^+_{-k\downarrow} - \Delta e^{-2i\theta} \sum_k c_{-k\downarrow} c_{k\uparrow}. \end{aligned} \tag{6.28}$$

Here, we have included the Hamiltonian of Weyl metal (Eq. 6.24), added interaction with electromagnetic field via Pierls substitution $k \to k - eA$, and introduced superconducting pairing Δ. We have added phase fluctuations θ of the superconducting order parameter, which occur due to the electromagnetic field, but they can be removed by gauge transformation of the fermion operators, $c \to e^{i\theta}c$, and the vector potential $A_\mu \to A_\mu - ip_\mu A_\mu$.

After we introduce Nambu spinors (6.25), we can rewrite the action as:

$$-S = \sum_k \psi^+ (G^{-1} + H_A)\psi,$$

where the superconducting Green function G is defined as:

$$G = (iw - H_0)^{-1}, \tag{6.29}$$

and H_0 is the Hamiltonian of the Nambu spinors (6.26).

The Hamiltonian describing electromagnetic interaction can be written in two blocks:

$$H_A = \begin{pmatrix} h_A & 0 \\ 0 & -h_A \end{pmatrix}, \tag{6.30}$$

and each block has an expression:

$$h_A = \begin{pmatrix} iA_0 & -A_2 - iA_1 \\ -A_2 + iA_1 & iA_0 \end{pmatrix}.$$

To proceed with the calculations, we have to write the Green function (6.29) explicitly, i.e. invert the matrix $iw - H$. After long calculations, we find it convenient to write the answer in terms of 2×2 blocks:

$$G = \begin{pmatrix} G_e & \tilde{G}_\Delta \\ G_\Delta & G_h \end{pmatrix}, \tag{6.31}$$

which have the following explicit expressions:

$$\det(G^{-1})G_\Delta$$
$$= \Delta\left(2imw + 2(k_2 m - ik_1\mu)\sigma_1 + 2(-k_1 m - ik_2\mu)\sigma_2 - (\mu^2 + \Delta^2 + k^2 + w^2 - m^2)\right)$$

$$\det(G^{-1})\tilde{G}_\Delta$$
$$= \Delta\left(2imw + 2(k_2 m + ik_1\mu)\sigma_1 + 2(-k_1 m + ik_2\mu)\sigma_2 - (\mu^2 + \Delta^2 + k^2 + w^2 - m^2)\right)$$

$$\det(G^{-1})G_e$$
$$= \Delta^2(\mu - iw) - k_2\sigma_1(\Delta^2 + k^2 + m^2 - (\mu - iw)^2) + k_1\sigma_2(\Delta^2 + k^2 + m^2 - (\mu - iw)^2)$$
$$+m\sigma_3(\Delta^2 - k^2 - m^2 + (\mu - iw)^2)$$

$$\det(G^{-1})G_h$$
$$= \Delta^2(\mu + iw) - k_2\sigma_1(\Delta^2 + k^2 + m^2 - (\mu + iw)^2) + k_1\sigma_2(\Delta^2 + k^2 + m^2 - (\mu + iw)^2)$$
$$+m\sigma_3(\Delta^2 - k^2 - m^2 + (\mu + iw)^2)$$

The determinant entering these equations is given by:

$$\det(G^{-1})$$
$$= \Delta^4 + 2\Delta^2(k^2 + w^2 + \mu^2 - m^2) + (k^2 + m^2 - \mu^2)^2 + 2w^2(k^2 + m^2 + \mu^2) + w^4.$$

Further, we proceed with the calculations in a way similar to the Sec. 2.4. Specifically, we have to consider quadratic contribution to the effective action for the electromagnetic field, which is given by:

$$S^{(2)} = \sum_{k,p} \frac{e^2}{2} \mathrm{tr}\left(G(k)H_A(-p)G(k+p)H_A(p)\right).$$

We transform this equation by decomposing the Green function G and the interaction Hamiltonian H_A into 2×2 blocks, and writing their explicit expressions given by the Eqs. 6.31 and 6.30. While performing the calculations, we have to take traces of Pauli matrices. We note, that it is convenient to do by introducing four-dimensional sigma-matrices as: $\sigma_\mu = (1, \sigma_\mu)$, $\bar{\sigma}_\mu = (1, -\sigma_\mu)$, and using the relation:

$$\mathrm{tr}\sigma_\mu\bar{\sigma}_\nu\sigma_\rho\bar{\sigma}_\sigma = 2\left(\eta_{\mu\nu}\eta_{\rho\sigma} - \eta_{\mu\rho}\eta_{\nu\sigma} + \eta_{\mu\sigma}\eta_{\nu\rho}\right) + 2i\epsilon_{\mu\nu\rho\sigma},$$

where $\eta_{\mu\nu}$ is a Minkovski metric tensor equal to $\mathrm{diag}(1, -1, -1, -1)$.

Since the total effective action contains a lot of terms, which would be too difficult to write explicitly, we have to select the terms, which contribute to the anomalous Hall conductivity, that we are interested in. We notice, that the anomalous Hall conductivity arises due to Chern-Simons term $\epsilon_{\mu\nu\lambda}k_\mu A_\nu A_\lambda$. Its main feature is that it is *odd* under time-reversal symmetry, which distinguishes it from conventional electromagnetic action $F^2_{\mu\nu}$, or massive electromagnetic term $m^2A^2_\mu$ (the latter is responsible for Meissner effect in superconductors, i.e. exponential decay of the electromagnetic field), which both are even under time reversal. Thus, if we are interested in the anomalous Hall conductivity, we can select only terms, which are odd under time reversal symmetry. Such terms entering the second-order quantum effective action are the following:

$$\begin{aligned}
&\frac{1}{2e^2}\mathrm{det}G^{-1}(k)\mathrm{det}G^{-1}(q)S^{(2)} = \text{even terms} \qquad (6.32)\\
+\;& 2\mu^2(m_k - m_q)\left[(\Delta^2 - k_\mu^2 - m_k^2 + \mu^2)w_q + w_k(\Delta^2 - q_\mu^2 - m_q^2 + \mu^2)\right]\\
&\quad\times(A_1(-p)A_2(p) - A_2(-p)A_1(p))\\
+\;& \epsilon_{\mu\nu\lambda}k_\mu A_\nu(-p)A_\lambda(p)\left[-m_q(\Delta^2 - q_\mu^2 - m_q^2 + \mu^2)(\Delta^2 + k_\mu^2 + m_k^2 - \mu^2)\right.\\
&\left.-4\mu^2 m_q w_k w_q + 2\Delta^2(\Delta^2 + q_\mu^2 + \mu^2 - m_q^2)m_k\right]\\
+\;& \epsilon_{\mu\nu\lambda}q_\mu A_\nu(-p)A_\lambda(p)\left[m_k(\Delta^2 - k_\mu^2 - m_k^2 + \mu^2)(\Delta^2 + q_\mu^2 + m_q^2 - \mu^2)\right.\\
&\left.+4\mu^2 m_k w_k w_q - 2\Delta^2(\Delta^2 + k_\mu^2 + \mu^2 - m_k^2)m_q\right]
\end{aligned}$$

For shortness, here we have introduced the momentum $q = k+p$. In addition, to simplify this expression, we have made a replacement of momenta: $k \leftrightarrow q, p \leftrightarrow -p$.

Next, we have to simplify this effective action. We start from integrating out the fluctuations of the superconducting order parameter, and afterwards, we perform Matsubara frequency summation and momentum integration.

6.7.2 Integration of the superconducting phase

As we mentioned in the beginning, external electromagnetic field results in the order parameter Δ having arbitrary space (or equivalently momentum) dependent phase $e^{2i\theta}$. We performed gauge transformation of the action (6.28), which removed the phase dependence from the order parameter. As a result, we obtained effective action for the electromagnetic field, which enters in a combination with the

phase gradient: $A_\mu(p) - ip_\mu\theta$. In other words, we have obtained an action, which generally can be written as:

$$S = \sum_p \left(A_\mu(-p) + ip_\mu\theta(-p)\right) Q_{\mu\nu}(p) \left(A_\mu(p) - ip_\mu\theta(p)\right)$$

Since the superconducting order parameter is a quantum field, we have to integrate out its phase fluctuation explicitly (this method has been previously used in the context of chiral p-wave superconductor [78]). If we do it, we obtain effective action of pure electromagnetic field:

$$S = \sum_p A_\mu(-p) K_{\mu\nu} A_\nu(p).$$

Here, the new operator $K_{\mu\nu}$ is related to the old operator $Q_{\mu\nu}$ as:

$$K_{\mu\nu} = Q_{\mu\nu} - \frac{Q_{\mu\rho}p_\rho p_\sigma Q_{\sigma\nu}}{Q_{\alpha\beta}p_\alpha p_\beta} \tag{6.33}$$

Now, we would like to understand the consequences of this equation. The most general momentum expansion of $Q_{\mu\nu}$ consistent with rotational symmetry is:

$$\begin{aligned} Q_{00} &= Q^S_\Omega, \\ Q_{0i} &= Q^S_{\Omega p} p_i + \epsilon_{0ij} p_j Q^A_p, \\ Q_{ij} &= Q^S_p \delta_{ij} + \Omega \epsilon_{0ij} Q^A_\Omega. \end{aligned}$$

Explicitly, we have decomposed the tensor $Q_{\mu\nu}$ into symmetric and antisymmetric parts, and used the fact, due to rotational symmetry, spatial indices can originate only from the vector field momentum - the only vector available. We can substitute these decompositions into the Eq. (6.33), and thus obtain general form of the operators $K_{\mu\nu}$:

$$\begin{aligned} K_{0i} &= \frac{-Q^S_\Omega Q^S_p \Omega p_i + Q^S_p Q^A_p \epsilon_{0ij} p_j p^2 + Q^S_\Omega Q^A_\Omega \epsilon_{0ij} p_j \Omega^2}{Q^S_\Omega \Omega^2 + Q^S_p p^2}, \\ K_{ij} &= \frac{1}{Q^S_\Omega \Omega^2 + Q^S_p p^2} \left\{ Q^S_p Q^S_\Omega \Omega^2 \delta_{ij} + (Q^A_p)^2 p^2 \delta_{ij} + Q^S_\Omega Q^A_\Omega \Omega^3 \epsilon_{0ij} \right. \\ &\quad + Q^S_p Q^A_\Omega \Omega p^2 \epsilon_{0ij} - (Q^S_p)^2 p_i p_j - Q^S_p Q^S_{p\Omega} \Omega p_i p_j \\ &\quad - Q^S_p (Q^A_p - Q^A_\Omega) \Omega p_i p_k \epsilon_{0jk} - Q^S_p Q^S_{\Omega p} \Omega p_i p_j \\ &\quad \left. - Q^S_p (Q^A_\Omega - Q^A_p) \Omega p_j p_l \epsilon_{0il} \right\}. \end{aligned}$$

Now we would like to use the fact, that our final goal is to compute anomalous Hall conductivity, which originates from the antisymmetric Chern-Simons term. For this reason, we are interested specifically in the antisymmetric contribution to the operators $K_{\mu\nu}$. It has the following explicit expression:

$$K^A_{0i} = \epsilon_{0ij} p_j \frac{Q^S_\Omega Q^A_\Omega \Omega^2 + Q^S_p Q^A_p p^2}{Q^S_\Omega \Omega^2 + Q^S_p p^2},$$
$$K^A_{ij} = \Omega \epsilon_{0ij} \frac{Q^S_\Omega Q^A_\Omega \Omega^2 + Q^S_p Q^A_p p^2}{Q^S_\Omega \Omega^2 + Q^S_p p^2}.$$

These equations can be greatly simplified in the limit $p \to 0$, i.e. in the case of spatially uniform electromagnetic field:

$$K^A_{0i} = \epsilon_{0ij} p_j Q^A_\Omega,$$
$$K^A_{ij} = \Omega \epsilon_{0ij} Q^A_\Omega. \tag{6.34}$$

We note, that we have to take the limit $p \to 0$ *before* taking the limit $\Omega \to 0$ because we are interested in a transport quantity (see [79] for details). We also note, that the equations (6.34) have the following physical meaning. If we compute Chern-Simons term, we may, in general, obtain different coefficients in front of $\Omega A_i A_j$ and $p_i A_0 A_j$. However, the Eq. 6.34 tells us, that anomalous Hall conductivity is determined specifically by the coefficient in front of $\Omega A_i A_j$.

6.7.3 Summation over momenta and frequencies

Now let us go back to the Eq. (6.32). In the last subsection, we have figured out, that we are interested only in the terms proportional to $\epsilon_{0ij} A_i A_j$. Also, since we take the limit $p \to 0$ before taking the limit $\Omega \to 0$, we need to select the terms, which do not vanish at $m_k = m_q$. Thus, we write the effective action (6.32) as:

$$\frac{1}{2e^2} \det G^{-1}(k) \det G^{-1}(q) S^{(2)} = \text{even terms} + \text{terms containing } A_0 \tag{6.35}$$
$$+8\epsilon_{0ij} A_i(-p) A_j(p) \left[m_q w_k^3 w_q^2 + w_k w_q^2 (m_q(\Delta^2 + k^2 + m_k^2 - \mu^2) + 2\Delta^2 m_k) \right.$$
$$-m_q(\Delta^2 - q^2 - m_q^2 + \mu^2) w_k^3 - 4\mu^2 m_q w_k^2 w_q$$
$$\left. -m_q(\Delta^2 - q^2 - m_q^2 + \mu^2)(\Delta^2 + k^2 + m_k^2 - \mu^2) + 2\Delta^2 m_k (\Delta^2 + q^2 + \mu^2 - m_q^2) \right]$$

As a next step, we have to perform the summation over Matsubara frequencies. To do it, we decompose determinant of the Green function as:

$$\det(G^{-1}) = (iw - iE_+)(iw + E_+)(iw - E_-)(iw + E_-),$$

where $E_\pm$ are energies of the excitations given by, Eq. (6.27). We can evaluate the Matsubara sum by using the method described in Sec. 2.4.3, i.e. by introducing the Fermi function $n_F(z)$, which poles are located at the Matsubara frequencies, and rewriting the sum as an integral over complex plane z. If we assume that the external spatial momentum, as well as the temperature, is zero, i.e. $k = q$, $m_k = m_q$, and consider the leading order over the external frequency $\Omega = w_q - w_k$, we obtain the following identities:

$$\begin{aligned}
\frac{1}{\beta}\sum \frac{w_k^3 w_q^2}{\det(G^{-1}(k))\det(G^{-1}(q))} &= -\frac{\Omega}{8(E_+ + E_-)^3} \\
\frac{1}{\beta}\sum \frac{w_k w_q^2}{\det(G^{-1}(k))\det(G^{-1}(q))} &= \frac{\Omega}{8E_+E_-(E_+ + E_-)^3} \\
\frac{1}{\beta}\sum \frac{w_k^3}{\det(G^{-1}(k))\det(G^{-1}(q))} &= -\frac{3\Omega}{8E_+E_-(E_+ + E_-)^3} \\
\frac{1}{\beta}\sum \frac{w_k^2 w_q}{\det(G^{-1}(k))\det(G^{-1}(q))} &= -\frac{\Omega}{8E_+E_-(E_+ + E_-)^3} \\
\frac{1}{\beta}\sum \frac{w_k}{\det(G^{-1}(k))\det(G^{-1}(q))} &= -\frac{\Omega(E_+^2 + E_-^2 + 3E_+E_-)}{8E_+^3E_-^3(E_+ + E_-)^3}
\end{aligned}$$

After we substitute them into the Chern-Simons term (6.35), we can simplify it and obtain:

$$\frac{2}{e^2}S^{(2)} = V\beta \int \frac{dk_z}{2\pi} \int \frac{d^2k}{(2\pi)^2} 4\epsilon_{0ij}\Omega A_i A_j \frac{m}{(E_+ + E_-)^3} \left\{1 + \frac{k^2 + m^2 - \mu^2 - \Delta^2}{E_+E_-}\right\}$$

The integral over the momentum perpendicular to the direction of the nodes can be computed by making change of variables

$$x = \sqrt{(k^2 + m^2)\mu^2 + m^2\Delta^2}$$

and multiplying the numerator and the denominator by the factor

$(E_+ - E_-)^3$. The resulting answer for the effective action is:

$$\begin{aligned} S^{(2)} &= 2V\beta e^2 \epsilon_{0ij}\Omega A_i A_j \int \frac{dk_z}{(2\pi)^2} m \\ &\times \left\{ -\frac{\Delta^2}{8\mu^3} \log\left(\frac{\mu|\sqrt{\mu^2+\Delta^2}+|m|| + |m|\sqrt{\mu^2+\Delta^2}+\mu^2}{\mu|\sqrt{\mu^2+\Delta^2}-|m|| + |m|\sqrt{\mu^2+\Delta^2}-\mu^2} \right) \right. \\ &\left. -\frac{\sqrt{\mu^2+\Delta^2}}{8\mu^2|m|} \left(|\sqrt{\mu^2+\Delta^2}-|m|| - |\sqrt{\mu^2+\Delta^2}+|m|| \right) \right\}. \end{aligned}$$

It can be simplified and rewritten as:

$$\begin{aligned} S^{(2)} &= \frac{1}{2} e^2 V\beta \epsilon_{0ij}\Omega A_i A_j \int \frac{dk_z}{(2\pi)^2} \\ \times & \quad \left\{ \mathrm{sign}(m) \left[1 + \frac{\Delta^2}{\mu^2} - \frac{\Delta^2|m|}{2\mu^3} \log\left(\frac{|m|+\mu}{|m|-\mu} \right) \right] \theta(|m| - \sqrt{\mu^2+\Delta^2}) \right. \\ & \left. \frac{m}{\mu} \left[\sqrt{1+\frac{\Delta^2}{\mu^2}} - \frac{\Delta^2}{2\mu^2} \log\left(\frac{\sqrt{\mu^2+\Delta^2}+\mu}{\sqrt{\mu^2+\Delta^2}-\mu} \right) \right] \theta(\sqrt{\mu^2+\Delta^2} - |m|) \right\}, \end{aligned}$$

which leads to the following answer for the anomalous Hall conductivity:

$$\begin{aligned} \sigma_{xy}^{SC} = \frac{e^2}{4\pi^2} \int_0^{\pi/d} dk_z & \left\{ \mathrm{sign}(m) \left[1 + \frac{\Delta^2}{\mu^2} - \frac{\Delta^2|m|}{2\mu^3} \log\left(\frac{|m|+\mu}{|m|-\mu} \right) \right] \theta(|m| - \sqrt{\mu^2+\Delta^2}) \right. \\ & \left. + \frac{m}{\mu} \left[\sqrt{1+\frac{\Delta^2}{\mu^2}} - \frac{\Delta^2}{2\mu^2} \log\left(\frac{\sqrt{\mu^2+\Delta^2}+\mu}{\sqrt{\mu^2+\Delta^2}-\mu} \right) \right] \theta(\sqrt{\mu^2+\Delta^2} - |m|) \right\} \end{aligned} \tag{6.36}$$

One can also see that, in the limit $\Delta = 0$, i.e. in the case of normal Weyl metal, the Hall conductivity is reduced to the familiar result obtained in the Ref. [28]:

$$\sigma_{xy}^{non-SC} = \frac{e^2}{4\pi^2} \int_0^{\pi/d} dk_z \left\{ \mathrm{sign}(m)\theta(|m|-\mu) + \frac{m}{\mu}\theta(\mu - |m|) \right\}. \tag{6.37}$$

An interesting property of the last equation is that, in the case, when $m(k_z)$ is linear, the anomalous Hall conductivity does not depend on chemical potential.

Now, if we look at the superconducting anomalous Hall conductivity (6.36) we can see, that in the limit $\Delta << \mu, |m|$, the difference between the integrands entering the Eqs.(6.36) and (6.37) is suppressed by a factor $\Delta^2/|m|^2$. This represents the expected fact, that contribution to the anomalous Hall conductivity from the states far from the Fermi surface does not differ in superconducting and non-superconducting cases. Therefore, the difference $\sigma_{xy}^{SC} - \sigma_{xy}^{non-SC}$ can be written as an integral over the range of k_z with $|m(k_z)| < \mu + \omega_D$. Furthermore, if we also assume that m is linear within the range of momentum integration, the latter becomes symmetric and the integrand becomes odd relative to the center of each Weyl cone. As a result, *in the regime, when m is linear over k_z, the difference $\sigma_{xy}^{SC} - \sigma_{xy}^{non-SC}$ vanishes.*

Thus, we conclude, that under the approximation of linear band dispersion, the value of anomalous Hall conductivity in Weyl metal is universal. It is neither affected by the presence of small chemical potential, nor by superconducting instability. By considering all four bands, which are relevant for the formation of the Weyl metal (see Ref. [28] for more details), one can see that the anomalous Hall conductivity is simply proportional to the distance between the Weyl points. Its deviation from this value can be created only by non-linear corrections to the band spectrum.

6.8 Model-independent calculation of anomalous Hall conductivity in a superconductor

Once we established that non-trivial anomalous Hall conductivity may exist in a superconductor, we may wonder, if it has a general expression, analogous to the TKNN formula, obtained in Sec. 2.4. In this section, we present an attempt to obtain such expression for an arbitrary multiband model with BCS pairing. We start from a general superconducting Hamiltonian:

$$h = c_\alpha^+ h_{\alpha\beta} c_\beta - \Delta c_{k\uparrow}^+ c_{-k\downarrow}^+ - \bar{\Delta} c_{-k\downarrow} c_{k\uparrow}, \tag{6.38}$$

where we assume summation over spin indices α, β. The term describing its interaction with electromagnetic field has the conven-

tional form, obtained by Pierls substitution:

$$h_A = -eA_\mu \frac{\partial h}{\partial k_\mu}.$$

Now, we would like to repeat the steps described in the Sec. 6.32.To do it, we introduce Nambu spinor: $\Psi(k) = (c_{k\uparrow}, c_{k\downarrow}, c^+_{-k\downarrow}, -c^+_{-k\uparrow})^T$ and rewrite the total Hamiltonian as:

$$\begin{aligned} H_{sc} &= \Psi^+(H_0 + H_A)\Psi, \\ H_0(k) &= \begin{pmatrix} h(k) - \mu & \Delta \\ \Delta & h(-k) + \mu \end{pmatrix}, \\ H_A(k) &= -eA_\mu \begin{pmatrix} \frac{\partial h(k)}{\partial k_\mu} & 0 \\ 0 & \frac{\partial h(-k)}{\partial k_\mu} \end{pmatrix}. \end{aligned}$$

As we have established previously, anomalous Hall conductivity is evaluated from Chern-Simons term, which, in turn, is obtained from the quadratic term of the effective action:

$$S_{eff} = \frac{1}{2}\mathrm{tr} G(\omega, k) H_A(-p) G(\omega + \Omega, k) H_A(p), \tag{6.39}$$

where $G(k)$ is Green function determined as: $G = (i\omega - H_0)^{-1}$. In the Sec. 2.4, we have evaluated this term by finding explicit expression for G, but now we take a different approach. Similarly to the Sec. 2.4, we write the Green function in terms of projectors to the eigenstates of the system as:

$$G(k) = \sum_s \frac{|z_s\rangle\langle z_s|}{iw - E_{ks}},$$

and substitute it into the effective action (6.39). After it, we perform the summation over Matsubara frequencies, thus rewriting the effective action in the form:

$$S_{eff} = \frac{\beta}{2} \sum_{ss'k} \langle z_s | H_A(-\Omega) | z_{s'} \rangle \langle z_{s'} | H_A(\Omega) | z_s \rangle \times \frac{n_F(E_{ks}) - n_F(E_{ks'})}{i\Omega + E_{ks} - E_{ks'}}.$$

By using the Eq. (6.39), and the relation between the effective actions before and after integrating over superconducting order parameter, one can see, that it leads to the following expression for

the Hall conductivity:

$$\sigma_{xy} = -\sum_{ss'k} \langle z_s | \frac{\delta H_A}{\delta A_x} | z_{s'} \rangle \langle z_{s'} | \frac{\delta H_A}{\delta A_y} | z_s \rangle \times \frac{n_F(E_{ks}) - n_F(E_{ks'})}{(E_{ks} - E_{ks'})^2}.$$

In the limit of zero temperature, the last equation can be rewritten as:

$$\sigma_{xy} = -e^2 \sum_k \sum_{\substack{s-filled \\ s'-empty}} \frac{1}{(E_{ks} - E_{ks'})^2} \tag{6.40}$$

$$\times \left\{ \langle z_s | \frac{\partial H_0}{\partial k_x} \tau_3 | z_{s'} \rangle \langle z_{s'} | \frac{\partial H_0}{\partial k_y} \tau_3 | z_s \rangle - \langle z_s | \frac{\partial H_0}{\partial k_y} \tau_3 | z_{s'} \rangle \langle z_{s'} | \frac{\partial H_0}{\partial k_x} \tau_3 | z_s \rangle \right\}.$$

This expression for the anomalous Hall conductivity is similar to the well-known TKNN formula. However, an important difference is the presence of the Pauli matrix τ_3 in Nambu space, which represents the fact that elementary excitations in a superconducting system do not have well-defined charge. The momentum summation in the last equation is taken over the half of the first Brillouin zone (e.g. $k_z > 0$), to avoid double counting caused by introducing Nambu spinors. However, if we consider the difference between the superconducting and non-superconducting anomalous Hall conductivity $\sigma_{xy}^{(SC)} - \sigma_{xy}^{(Non-SC)}$, the range of momentum summation can be limited only to the states affected by the presence of superconductivity, i.e. near half of the Fermi points/surfaces.

The equation for anomalous Hall conductivity (6.40) can be used to see explicitly, that, in any TRI system, total anomalous Hall conductivity is zero. Indeed, one can check that states connected with each other by TR transformation $z(k) \to i\sigma_2 z^*(-k)$ give opposite contribution to its explicit expression (6.40). In the considered model of Weyl metal, TRS is explicitly broken, which allows the total anomalous Hall conductivity to be non-zero. However, if we approximate energy spectrum of Weyl metal as linear, we find, that it obeys an approximate symmetry:

$$h(\vec{K} - \vec{k}) = -h(\vec{K} + \vec{k}), \tag{6.41}$$

which, in turn, implies that, in the low energy limit, Weyl metal possesses an analog of TRS taken not relative to the origin, but relative to the Weyl node:

$$z(\vec{K} + \vec{k}) \to i\sigma_2 z^*(\vec{K} - \vec{k}). \tag{6.42}$$

Now we would like to study the effect of this symmetry on the anomalous Hall conductivity. Let us write each term in the sum as $d\sigma_{xy}$, so that $\sigma_{xy} = \sum_k d\sigma_{xy}$, and consider the difference between anomalous Hall conductivities in superconducting and normal case: $\sigma_{xy}^{(SC)} - \sigma_{xy}^{(Non-SC)}$. Since such difference contains only low energy terms, it can be split between two Weyl cones:

$$\begin{aligned}
&\sigma_{xy}^{(SC)} - \sigma_{xy}^{(Non-SC)} \\
&= -e^2 \sum_{k_z>0} \sum_{\substack{s-filled \\ s'-empty}} \left(d\sigma_{xy}^{SC}(\vec{K}+\vec{k}, s, s') - d\sigma_{xy}^{non-SC}(\vec{K}+\vec{k}, s, s') \right) \\
&\quad + e^2 \sum_{k_z<0} \sum_{\substack{s-filled \\ s'-empty}} \left(d\sigma_{xy}^{SC}(\vec{K}-\vec{k}, s, s') - d\sigma_{xy}^{non-SC}(\vec{K}-\vec{k}, s, s') \right),
\end{aligned} \tag{6.43}$$

One can see, that in the approximation of linear energy spectrum near the node, two sums taken over the opposite parts of the Weyl cones exactly cancel each other. Thus, we conclude that the presence of the analog of TRS in the form of the Eq. (6.42), ensures that the difference between the Hall conductivities in superconducting and non-superconducting Weyl metal is zero. In general, this result holds if the states forming Cooper pairs, i.e. the states giving non-zero contribution to the $\sigma_{xy}^{(SC)} - \sigma_{xy}^{(Non-SC)}$ are located in the part of the BZ, where h is odd under the reflection relative to the node, i.e. $h(\vec{K}-\vec{k}) = -h(\vec{K}+\vec{k})$.

We also note, that this argument can be applied to multi-Weyl metals. In this case, the most general Hamiltonian still has the form (6.38) with its free part equal to: $H_0 = d_i\sigma_i$, and its components written as:

$$\begin{aligned}
h_{1,2} &= h_{1,2}(k_x, k_y), \\
h_3 &= m(k_z),
\end{aligned}$$

where the leading terms of $h_{1,2}$ have powers of k equal to the charge of the Weyl point (see [24] for the possible explicit expressions), and m is linear over k_z.

In the case of cubic band touching, the Hamiltonian still possesses the symmetry (6.41), and consequently still invariant under the transformations (6.42). Thus, the whole reasoning for the con-

ventional Weyl metals can be transferred to the Weyl metals with cubic band touching.

In the case of quadratic band touching, the Hamiltonian is no longer invariant under (6.41), and as a result, the Weyl cones are not invariant under the symmetry (6.42). However, one can consider a combination of the transformation (6.42) with rotation by $\pi/2$ in the xy plane. Indeed, the Hamiltonian for double-Weyl metals has a symmetry:

$$h(k_x, k_y, m) = -h(k_y, -k_x, -m),$$

which ensures invariance under transformations

$$z(k_x, k_y, m) \to i\sigma_2 z^*(k_y, -k_x, -m).$$

By applying the same argument as before, one can see that, in the case of the quadratic band touching, the result $\sigma_{xy}^{(SC)} - \sigma_{xy}^{(Non-SC)} = 0$ still holds in the low energy limit. Thus, we conclude that, in a double Weyl metal, independence of anomalous Hall conductivity on the presence of superconductivity occurs due to 'analog' of time reversal symmetry, which switches spin, but rotates momentum over cubic angle.

Chapter 7

Dirac metal

7.1 Basic concepts

Dirac metal is a material, which spectrum is described by four-component massless Dirac equation. Historically, Dirac equation in the form $H = \gamma_i k_i + m\gamma_0$ was first introduced to describe massive relativistic electrons. It has two double degenerate solutions with positive and negative energies. In the massless limit, Dirac equation can be decomposed into two Weyl equations with opposite chiralities.

In the condensed matter context, we are interested in the massless Dirac equation, because it describes gapless phases. Since, the massless Dirac equation can be decomposed into two Weyls, it is convenient to view each Dirac point as two copies of Weyl points with opposite chiralities. However, two such points would have the opposite monopole charges, and thus the resulting Dirac point will not be topologically protected. An example, illustrating this point, is a model of topological/normal insulator (see Sec. 3.6), where Dirac point is a critical point between Weyl metal and the insulating phases. Thus, to stabilize Dirac points, we need additional protection, which can be realized, for example, due to discrete rotational symmetry. In this sense, Dirac metal is similar to a double Weyl metal: in both of them, the Dirac/Weyl points are protected via the same mechanism: discrete rotational symmetry.

In the Ref. [52], the full classification of Dirac metals protected by the rotational symmetry was performed, and it was found, that they can be realized via a few possible Hamiltonians. We consider

one of them. Specifically, we write our Hamiltonian as:

$$H_0 = v_F k_x \Gamma_1 + v_F k_y \Gamma_2 + m(k)\Gamma_3 + \frac{\gamma k_z}{2}(k_y^2 - k_x^2)\Gamma_4 + \gamma k_z k_x k_y \Gamma_5 \quad (7.1)$$

If we neglect the factor γ, then the Hamiltonian consists of only three terms, and it can be decomposed into two copies of the Weyl Hamiltonians 3.15, describing one pair of Weyl points each. We choose representation of the gamma-matrices, which makes this decomposition explicit:

$$\Gamma_1 = \sigma_x \otimes s_z, \qquad \Gamma_2 = -\sigma_y, \qquad \Gamma_3 = \sigma_z,$$
$$\Gamma_4 = \sigma_x \otimes s_x, \qquad \Gamma_5 = \sigma_x \otimes s_y.$$

We note, that in contrast to Weyl metal, the Dirac Hamiltonian is invariant under both inversion and time-reversal symmetries, which is consistent with double degeneracy of the bands. If we view it as two copies of Weyl metals, we can say that, under time reversal, one copy gets transformed into the other.

However, the whole Hamiltonian 7.1 also contains two terms proportional to γ, which mix these Weyl copies. As a result, Dirac point can no longer be viewed as two copies of Weyl points, and therefore it is no longer topologically protected. As we will see later, this fact affects the surface states properties: at zero γ there are two copies of Fermi arcs, each of which is exactly same as in Weyl metal, but at non-zero γ, they hybridize with each other.

As we mentioned previously, Dirac points are protected by rotational symmetry. If one considers realistic material (e.g. Na_3Bi), and explore, how the Hamiltonian 7.1 arises in it, one can find that its true rotational symmetry generator along the z axis has the form: $C = (2 - \sigma_z) \otimes s_z$. In other, words, this Hamiltonian describes a model, such that valence electrons along the z axis have rotational eigenvalues $j = \pm 3/2$, but conduction electrons have rotational eigenvalues $\pm 1/2$. The fact, that conduction and valence electrons have different rotational eigenvalues explains, why the Dirac point is protected. Indeed, to gap the Dirac point out, one has to add a rotationally invariant term, that would be non-zero along the rotation axis, and would mix states from the opposite bands. Such term has to be proportional to phase of perpendicular momentum, and if we assume that the Hamiltonian is an analytic function, it has to contain at least linear powers of $k_\perp$, i.e. it cancels along the

rotation axis. Thus, we conclude that it is not possible to add to the Hamiltonian 7.1 a term, that would not break rotational symmetry, but would gap the Dirac points out.

7.2 Dirac metal and topological crystalline insulator

As we pointed out, the basic model of Dirac metal contains three symmetries: time reversal, inversion, and discrete rotational. However, the full crystal group of a material contains a lot of other symmetries. For instance, the full crystal group of Dirac metal Na_3Bi contains mirror symmetry along planes *along* the z axis, i.e. planes passing along Dirac points. We would like to explore the effects of such symmetry.

Specifically, we can add to the Hamiltonian 7.1 a term, which preserves such mirror symmetry, but breaks the rotational symmetry, thus gapping the Dirac points out. We write this term as:

$$H_1 = \Delta_1 k_z \Gamma_4. \tag{7.2}$$

This term breaks the rotational symmetry, because of non-trivial transformation of each wavefunction component. To ensure, that it preserves the mirror symmetry in xz plane, we write the latter explicitly as:

$$H(k_x, -k_y, k_z) = \mathcal{M} H(k_x, k_y, k_z) \mathcal{M}^{-1},$$

and note that its generator has the form:

$$\mathcal{M} = i\Gamma_2\Gamma_5. \tag{7.3}$$

As we mentioned previously, the term 7.2 breaks the rotational symmetry, and thus gaps the Dirac points out. As a result, the system described by the sum of Hamiltonians 7.1 and 7.2 is an insulator. We would like to explore its properties in more details.

The first question we can address, is whether the resulting system is a topological or normal insulator. Indeed, this question has a very simple answer. In the Ref. [64], it was demonstrated, that a system with inversion symmetry is a topological insulator, if a product of its inversion eigenvalues is different at different time reversal

invariant momenta within the Brillouin zone. By placing the total Hamiltonian on the lattice:

$$\begin{aligned} H_0 &= v_F \sin k_x \Gamma_1 + v_F \sin k_y \Gamma_2 + m(k)\Gamma_3 \\ &\quad +\gamma k_z(\cos k_x - \cos k_y)\Gamma_4 + \gamma k_z \sin k_x \sin k_y \Gamma_5, \\ H_1 &= \Delta_1 \sin k_z \Gamma_4, \end{aligned} \tag{7.4}$$

and checking its inversion symmetry eigenvalues explicitly, we can find out, that their product is indeed different. The system is a strong topological insulator, and thus its surface state spectrum contains two-dimensional Dirac cone centered at the Γ point (i.e. at the origin) of the Brillouin zone.

Now, we would like to explore the effects of mirror symmetry. We note that the Hamiltonian (7.4) commutes with the mirror symmetry operator (7.3) at the momenta lying in the mirror invariant plane, i.e. at $k_y = 0$. In this special case, the Hamiltonian (7.4) decouples into two 2×2 Hamiltonians with fixed mirror eigenvaues equal to ± 1. Each of these Hamiltonians has the form:

$$\begin{aligned} H_\pm &= v_F \sin k_x \tau_1 \pm m(k)\tau_3 \\ &\quad + (\gamma(1 - \cos k_x) + \Delta_1) \sin k_z \tau_2. \end{aligned} \tag{7.5}$$

Since these Hamiltonians are similar to a simple model of 2D Chern insulator, it is easy to compute their Chern numbers, using the method described in Sec. 4.2. We can find, that the filled bands of each of the Hamiltonians 7.5 have the Chern numbers $C = \pm \mathrm{sign}\Delta_1$. In other words, the bands with opposite mirror eigenvalues have the opposite Chern numbers. Thus, in the total system, the Chern numbers cancel out each other, but the system is still topologically non-trivial. Indeed, it can be characterized by *mirror Chern number* [80] defined as the difference between the Chern numbers for the bands with opposite mirror eigenvalues. Such kind of topological materials is known as *topological crystalline insulator* [15, 18].

However, even more interesting property of the system defined by the Hamiltonians 7.5 is that the Chern numbers change their signs, as the gap parameter Δ_1 changes sign. We remind, that $\Delta_1 = 0$ is the point, where the system becomes Dirac metal. Thus, we arrive to the conclusion, that *Dirac metal with two spatially separated Dirac points can be viewed as a critical point between two phases of topological crystalline insulators with different Chern numbers.*

7.3 Surface states in Dirac metal and topological crystalline insulator

In the previous section, we have established that Dirac metal is a critical point between two different topological crystalline insulators. Now, we would like to explore, how this fact affects the surface states. We can make all qualitative conclusions from the topological properties described in the previous section, and then check the results numerically.

First, the fact that system with non-zero gap Δ_1 is a topological insulator, implies that its surface spectrum contains two-dimensional Dirac cone localized at the center of the Brillouin zone.

Next, the fact that the system is a topological crystalline insulator, i.e. possess non-trivial Chern numbers in the mirror invariant plane $k_y = 0$, makes it possible to describe topological structure of the surface states at $k_y = 0$. Indeed, as we mentioned previously, the total Hamiltonian of the model consists of two blocks with Chern numbers ± 1 each. We know, that each block contains one chiral surface state of a given 'handedness' on each surface (i.e. it disperses either from left to right, or from right to left). As a result, the whole model contains a pair of two surface states of opposite 'handednesses'. These two states cross each other exactly at the point, where they have to form the Dirac cone, i.e. at $\vec{k} = 0$. We show their structure on the Fig. 7.1a.

As the gap parameter Δ_1 acquires the opposite sign, each Chern number, as well, change its sign. Thus, at the opposite side of the transition, surface states have the opposite 'handednesses' (see Fig. 7.1d). Now let us look at the transition point in more details. If γ were equal to zero, transition between these two phases would occur through the point, where the surface states spectrum is flat. We know this, because, at $\gamma = 0$, the system consists of two copies of Weyl metals, each of which possesses Fermi arcs with the spectrum $E = \pm v_f k_y$: in the mirror invariant plane $k_y = 0$ their energies would be equal to zero. However, this is no longer the case, when γ is non-zero. Indeed, this is numerically demonstrated on the plot of the surface states in Dirac metal, shown on the Fig. 7.1b.

At the transition point, the surface states have to meet two conditions: first, their 'handedness' has to change, and second, this change has to occur in such a way, that, at the critical point, their

Dirac velocity at $\vec{k} = 0$ has to remain non-zero. The first condition can be reformulated in a way, that if a surface state from one side of the transition terminate at one (conduction/valence) band, then, on the other side of the transition, it has to terminate at the opposite band (valence/conduction). Thus, at the critical point, i.e. in the Dirac metal, the surface state branches 'switch' the zones, where they terminate. This may happen only if the surface states in the Dirac metal terminate exactly at the gap closing point, i.e. at the Dirac points. This is an important physical conclusion: *surface states in Dirac metal terminate exactly at the Dirac points*, despite being not protected topologically, as in Weyl metal.

Now let us explore the structure of the surface states near the transition. We mentioned, that on one side (at $\Delta_1 > 0$), the surface states form a Dirac cone localized at the Brillouin zone center. As the gap closes, there appears additional degeneracies at the gap closing point, but the Dirac cone at $\vec{k} = 0$ persists. This Dirac point also persists slightly away from the critical point (see Fig. 7.1c), where it coexists with two other Dirac cones, which arise from the bulk Dirac points at the transition point. As $|\Delta|$ increases, these two Dirac points smoothly move towards the center of the Brillouin zone. Since they appear as degeneracies between two surface state branches with the opposite mirror eigenvalues, we can conclude that the two Dirac points, shown on the Fig. 7.1c, are protected by the mirror symmetry.

To check the mirror symmetry protection of the two surface Dirac points, we have introduced an additional term to the Hamiltonian:

$$H_2 = \Delta_2 \sin k_z \Gamma_5, \tag{7.6}$$

which breaks the mirror symmetry in xz plane, and plotted the resulting surface states. We presented our results on the Fig. 7.2. Indeed, we have found, that if the new gap parameter Δ_2 is kept constant while Δ_1 changes, then the gap never closes. Fig. 7.1c shows that the states at the origin of the Brillouin zone are still protected, but two other Dirac cones, which were protected by the mirror symmetry become gapped. Furthermore, we have found that the transition between two phases with positive/negative Δ_1 can be accomplished without gap closing (see Fig. 7.2). Indeed, we can take the state at $\Delta_1 > 0$, $\Delta_2 = 0$, make Δ_2 non-zero, then change Δ_1 from positive to negative, and eventually turn Δ_2 back

to zero. Such transition between two phases with different mirror Chern numbers would occur without gap closing. Thus, we confirm that the two topological phases, which exist away from the Dirac metal, are protected by the mirror symmetry. They are topologically distinguishable, when it is present, but become indistinguishable, once it is broken.

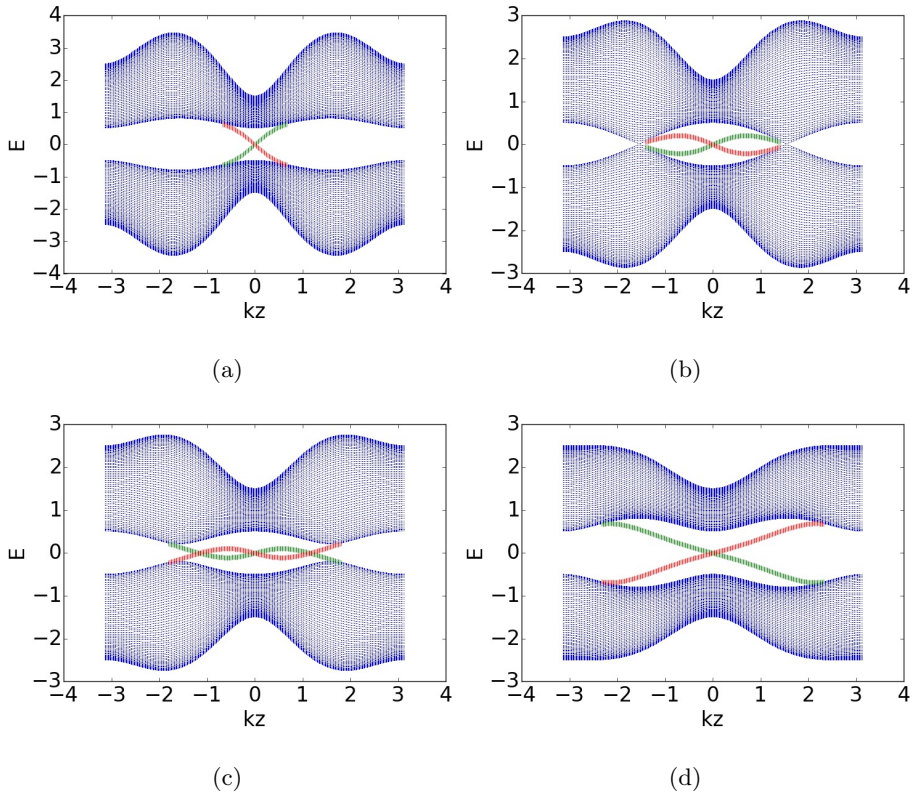

Figure 7.1: Dispersion structure of the model (7.5) at mirror eigenvalue +1. The values of Δ_1 are 0.8 (a), 0.0 (b), -0.2 (c), -0.8 (d). The parameters are: $v_F = 1.0$, $m = 0.5$, $b_{xy} = 0.5$, $b_z = 0.5$, $\gamma = 1.0$. Blue color refers to bulk states; Red and Green colors refer to surface states localized at the left and right boundary correspondingly. Surface states with a given mirror eigenvalue and localized at one surface have the same dispersion as states with the opposite mirror eigenvalue and localized at the opposite surface.

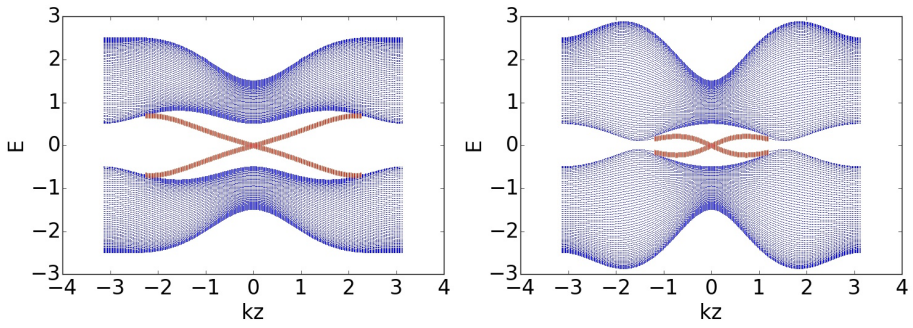

(a) (b)

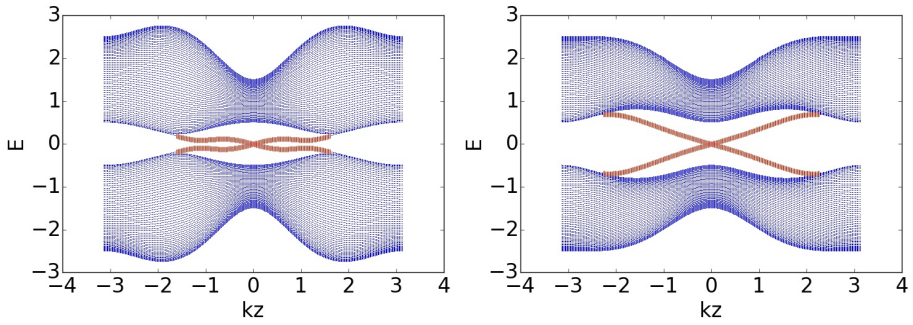

(c) (d)

Figure 7.2: Dispersion structure of the model (7.5) in the case of broken mirror symmetry. The values of Δ_1 are 0.8 (a), 0.0 (b), -0.2 (c), -0.8 (d). The parameters are: $v_F = 1.0$, $m = 0.5$, $b_{xy} = 0.5$, $b_z = 0.5$, $\gamma = 1.0$, $\Delta_2 = 0.1$.

Chapter 8

Conclusions

In this work, we have presented a general discussion about topological and superconducting properties of Weyl and Dirac metals. We have started from pedagogical revision of basic properties of Chern insulators, such as their Berry curvature and anomalous Hall effect. After it, we presented pedagogical introduction to Weyl metals, followed by a few problems solved by the author.

The first problem was to find surface states in Luttinger model. We found that Luttinger model without magnetic field possess two branches of surface states in the case, when bands disperse in the opposite directions. This is the case in the presence of particle-hole symmetry, as well as the case of its slight breaking. However, as particle-hole symmetry breaking increases, one of the surface state branches disappears. Eventually, the other surface state branch disappears too - it happens, when the bands start dispersing in the same directions. However, in this model, surface states are not protected topologically.

In the Luttinger model with external Zeeman field, quadratic band touching splits into four Weyl points.In other words, Luttinger model with external Zeeman field forms Weyl metal, and thus, similarly to any other Weyl metal, it possesses topological surface states forming Fermi arcs. More precisely, we found that such model possesses both topological and non-topological surface states. Interestingly, we found that in this model surface states disappear in a similar way to Luttinger model without magnetic field: they completely disappear, when the bands start dispersing in the same directions. However, we have also found a new feature, which

makes Luttinger model distinct from conventional topological materials. In conventional topological insulators, surface states disappear at critical points, where bulk bands touch each other. In contrast, in the Luttinger model, surface states may disappear if only the projections of the bulk bands touch each other, whereas the bulk bands still remain separated. We believe, that this is a new kind of topological phase transition, which may be relevant in all topological systems, where bands may disperse in different directions: for example, it may be Luttinger model, but it may also be type II Weyl metal, or any other related system.

We have also found that, in a given model, e.g. Luttinger model, under smooth change of parameters, signs of Weyl points charges may change. This is also a new form of topological phase transition, which would result in continuous gap closing in the whole range between the Weyl points, whose charge changes. It would be of interest to realize such transition experimentally, and to propose one possible scenario, we decided to consider a multilayer of different Weyl metals, where two thin layers from the opposite sides of the transition alternate with each other. Indeed, we have found that such multilayer possesses gapless states, which emerge as Bloch waves formed by Fermi arcs residing at each interface. We would like to note, that this scenario can be realized experimentally in many different ways. First, since there exist plenty of various semiconductors described by Luttinger model with different parameters, it seems natural to use them to create multilayer. Next, since Weyl points with spatially modulated separation can be created by applying spatially modulated Zeeman field, it is natural to search for these gapless states in a model of Weyl/Dirac metal accompanied by spin density wave, which in turn can be either intrinsic or extrinsic. Indeed, after completing this work, we have found that Dirac metals naturally host spin density waves. Finally, we would like to note, that since in such phase, there are in fact a lot of states at zero energy, it might be strongly modified by electron-electron interactions. For example, such gapless phase may be a new candidate for unconventional superconductivity or other strongly coupled phases.

We also studied the problem of possible superconducting instabilities in Weyl metal. We found that in a simple model of Weyl metal, where Weyl points are located at the same energies, conventional zero momentum pairing is more favorable that finite momen-

tum pairing (FFLO). However, after a few years since our results were published, there is still little evidence, that our predictions are correct. Only in a few materials with Weyl points, superconductivity was discovered at special conditions, e.g. high pressure. Despite that, we still think that there is a change to verify our predictions. Indeed, Weyl points may exist in a huge amount of materials: the only necessary constraint is breaking of time-reversal or inversion symmetries, and in fact, during the last few years, plenty of different Weyl metals were experimentally discovered. It is natural to seach for superconductivity in materials, where electron-electron coupling is as strong as possible, as well Fermi level and density of states are as large as possible. It is easy to see, that density of states is, in turn, larger in systems with larger Fermi velocities, and therefore it is natural to explore them. Finally, we note that it is natural, that intrinsic superconductivity has been discovered in type II Weyl metal: its Fermi pockets have larger area than Fermi spheres, and therefore it has higher density of states at Fermi level.

The last problem we considered was related to exploring surface states in Dirac metal. We started from considering mirror invariant planes connecting the Dirac points, which are present, as crystal symmetries, in Dirac metal Na_3Bi. We found that it is possible to break rotational symmetry protecting the Dirac points, while preserving such mirror symmetries. As a result, it is possible to gap the Dirac points out, thus converting the Dirac metal into a topological crystalline insulator. We note, that this can be realized experimentally in an number of different ways: one can apply high pressure, or find structural phase transition in Dirac metal, or consider any other way of breaking rotational symmetry, such as e.g. nematic order. We have found that Dirac metal can be viewed as a critical point between two different phases of topological crystalline insulators with different mirror Chern numbers. This fact implies that Dirac metal is a critical point, where handedness of surface states changes, which, in turn, leads, to an important physical conclusion: surface states in Dirac metal always terminate at Dirac points despite being not topologically protected. Thus our work supplements previous works, which established that suraface states in Dirac metal contain a small gap, which results from absence of topological protection. However, we would like to note, that such gap has never been observed experimentally, because it is smaller than Fermi level

in realistic samples. Thus, to confirm our predictions, it would be of interest, to create Dirac metal samples with as low Fermi level as possible. This can be achieved, e.g. by adding acceptor impurities.

Bibliography

[1] G. Bednik, A. A. Zyuzin, and A. A. Burkov. Superconductivity in weyl metals. *Phys. Rev. B*, 92:035153, Jul 2015.

[2] G Bednik, A A Zyuzin, and A A Burkov. Anomalous hall effect in weyl superconductors. *New Journal of Physics*, 18(8):085002, 2016.

[3] G. Bednik. Surface states in dirac semimetals and topological crystalline insulators. *Phys. Rev. B*, 98:045140, Jul 2018.

[4] K. v. Klitzing, G. Dorda, and M. Pepper. New method for high-accuracy determination of the fine-structure constant based on quantized hall resistance. *Phys. Rev. Lett.*, 45:494–497, Aug 1980.

[5] R. B. Laughlin. Quantized hall conductivity in two dimensions. *Phys. Rev. B*, 23:5632–5633, May 1981.

[6] D. J. Thouless, M. Kohmoto, M. P. Nightingale, and M. den Nijs. Quantized hall conductance in a two-dimensional periodic potential. *Phys. Rev. Lett.*, 49:405–408, Aug 1982.

[7] Quantal phase factors accompanying adiabatic changes. *Proceedings of the Royal Society of London A: Mathematical, Physical and Engineering Sciences*, 392(1802):45–57, 1984.

[8] Mahito Kohmoto. Topological invariant and the quantization of the hall conductance. *Annals of Physics*, 160(2):343 – 354, 1985.

[9] F. D. M. Haldane. Model for a quantum hall effect without landau levels: Condensed-matter realization of the "parity anomaly". *Phys. Rev. Lett.*, 61:2015–2018, Oct 1988.

[10] A. K. Geim and K. S. Novoselov. The rise of graphene. *Nature Materials*, 6:183 EP –, Mar 2007.

[11] C. L. Kane and E. J. Mele. Quantum spin hall effect in graphene. *Phys. Rev. Lett.*, 95:226801, Nov 2005.

[12] Markus König, Steffen Wiedmann, Christoph Brüne, Andreas Roth, Hartmut Buhmann, Laurens W. Molenkamp, Xiao-Liang Qi, and Shou-Cheng Zhang. Quantum spin hall insulator state in HgTe quantum wells. *Science*, 318(5851):766–770, 2007.

[13] B. Andrei Bernevig, Taylor L. Hughes, and Shou-Cheng Zhang. Quantum spin hall effect and topological phase transition in hgte quantum wells. *Science*, 314(5806):1757–1761, 2006.

[14] Xiao-Liang Qi and Shou-Cheng Zhang. Topological insulators and superconductors. *Rev. Mod. Phys.*, 83:1057–1110, Oct 2011.

[15] Liang Fu. Topological crystalline insulators. *Phys. Rev. Lett.*, 106:106802, Mar 2011.

[16] Timothy H. Hsieh, Hsin Lin, Junwei Liu, Wenhui Duan, Arun Bansil, and Liang Fu. Topological crystalline insulators in the snte material class. *Nature Communications*, 3:982 EP –, Jul 2012. Article.

[17] Su-Yang Xu et al. Observation of a topological crystalline insulator phase and topological phase transition in $Pb_{1_x}Sn_xTe$. *Nat. Commun.*, 3:2191, Nov 2012.

[18] Yoichi Ando and Liang Fu. Topological crystalline insulators and topological superconductors: From concepts to materials. *Annual Review of Condensed Matter Physics*, 6(1):361–381, 2015.

[19] Xiangang Wan, Ari M. Turner, Ashvin Vishwanath, and Sergey Y. Savrasov. Topological semimetal and fermi-arc surface states in the electronic structure of pyrochlore iridates. *Phys. Rev. B*, 83:205101, May 2011.

[20] N. P. Armitage, E. J. Mele, and Ashvin Vishwanath. Weyl and dirac semimetals in three-dimensional solids. *Rev. Mod. Phys.*, 90:015001, Jan 2018.

[21] Binghai Yan and Claudia Felser. Topological materials: Weyl semimetals. *Annual Review of Condensed Matter Physics*, 8(1):337–354, 2017.

[22] Guang Bian, Tay-Rong Chang, Raman Sankar, Su-Yang Xu, Hao Zheng, Titus Neupert, Ching-Kai Chiu, Shin-Ming Huang, Guoqing Chang, Ilya Belopolski, Daniel S. Sanchez, Madhab Neupane, Nasser Alidoust, Chang Liu, BaoKai Wang, Chi-Cheng Lee, Horng-Tay Jeng, Chenglong Zhang, Zhujun Yuan, Shuang Jia, Arun Bansil, Fangcheng Chou, Hsin Lin, and M. Zahid Hasan. Topological nodal-line fermions in spin-orbit metal pbtase2. *Nature Communications*, 7:10556 EP –, Feb 2016. Article.

[23] Motoaki Hirayama, Ryo Okugawa, Takashi Miyake, and Shuichi Murakami. Topological dirac nodal lines and surface charges in fcc alkaline earth metals. *Nat Commun*, 8:14022, Jan 2017. 28074835[pmid].

[24] Chen Fang, Matthew J. Gilbert, Xi Dai, and B. Andrei Bernevig. Multi-weyl topological semimetals stabilized by point group symmetry. *Phys. Rev. Lett.*, 108:266802, Jun 2012.

[25] A. A. Burkov and Leon Balents. Weyl semimetal in a topological insulator multilayer. *Phys. Rev. Lett.*, 107:127205, Sep 2011.

[26] A.A. Burkov. Anomalous hall effect in weyl metals. *Phys. Rev. Lett.*, 113:187202, Oct 2014.

[27] A.A. Burkov. Chiral anomaly and diffusive magnetotransport in weyl metals. *Phys. Rev. Lett.*, 113:247203, Dec 2014.

[28] A. A. Burkov. Negative longitudinal magnetoresistance in dirac and weyl metals. *Phys. Rev. B*, 91:245157, Jun 2015.

[29] A. A. Burkov, M. D. Hook, and Leon Balents. Topological nodal semimetals. *Phys. Rev. B*, 84:235126, Dec 2011.

[30] Tobias Meng and Leon Balents. Weyl superconductors. *Phys. Rev. B*, 86:054504, Aug 2012.

[31] Gil Young Cho, Jens H. Bardarson, Yuan-Ming Lu, and Joel E. Moore. Superconductivity of doped weyl semimetals: Finite-momentum pairing and electronic analog of the ^{3}he-a phase. *Phys. Rev. B*, 86:214514, Dec 2012.

[32] Huazhou Wei, Sung-Po Chao, and Vivek Aji. Odd-parity superconductivity in weyl semimetals. *Phys. Rev. B*, 89:014506, Jan 2014.

[33] Peter Fulde and Richard A. Ferrell. Superconductivity in a strong spin-exchange field. *Phys. Rev.*, 135:A550–A563, Aug 1964.

[34] A. I. Larkin and Y. N. Ovchinnikov. Inhomogeneous state of superconductors. *Sov. Phys.-JETP*, 20:762–769, Apr 1964.

[35] Shin-Ming Huang, Su-Yang Xu, Ilya Belopolski, Chi-Cheng Lee, Guoqing Chang, BaoKai Wang, Nasser Alidoust, Guang Bian, Madhab Neupane, Chenglong Zhang, Shuang Jia, Arun Bansil, Hsin Lin, and M. Zahid Hasan. A weyl fermion semimetal with surface fermi arcs in the transition metal monopnictide taas class. *Nature Communications*, 6:7373 EP –, Jun 2015. Article.

[36] Su-Yang Xu, Nasser Alidoust, Ilya Belopolski, Zhujun Yuan, Guang Bian, Tay-Rong Chang, Hao Zheng, Vladimir N. Strocov, Daniel S. Sanchez, Guoqing Chang, Chenglong Zhang, Daixiang Mou, Yun Wu, Lunan Huang, Chi-Cheng Lee, Shin-Ming Huang, BaoKai Wang, Arun Bansil, Horng-Tay Jeng, Titus Neupert, Adam Kaminski, Hsin Lin, Shuang Jia, and M. Zahid Hasan. Discovery of a weyl fermion state with fermi arcs in niobium arsenide. *Nature Physics*, 11:748 EP –, Aug 2015. Article.

[37] L. X. Yang, Z. K. Liu, Y. Sun, H. Peng, H. F. Yang, T. Zhang, B. Zhou, Y. Zhang, Y. F. Guo, M. Rahn, D. Prabhakaran, Z. Hussain, S.-K. Mo, C. Felser, B. Yan, and Y. L. Chen. Weyl semimetal phase in the non-centrosymmetric compound taas. *Nature Physics*, 11:728 EP –, Aug 2015.

[38] Su-Yang Xu, Ilya Belopolski, Daniel S. Sanchez, Chenglong Zhang, Guoqing Chang, Cheng Guo, Guang Bian, Zhujun Yuan, Hong Lu, Tay-Rong Chang, Pavel P. Shibayev,

Mykhailo L. Prokopovych, Nasser Alidoust, Hao Zheng, Chi-Cheng Lee, Shin-Ming Huang, Raman Sankar, Fangcheng Chou, Chuang-Han Hsu, Horng-Tay Jeng, Arun Bansil, Titus Neupert, Vladimir N. Strocov, Hsin Lin, Shuang Jia, and M. Zahid Hasan. Experimental discovery of a topological weyl semimetal state in tap. *Science Advances*, 1(10), 2015.

[39] Yufeng Li, Yonghui Zhou, Zhaopeng Guo, Fei Han, Xuliang Chen, Pengchao Lu, Xuefei Wang, Chao An, Ying Zhou, Jie Xing, Guan Du, Xiyu Zhu, Huan Yang, Jian Sun, Zhaorong Yang, Wenge Yang, Ho-Kwang Mao, Yuheng Zhang, and Hai-Hu Wen. Concurrence of superconductivity and structure transition in weyl semimetal tap under pressure. *npj Quantum Materials*, 2(1):66, 2017.

[40] He Wang, Huichao Wang, Yuqin Chen, Jiawei Luo, Zhujun Yuan, Jun Liu, Yong Wang, Shuang Jia, Xiong-Jun Liu, Jian Wei, and Jian Wang. Discovery of tip induced unconventional superconductivity on weyl semimetal. *Science Bulletin*, 62(6):425 – 430, 2017.

[41] Leena Aggarwal, Sirshendu Gayen, Shekhar Das, Ritesh Kumar, Vicky SGjGdzh, Claudia Felser, Chandra Shekhar, and Goutam Sheet. Mesoscopic superconductivity and high spin polarization coexisting at metallic point contacts on weyl semimetal taas. *Nature Communications*, 8:13974 EP –, Jan 2017. Article.

[42] Maja D. Bachmann, Nityan Nair, Felix Flicker, Roni Ilan, Tobias Meng, Nirmal J. Ghimire, Eric D. Bauer, Filip Ronning, James G. Analytis, and Philip J. W. Moll. Inducing superconductivity in weyl semimetal microstructures by selective ion sputtering. *Science Advances*, 3(5), 2017.

[43] Z. Guguchia, F. von Rohr, Z. Shermadini, A. T. Lee, S. Banerjee, A. R. Wieteska, C. A. Marianetti, B. A. Frandsen, H. Luetkens, Z. Gong, S. C. Cheung, C. Baines, A. Shengelaya, G. Taniashvili, A. N. Pasupathy, E. Morenzoni, S. J. L. Billinge, A. Amato, R. J. Cava, R. Khasanov, and Y. J. Uemura. Signatures of the topological s^{+-} superconducting order parameter in the type iiweyl semimetal $MoTe_2$. *Nature Communications*, 8(1):1082, 2017.

[44] J. M. Luttinger. Quantum theory of cyclotron resonance in semiconductors: General theory. *Phys. Rev.*, 102:1030–1041, May 1956.

[45] T. Jungwirth, Qian Niu, and A. H. MacDonald. Anomalous hall effect in ferromagnetic semiconductors. *Phys. Rev. Lett.*, 88:207208, May 2002.

[46] Shuichi Murakami, Naoto Nagosa, and Shou-Cheng Zhang. SU(2) non-abelian holonomy and dissipationless spin current in semiconductors. *Phys. Rev. B*, 69:235206, Jun 2004.

[47] Eun-Gook Moon, Cenke Xu, Yong Baek Kim, and Leon Balents. Non-fermi-liquid and topological states with strong spin-orbit coupling. *Phys. Rev. Lett.*, 111:206401, Nov 2013.

[48] Jennifer Cano, Barry Bradlyn, Zhijun Wang, Max Hirschberger, N. P. Ong, and B. A. Bernevig. Chiral anomaly factory: Creating weyl fermions with a magnetic field. *Phys. Rev. B*, 95:161306, Apr 2017.

[49] Lucile Savary, Eun-Gook Moon, and Leon Balents. New type of quantum criticality in the pyrochlore iridates. *Phys. Rev. X*, 4:041027, Nov 2014.

[50] Pallab Goswami, Bitan Roy, and Sankar Das Sarma. Competing orders and topology in the global phase diagram of pyrochlore iridates. *Phys. Rev. B*, 95:085120, Feb 2017.

[51] S. M. Young, S. Zaheer, J. C. Y. Teo, C. L. Kane, E. J. Mele, and A. M. Rappe. Dirac semimetal in three dimensions. *Phys. Rev. Lett.*, 108:140405, Apr 2012.

[52] Naoto Nagaosa Bohm-Jung Yang. Classification of stable three-dimensional dirac semimetals with nontrivial topology. *Nat. Commun.*, 5:5898, September 2014.

[53] Zhijun Wang, Yan Sun, Xing-Qiu Chen, Cesare Franchini, Gang Xu, Hongming Weng, Xi Dai, and Zhong Fang. Dirac semimetal and topological phase transitions in A_3bi (a = Na, k, rb). *Phys. Rev. B*, 85:195320, May 2012.

[54] Z. K. Liu et al. Discovery of a three-dimensional topological dirac semimetal na3bi. *Science*, 343:864–867, February 2014.

[55] Su-Yang Xu, Chang Liu, Satya K. Kushwaha, Raman Sankar, Jason W. Krizan, Ilya Belopolski, Madhab Neupane, Guang Bian, Nasser Alidoust, Tay-Rong Chang, Horng-Tay Jeng, Cheng-Yi Huang, Wei-Feng Tsai, Hsin Lin, Pavel P. Shibayev, Fang-Cheng Chou, Robert J. Cava, and M. Zahid Hasan. Observation of fermi arc surface states in a topological metal. *Science*, 347(6219):294–298, 2015.

[56] Sergey Borisenko, Quinn Gibson, Danil Evtushinsky, Volodymyr Zabolotnyy, Bernd Büchner, and Robert J. Cava. Experimental realization of a three-dimensional dirac semimetal. *Phys. Rev. Lett.*, 113:027603, Jul 2014.

[57] Zhijun Wang, Hongming Weng, Quansheng Wu, Xi Dai, and Zhong Fang. Three-dimensional dirac semimetal and quantum transport in cd_3as_2. *Phys. Rev. B*, 88:125427, Sep 2013.

[58] M. et al. Neupane. Observation of a three-dimensional topological dirac semimetal phase in high-mobility cd3as2. *Nat. Commun.*, 5:3786, May 2014.

[59] M. et al. Neupane. A stable three-dimensional topological dirac semimetal cd3as2. *Nat. Mater.*, 13:677–681, July 2014.

[60] R. Y. Chen, Z. G. Chen, X.-Y. Song, J. A. Schneeloch, G. D. Gu, F. Wang, and N. L. Wang. Magnetoinfrared spectroscopy of landau levels and zeeman splitting of three-dimensional massless dirac fermions in $zrte_5$. *Phys. Rev. Lett.*, 115:176404, Oct 2015.

[61] Philip J. W. Moll, Nityan L. Nair, Toni Helm, Andrew C. Potter, Itamar Kimchi, Ashvin Vishwanath, and James G. Analytis. Transport evidence for fermi-arc-mediated chirality transfer in the dirac semimetal cd3as2. *Nature*, 535:266 EP –, Jul 2016.

[62] Cheng Zhang, Awadhesh Narayan, Shiheng Lu, Jinglei Zhang, Huiqin Zhang, Zhuoliang Ni, Xiang Yuan, Yanwen Liu, Ju-Hyun Park, Enze Zhang, Weiyi Wang, Shanshan Liu, Long Cheng, Li Pi, Zhigao Sheng, Stefano Sanvito, and Faxian Xiu. Evolution of weyl orbit and quantum hall effect in dirac semimetal cd3as2. *Nat. Commun.*, 8(1):1272, 2017.

[63] Mehdi Kargarian, Mohit Randeria, and Yuan-Ming Lu. Are the surface fermi arcs in dirac semimetals topologically protected? *Proceedings of the National Academy of Sciences*, 113(31):8648–8652, 2016.

[64] B. ANDREI BERNEVIG and Taylor L. Hughes. *Topological Insulators and Topological Superconductors*. Princeton University Press, 2013.

[65] Valery Rubakov and Stephen S Wilson. *Classical Theory of Gauge Fields*. Princeton University Press, 2002.

[66] C.A. Brau. *Modern Problems in Classical Electrodynamics*. OUP USA, 2004.

[67] A. Altland and B. Simons. *Condensed Matter Field Theory*. Cambridge University Press, 2006.

[68] Tohru Eguchi, Peter B. Gilkey, and Andrew J. Hanson. Gravitation, gauge theories and differential geometry. *Physics Reports*, 66(6):213 – 393, 1980.

[69] M. Nakahara. *Geometry, Topology and Physics, Second Edition*. Graduate student series in physics. Taylor & Francis, 2003.

[70] E. Yankowsky, A.S. Schwarz, and S. Levy. *Quantum Field Theory and Topology*. Grundlehren der mathematischen Wissenschaften. Springer Berlin Heidelberg, 2013.

[71] Chao-Xing Liu, Xiao-Liang Qi, Hai-Jun Zhang, Xi Dai, Zhong Fang, and Shou-Cheng Zhang. Model hamiltonian for topological insulators. *Phys. Rev. B*, 82:045122, Jul 2010.

[72] A. A. Zyuzin, Si Wu, and A. A. Burkov. Weyl semimetal with broken time reversal and inversion symmetries. *Phys. Rev. B*, 85:165110, Apr 2012.

[73] Y. Chen, D. L. Bergman, and A. A. Burkov. Weyl fermions and the anomalous hall effect in metallic ferromagnets. *Phys. Rev. B*, 88:125110, Sep 2013.

[74] Takahiro Fukui, Yasuhiro Hatsugai, and Hiroshi Suzuki. Chern numbers in discretized brillouin zone: Efficient method of computing (spin) hall conductances. *Journal of the Physical Society of Japan*, 74(6):1674–1677, 2005.

[75] Roger S. K. Mong and Vasudha Shivamoggi. Edge states and the bulk-boundary correspondence in dirac hamiltonians. *Phys. Rev. B*, 83:125109, Mar 2011.

[76] Maxim Kharitonov, Julian-Benedikt Mayer, and Ewelina M. Hankiewicz. Universality and stability of the edge states of chiral-symmetric topological semimetals and surface states of the luttinger semimetal. *Phys. Rev. Lett.*, 119:266402, Dec 2017.

[77] A. A. Burkov. Mirror anomaly in dirac semimetals. *Phys. Rev. Lett.*, 120:016603, Jan 2018.

[78] Roman M. Lutchyn, Pavel Nagornykh, and Victor M. Yakovenko. Gauge-invariant electromagnetic response of a chiral $p_x + ip_y$ superconductor. *Phys. Rev. B*, 77:144516, Apr 2008.

[79] A. A. Burkov. Chiral anomaly and transport in weyl metals. *Journal of Physics: Condensed Matter*, 27(11):113201, 2015.

[80] Jeffrey C. Y. Teo, Liang Fu, and C. L. Kane. Surface states and topological invariants in three-dimensional topological insulators: Application to $\mathrm{bi}_{1-x}\mathrm{sb}_x$. *Phys. Rev. B*, 78:045426, Jul 2008.